

Flight Reports of MPO-MAG:

Commissioning Report

Covered Time Period : October 25th 2018 – December 6th 2018

Instrument: MPO-MAG
Document Title: Commissioning Report
Prepared by: MPO-MAG Team
Organisation: TU-Braunschweig - IGEP
Approved by:
Date of Issue: 2019-10-07

WBS Code:
Package Code :

BC-MPO
MAG

Doc. Title: Commissioning Report
Doc. Ref. : BC-MAG-TR-00120
Date : 2019-10-07

Issue: 1
Rev. : 0
Page : 3/92

TABLE OF CONTENTS

1	Introduction	6
2	Hardware Commissioning Setup	6
3	Commissioning Sequences	6
4	Hardware Commissioning Results: Calibration Modes	8
4.1	Noise and Sensitivity in Close and Open Loop Operation	8
4.1.1	IB	8
4.1.2	OB	12
4.1.3	Discussion	16
4.2	ADC /DAC Mode results (Cal 3)	17
4.2.1	IB	17
4.2.2	OB	20
4.2.3	Discussion	22
4.3	Find phase results (Cal 7)	23
4.3.1	IB	23
4.3.2	OB	25
4.4	Meander results (Cal 5)	28
4.4.1	IB	28
4.4.2	OB	30
4.5	Step Function Results (Cal 1)	33
4.6	Counter results (Cal 2)	33
4.7	ADC noise test	34
4.7.1	IB	34
4.7.2	OB	35
5	Results of HK Measurements	42
5.1	Temperature of Sensor and Electronics	42
5.2	Heater operation	43
5.3	Voltages / Currents	44
6	Results Offset Calibration	45
7	Investigation of S/C Interferences	49
7.1	Boom Deployment	57
7.2	Reaction Wheels	59

7.3	MTM solar panel currents	64
7.4	MPO solar panel currents	65
7.5	Phebus	67
7.6	SEPS	71
7.7	HGA	79
8	Common measurement with MMO	82
9	Agenda for Future Activities	83
10	Appendix 1 – Commissioning sequence:	1

1 Introduction

In this document data received during the MPO-MAG Commissioning and the monitoring activities during the entire NECP are evaluated.

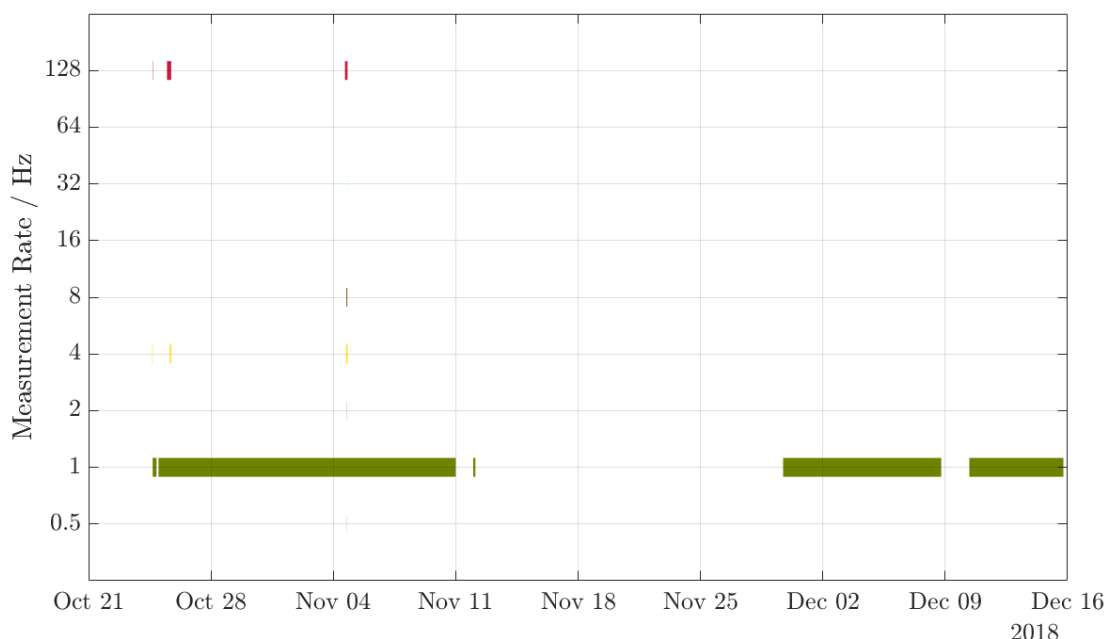
The switch-on of MPO-MAG was successful and the instrument operated nominally during the NECP. All data required to evaluate the instrument's status and performance were successfully recorded. The s/c interferences are on a acceptable level. Also, the parallel operation of MPO-MAG with MMO-MGF yield the mutual sensor orientation.

2 Hardware Commissioning Setup

The commissioning starts soon after successful boom deployment. Thus the test configuration was fully representative for the MPO configuration in the Mercury orbit. Note that s/c magnetic field will change after separation of MTM and MMO.

3 Commissioning Sequences

The magnetometer has been operated in open and close loop as well as in several calibration modes. The test sequence has been executed for the first time on 25/10/2018 and repeated on 04/11/2018. The first sequence was setup with a conservative configuration whereas the second one took the low s/c disturbance level into account. The used calibration sequence was executed on both main and redundant side. In between MPO-MAG works in 1Hz dual mode for monitoring interferences of sub systems and other instruments. The data availability is shown in the following plot:



The calibration test sequence consists of a 5min registration in a closed and open loop mode. In both modes +/- calibration fields (using +/-300 LSB steps of the compensation ADC) are added.

In the following sequence calibration sub-sequences (stored onboard) are executed.

The calibration sub-sequences are:

- ADC/DAC mode
- Findphase
- Meander
- Step Function
- Counter

The detailed command list of a calibration sequence can be found in Appendix 1.

4 Hardware Commissioning Results: Calibration Modes

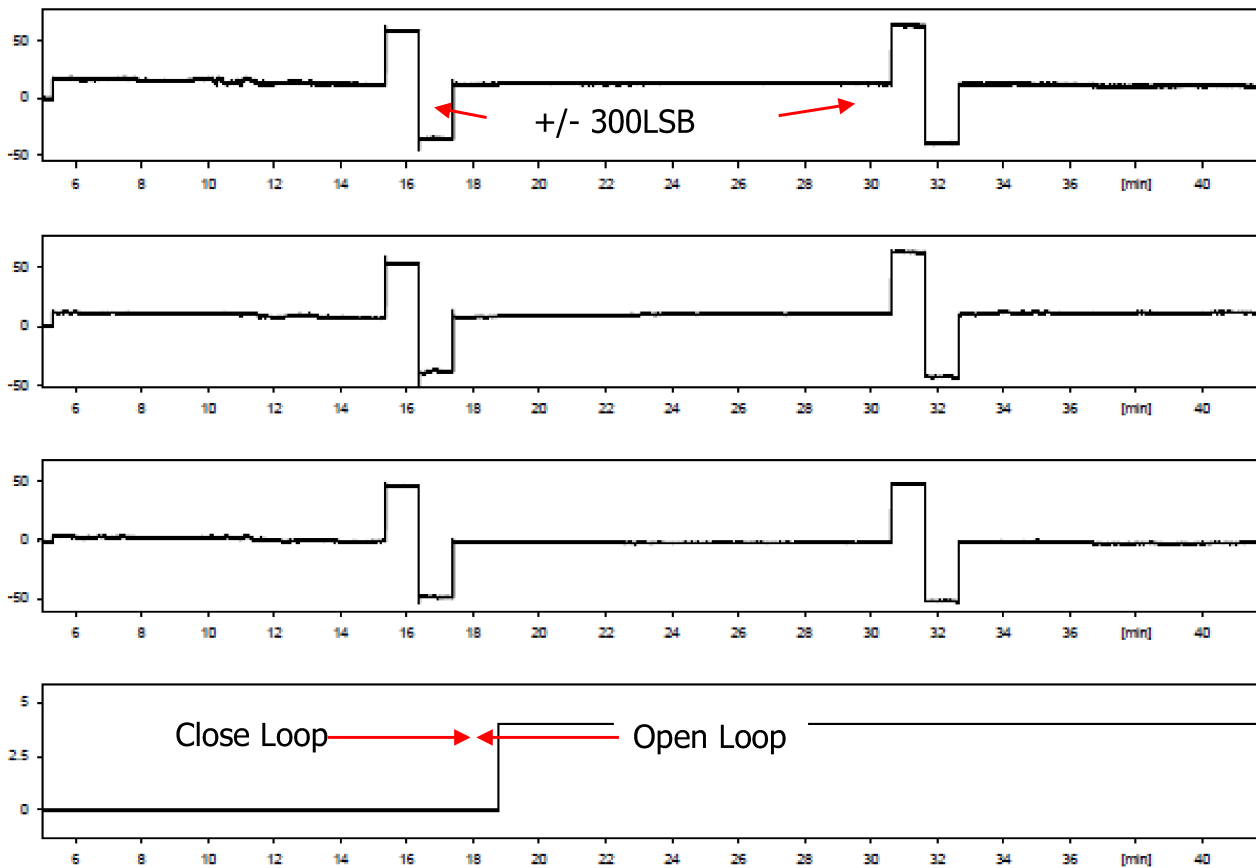
4.1 Noise and Sensitivity in Close and Open Loop Operation

During commissioning MPO-MAG has been operated in close (code 0) and open loop (code4) mode. Additionally, +/-300 LSB steps of the compensation DAC have been applied.

Noise and sensitivity data recording starts at 7014-16:02:31.49837

4.1.1 IB

IB overview:



The upper three panels show the magnetic field components X Y Z (sensor coordinates) in nT. In the lower panel a status byte is plotted which contains the information about the commanded mode (0=Close Loop; 4= Open Loop)

IB Steps:

IB	X	Steps	Y	Steps	Z	Steps
Close Loop	11,55	46,57	6,96	45,73	-0,79	47,73
	58,09	-46,75	53,13	-45,38	46,59	-47,37
	-35,23		-37,97		-48,50	
	11,49		7,85		-1,48	
Sensitivity Commiss..		46,66		45,56		47,55
Sensitivity SPT-2		46,89		46,26		47,21
Ratio Comm/SPT2		0,995		0,985		1,007
Open Loop	12,29	50,58	10,69	52,35	-2,17	50,29
	62,66	-51,80	63,07	-53,55	48,34	-49,97
	-39,72		-42,82		-51,91	
	11,87		10,76		-1,72	
Sensitivity Commiss..		51,19		52,95		50,13
Sensitivity SPT-2		43,23		44,15		48,04
Ratio Comm/SPT2		1,184		1,199		1,044

The table summarises the measurement results (grey) before executing steps, at upper level, at lower level and after steps in nT for each component. Step heights (see subsequent columns) are calculated on basis of a zero level derived from the averaged before and after steps level. Derived Sensitivity (red) is compared with the results during SPT-2 (blue). All numbers (except ratios) are given in nT.

In close loop the response of the feedback signal (via feedback DAC) to a field step applied by the compensation DAC is checked. Both, feedback as well as compensation DAC circuitries are supplying a current into the same Helmholtz coil system. Thus temperature related changes of the coil system size and geometry should not impact this value. The sensitivity should be independent on temperature. The measured deviation is less than 1,5% (of 46nT) which is with less than 1nT within the measurement accuracy. Thus feedback and compensation are working well.

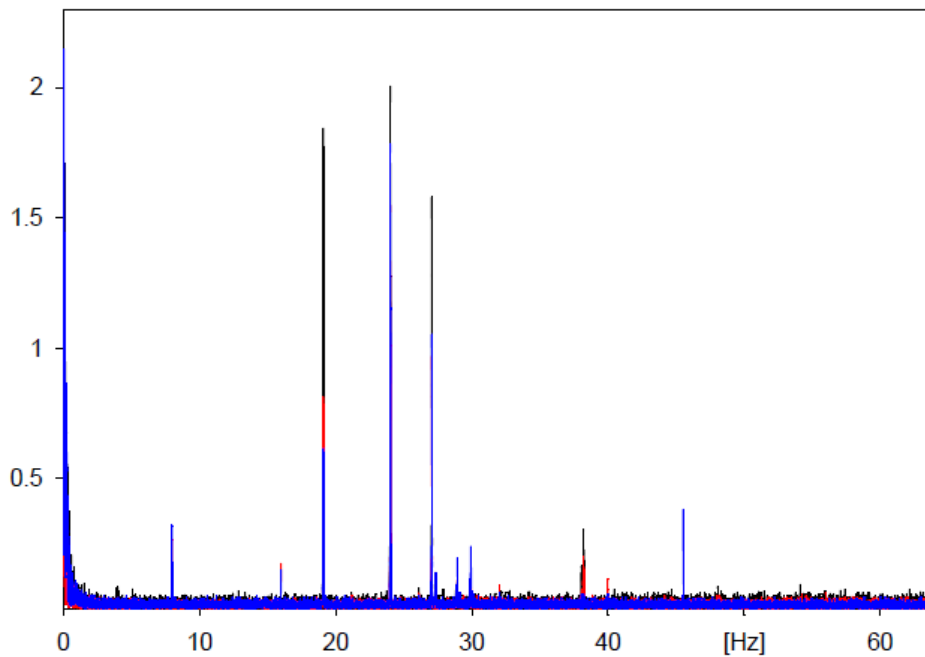
In open loop the steps generated by the compensation are measured by the pick-up system. Assuming the pickup system (pickup coil, ADC sampling and phase shift of ADC sampling vs. excitation) works unchanged since SPT-2, the temperature expansion of the feedback system due to the ambient temperature must be visible. The temperature during commissioning was with -70°C almost 90°C below the temperature during SPT-2. The temperature coefficient of the feedback system is 18ppm/°C. Thus the sensitivity must change systematically by 0,17%. The deviation however is with up to 20% much higher and therefore (as expected) related to the pickup system. The reasons for this high sensitivity of the pickup system are the temperature sensitivity of the excitation current and the temperature dependency of the pickup resonant circuit with its related phase shift.

The mismatch between Feedback and ADC sensitivity leads to errors if ADC and DAC values are summed up and it influences the feedback control loop (oscillations in case of overcompensation). The control loop deviation is +/-0.5nT maximum (see chapter 4.2.,

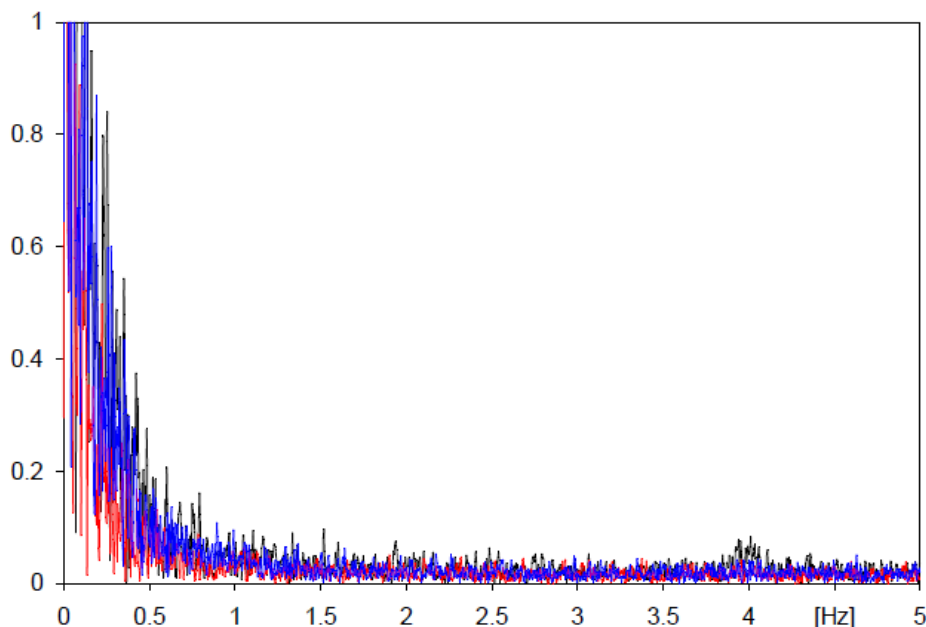
ADC / DAC cal mode), thus a 20% error of the ADC sensitivity would cause a measurement errors of $<0.1\text{nT}$.

IB Noise:

Close Loop

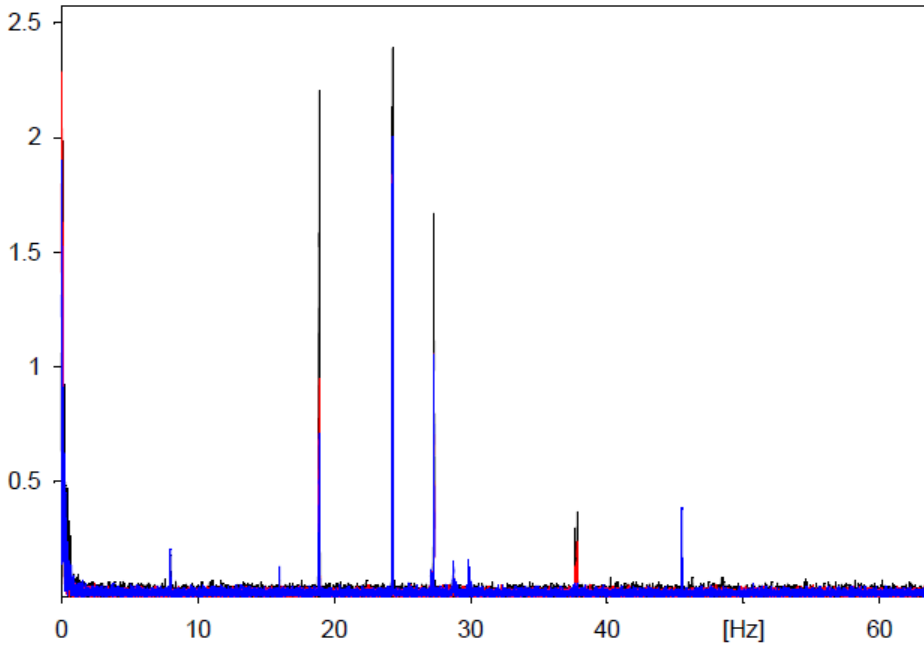


FFT of the three magnetic field components X (black), Y (red) and Z (blue) in $\text{nT}/\sqrt{\text{Hz}}$

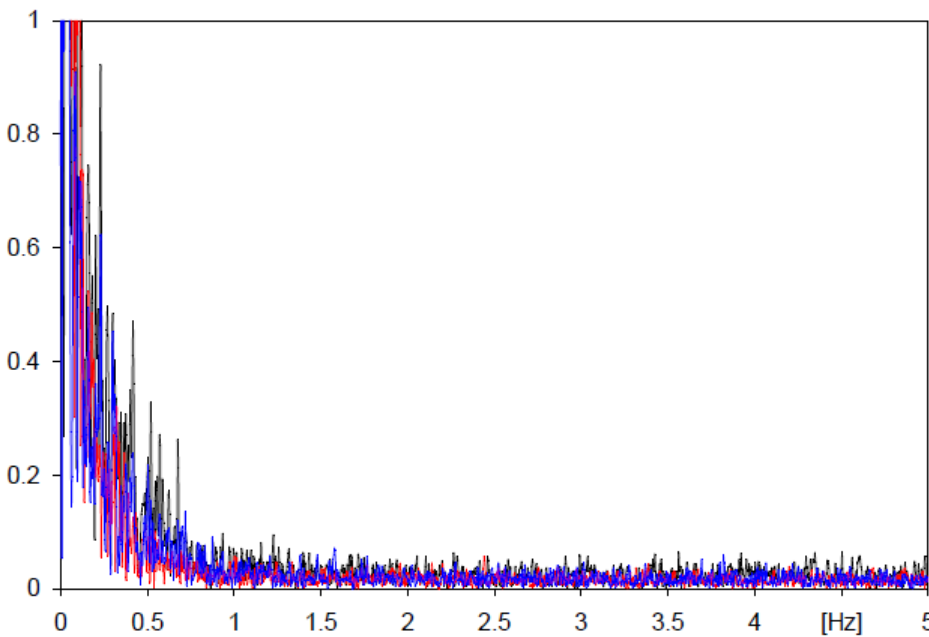


FFT of the three magnetic field components X (black), Y (red) and Z (blue) in $\text{nT}/\sqrt{\text{Hz}}$ zoomed out for a frequency range of 0-5Hz.

Open Loop:



FFT of the three magnetic field components X (black), Y (red) and Z (blue) in nT/Sqrt(Hz)



FFT of the three magnetic field components X (black), Y (red) and Z (blue) in nT/Sqrt(Hz) zoomed out for a frequency range of 0-5Hz.

IB/ CL

	X	Y	Z
@ 1Hz	45	29	45
@ 5Hz	21	15	17

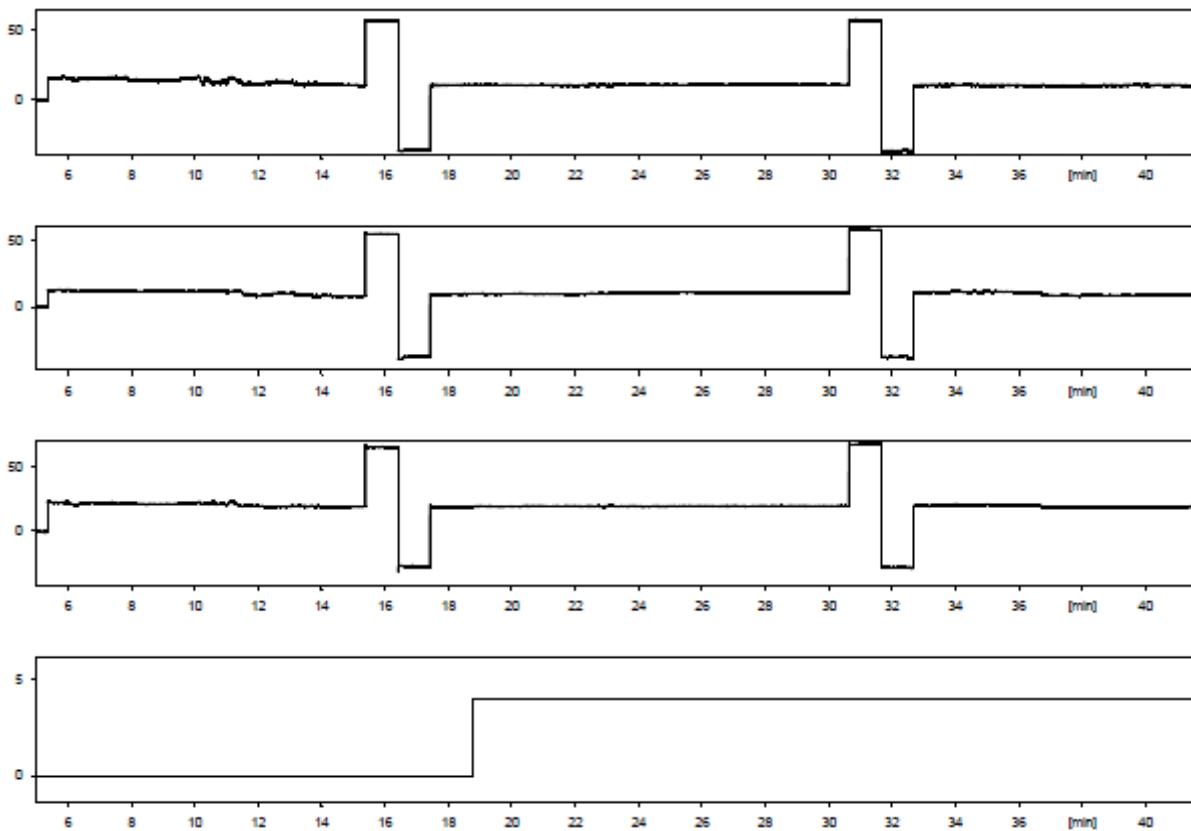
IB/ OL

	X	Y	Z
@ 1Hz	41	23	30
@ 5Hz	23	16	16

Noise in pT/Sqrt(Hz):

4.1.2 OB

OB overview:



The upper three panels show the magnetic field components X Y Z (sensor coordinates) in nT. In the lower panel a status byte is plotted which contains the information about the commanded mode (0=Close Loop; 4= Open Loop)

OB Steps:

IB	X	Steps	Y	Steps	Z	Steps
Close Loop	10,19	46,51	8,32	45,67	18,71	47,57
	56,66	-46,72	54,60	-45,28	66,13	-47,28
	-36,56		-36,34		-28,72	
	10,12		9,55		18,41	
Sensitivity Commiss..		46,61		45,47		47,43
Sensitivity SPT-2		47,02		46,27		47,36
Ratio Comm/SPT2		0,991		0,983		1,001
Open Loop	10,27	46,37	11,00	46,81	19,35	49,07
	56,51	-47,42	57,90	-47,74	68,58	-49,01
	-37,27		-36,64		-29,49	
	10,02		11,19		19,68	
Sensitivity Commiss..		46,89		47,27		49,04
Sensitivity SPT-2		44,84		45,41		48,63
Ratio Comm/SPT2		1,046		1,041		1,008

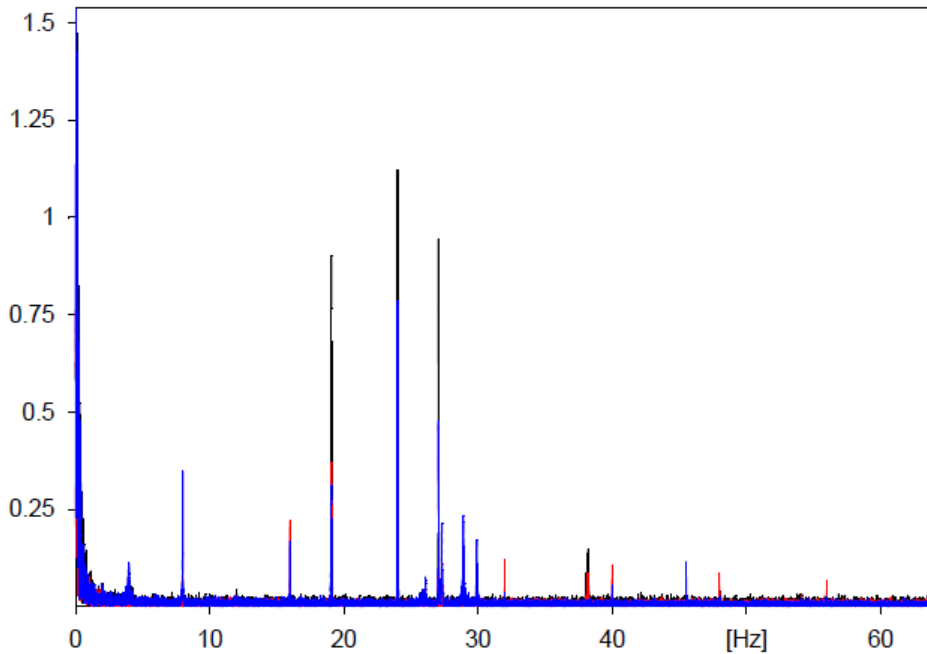
The table summarizes the measurement results (grey) before executing steps, at upper level, at lower level and after steps in nT for each component. Step heights (see subsequent columns) are calculated on basis of a zero level derived from the averaged before and after steps level. Derived Sensitivity (red) is compared with the results during SPT-2 (blue). All numbers (except ratios) are given in nT.

In close loop the response of the feedback signal (via feedback DAC) to a field step applied by the compensation DAC is checked. Both, feedback as well as compensation DAC circuitries are supplying a current into the same Helmholtz coil system. Thus temperature related changes of the coil system size and geometry should not impact this value. The sensitivity should be independent on temperature. The measured deviation is less than 1,7% (of 46nT) which is with less than 1nT within the measurement accuracy. Thus feedback and compensation are working well.

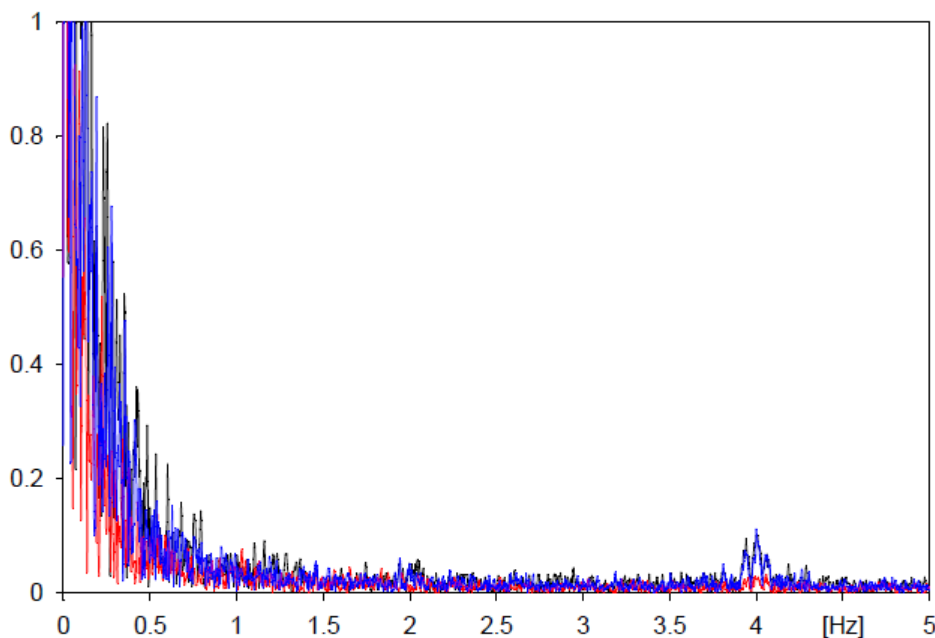
In open loop the steps generated by the compensation are measured by the pick-up system. Assuming the pickup system (pickup coil, ADC sampling and phase shift of ADC sampling vs. excitation) works unchanged since SPT-2, the temperature expansion of the feedback system due to the ambient temperature must be visible. The temperature during commissioning was with -70°C almost 90°C below the temperature during SPT-2. The temperature coefficient of the feedback system is 18ppm/°C. Thus the sensitivity must change systematically by 0,17%. The deviation however is with up to 5% much higher (but less than for IB) and therefore (as expected) related to the pickup system. The reasons for this high sensitivity of the pickup system are the temperature sensitivity of the excitation current and the temperature dependency of the pickup resonant circuit with its related phase shift.

OB Noise:

Close Loop

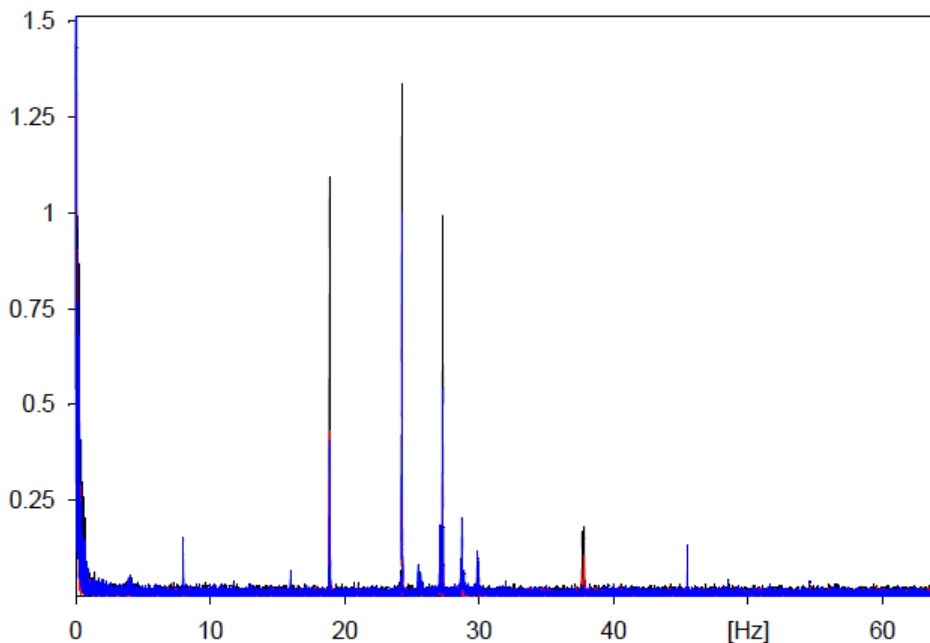


FFT of the three magnetic field components X (black), Y (red) and Z (blue) in nT/Sqrt(Hz)

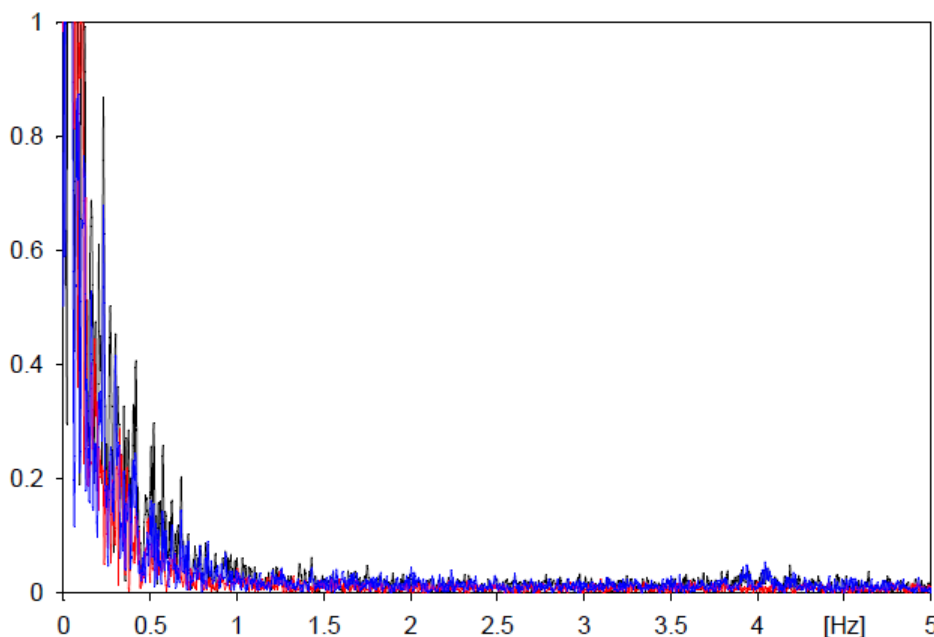


FFT of the three magnetic field components X (black), Y (red) and Z (blue) in nT/Sqrt(Hz) zoomed out for a frequency range of 0-5Hz.

Open Loop



FFT of the three magnetic field components X (black), Y (red) and Z (blue) in nT/Sqrt(Hz)



FFT of the three magnetic field components X (black), Y (red) and Z (blue) in nT/Sqrt(Hz) zoomed out for a frequency range of 0-5Hz.

OB/ CL	X	Y	Z	OB/ OL	X	Y	Z
@ 1Hz	40	29	31	1Hz	31	17	23
@ 5Hz	13	9	11	5Hz	12	8	10

Noise in pT/Sqrt(Hz):

4.1.3 Discussion

Only the noise of the outboard sensor at 5Hz is in accordance with the noise measurement performed in a shielded environment at -70°C. The power at lower frequencies is obviously dominated by the solar wind field and possible s/c noise (see difference between inboard and outboard sensor)

Noise in pT/Sqrt(Hz) at 1Hz from pre-flight measurements:

	OB X	OB Y	OB Z	IB X	IB Y	IB Z
-70°	12,9	7,1	9,3	14,0	9,6	12,4
-20°	9,1	5,1	6,7	11,0	6,2	12,2
+30°	5,1	3,9	6,5	7,7	5,4	9,8
+80°	6,7	3,6	5,7	6,9	4,8	8,2
+130°	6,3	3,2	6,0	6,5	4,5	8,3
+180°	5,9	3,2	4,9	6,2	3,8	5,5

The noise levels in pT/Sqrt(Hz) at 1Hz listed in this table are taken from the temperature calibration test in Graz (cf. BC-MAG-TR-00053).

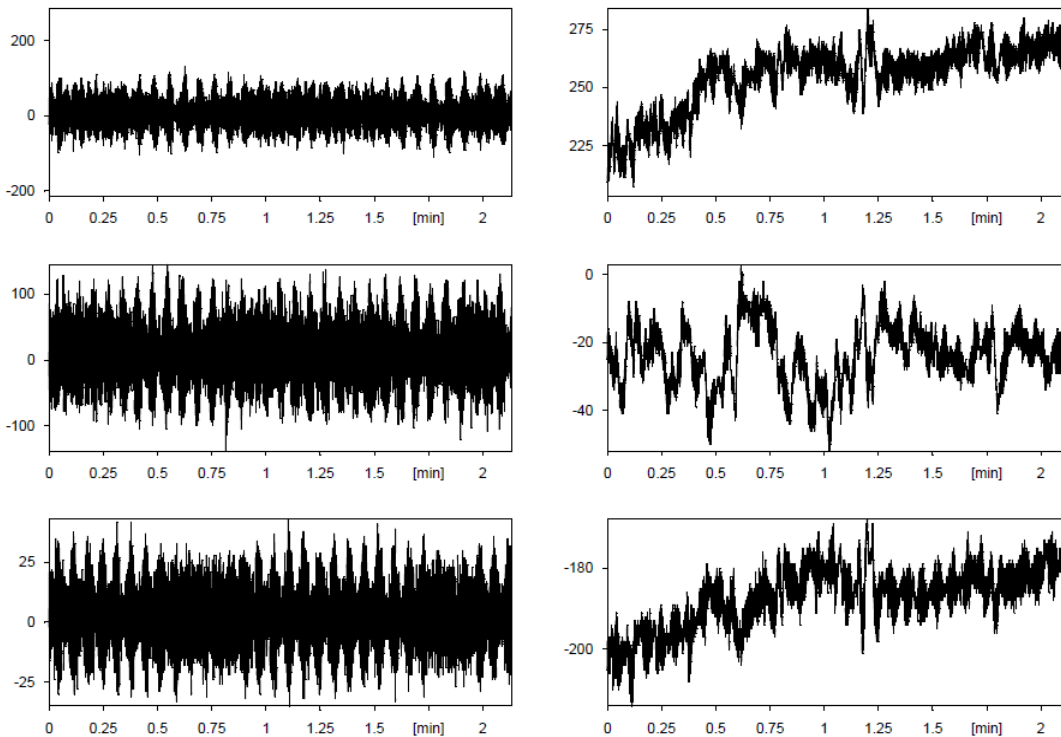
4.2 ADC /DAC Mode results (Cal 3)

In Cal Mode 3 the magnetometer is operating in standard (close loop) mode, however ADC and DAC values are transmitted separately. This mode is used for checking the feedback control loop properties.

ADC / DAC data recording starts at 7014-16:55:30.26998

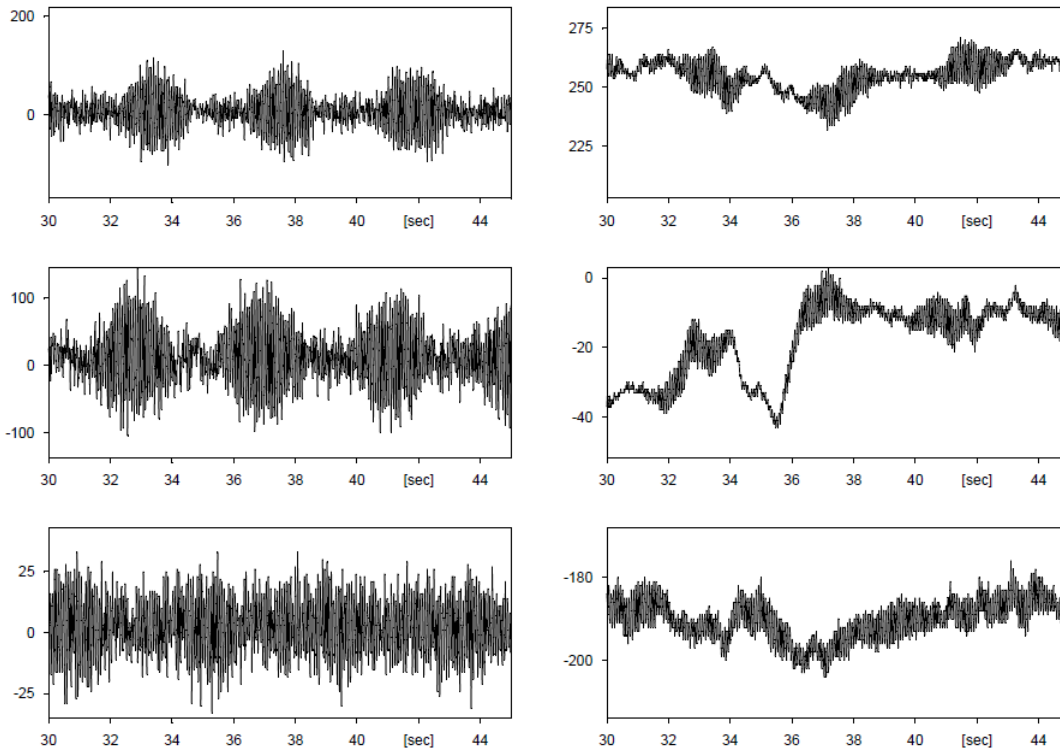
4.2.1 IB

In the following plots ADC counts (left hand side) and DAC counts (right hand side) are plotted. While the DAC values follow the external field, the ADC values are centered about zero.



The plot shows ADC values in LSBs left and DAC values in LSBs right. Upper, middle and lower panels show the components X, Y and Z.

During commissioning MPO MAG works for about 2 minutes in Cal-3 Mode. Because ADC and DAC values are transmitted sequentially the sampling frequency was only half of the maximum sampling rate of 128Hz. All sampled data are shown in the upper plot. In the following plot a period of 15 second is extracted.



The plot shows ADC values in LSBs left and DAC values in LSBs right. Upper, middle and lower panels show the components X, Y and Z.

For comparing the magnitudes of ADC and DAC both shall be scaled in nT.

Scaling of LSB ADC:

The ADC output is scaled in order to meet a 2048nT range by 24bit. This results in a resolution of 0.244pT/LSB. However data are transmitted with 16bit only. The extraction of 16 from 24bit is done by „ranging“. In 2048nT the upper 16bits are transmitted, in 8nT range the lower 16bits are transmitted. The resolution changes accordingly between 62,5pT/LSB and 0,244pT/LSB. During commissioning Cal Mode 3 is commanded into 128nT range mode. Its resolution is 3,906pT/LSB.

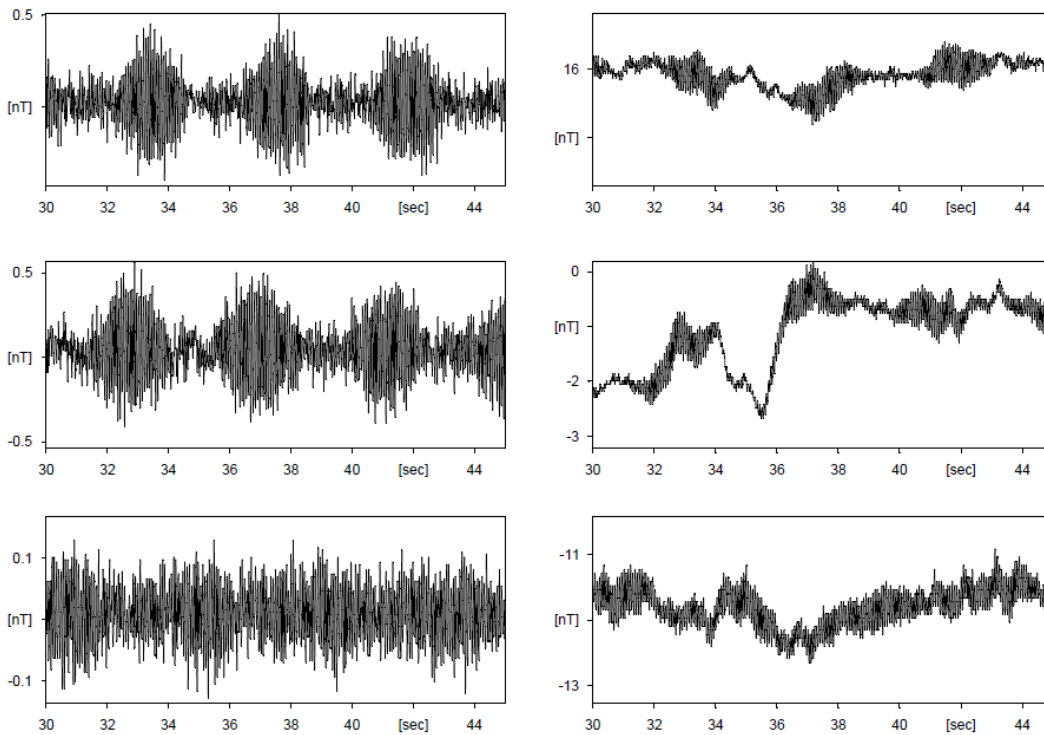
Scaling of LSB DAC

The scale value of DAC steps is independent on ranging. It depends on current per commanded DAC step and the coil constants of the Helmholtz system. It is adjusted by hardware to about 62pT/LSB for the feedback DAC and 156pT/LSB for the compensation DAC. Fine adjustment is done by K2 and K3 values.

Details can be found:

For IB: MPO_MerMag_FM1_S10_StartupProcedure.xls

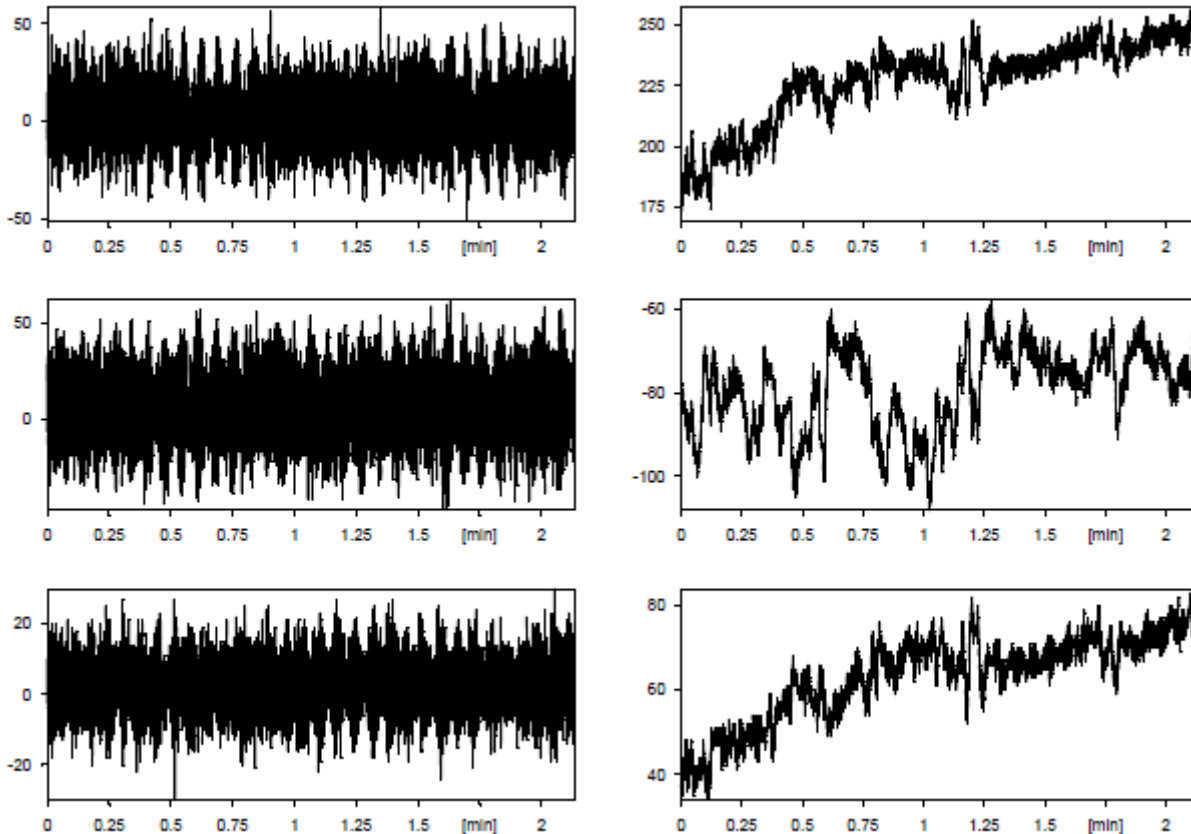
In the following plot the scaled ADC and DAC values are plotted. ADC values and feedback related signatures in the DAC values (if any) shall be in the same order of magnitude because a ADC measurement shall be acknowledged by a field with the same magnitude with opposite sign.



The plot shows ADC values in nT left and DAC values in nT right. Upper, middle and lower panels show the components X, Y and Z.

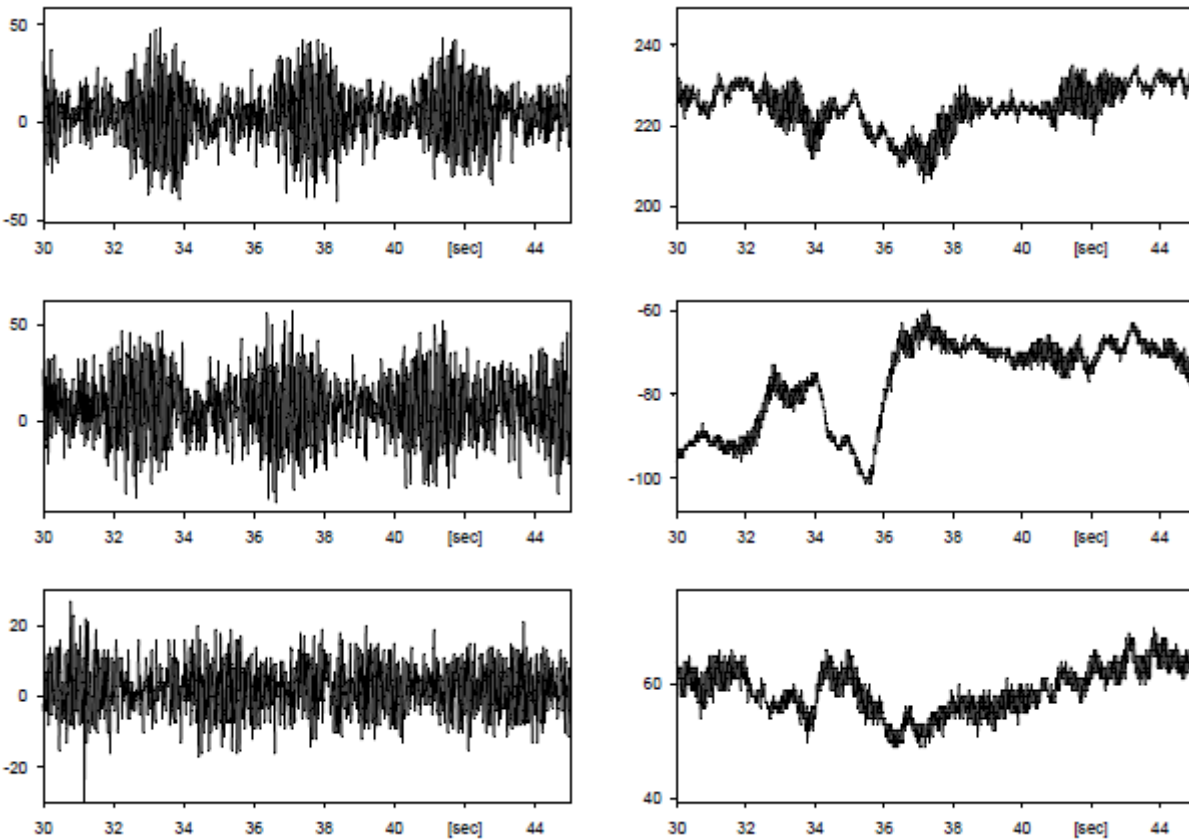
4.2.2 OB

In the following plots ADC counts (left hand side) and DAC counts (right hand side) are plotted. While the DAC values follow the external field, the ADC values are centered about zero.



The plot shows ADC values in LSBs left and DAC values in LSBs right. Upper, middle and lower panels show the components X, Y and Z.

During commissioning MPO MAG works for about 2 minutes in Cal-3 Mode. Because ADC and DAC values are transmitted sequentially the sampling frequency was only half of the maximum sampling rate of 128Hz. All sampled data are shown in the upper plot. In the following plot a period of 15 second is extracted.



The plot shows ADC values in LSBs left and DAC values in LSBs right. Upper, middle and lower panels show the components X, Y and Z.

For comparing the magnitudes of ADC and DAC both shall be scaled in nT.

Scaling of LSB ADC:

The ADC output is scaled in order to meet a 2048nT range by 24bit. This results in a resolution of 0.244pT/LSB. However data are transmitted with 16bit only. The extraction of 16 from 24bit is done by „ranging“. In 2048nT the upper 16bits are transmitted, in 8nT range the lower 16bits are transmitted. The resolution changes accordingly between 62,5pT/LSB and 0,244pT/LSB. During commissioning Cal Mode 3 is commanded into 128nT range mode. It's resolution is 3,906pT/LSB.

Scaling of LSB DAC

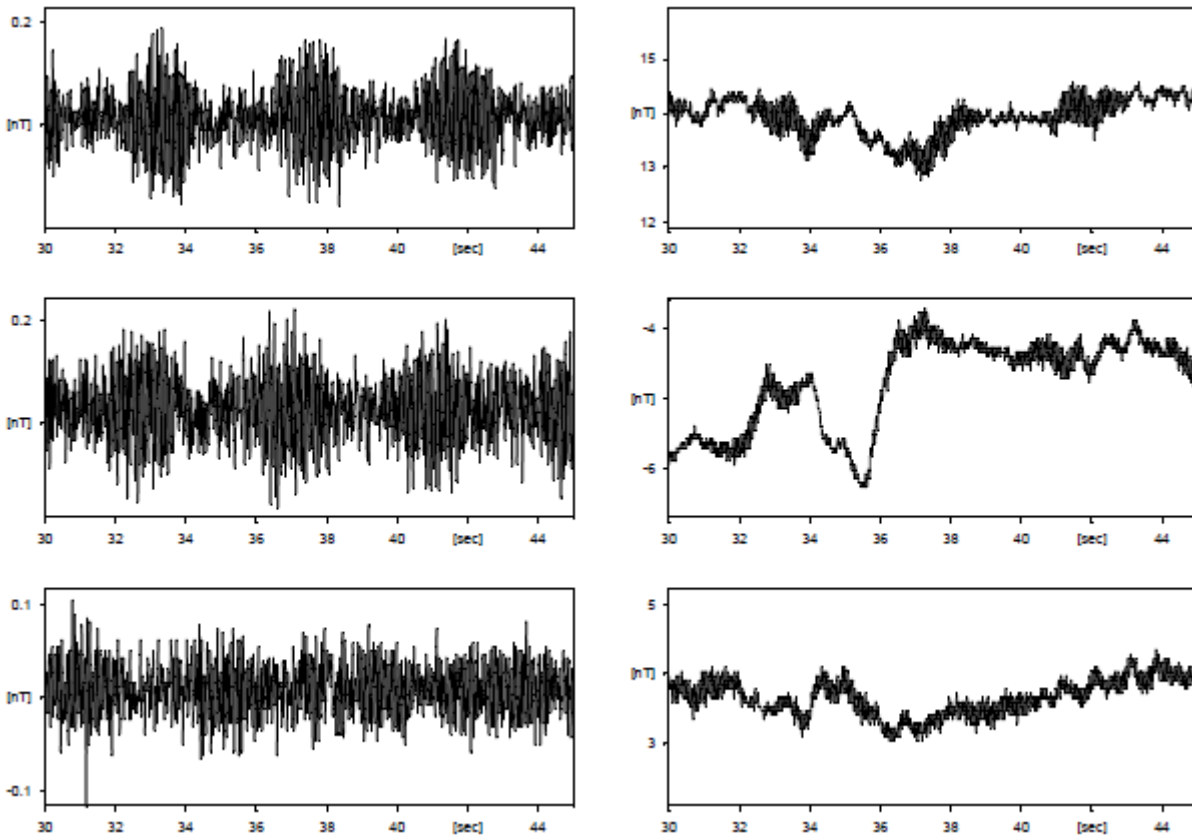
The scale value of DAC steps is independent on ranging. It depends on current per commanded DAC step and the coil constants of the Helmholtz system. It is adjusted by hardware to about 62pT/LSB for the feedback DAC and 156pT/LSB for the compensation DAC. Fine adjustment is done by K2 and K3 values.

Details can be found:

For OB: MPO_MerMag_FM2_S11_StartupProcedure.xls

In the following plot the scaled ADC and DAC values are plotted. ADC values and feedback related signatures in the DAC values (if any) shall be in the same order of magnitude

because a ADC measurement shall be acknowledged by a field with the same magnitude with opposite sign.



The plot shows ADC values in nT left and DAC values in nT right. Upper, middle and lower panels show the components X, Y and Z.

4.2.3 Discussion

ADC values are centered about zero, thus the feedback for cancelation of the field in the inner part of the sensor works well. However, oscillations are visible especially in the X and Y components of IB and OB. The reason is a tiny overcompensation due to a mismatch between K1 and K2 values due to the low sensor temperature and / or a too strong feedback factor. Correction of K1 (see following findphase chapter) and a reduction of the feedback factor should avoid this oscillation of the feedback system. Test using the QM shall be done for verification.

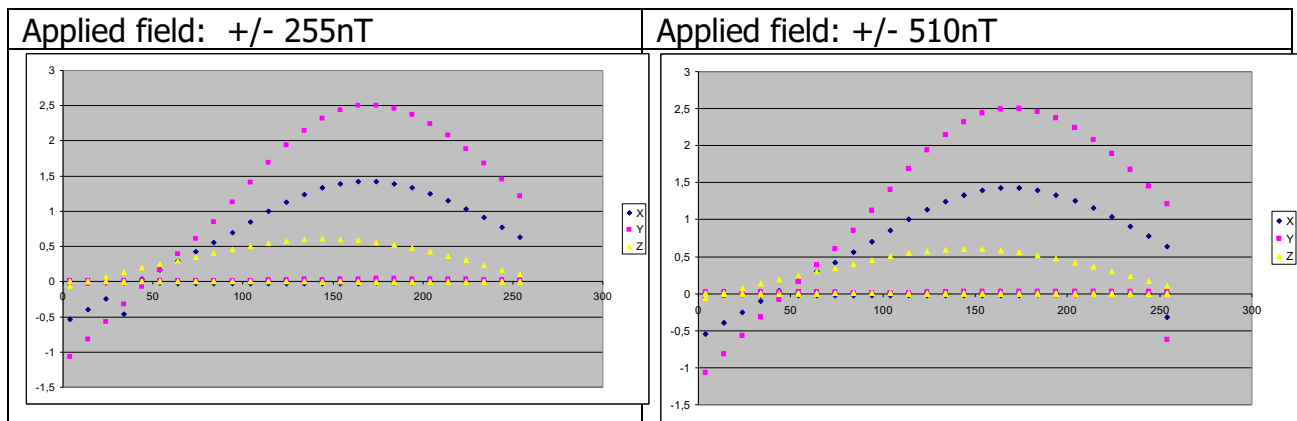
4.3 Find phase results (Cal 7)

Findphase is a calibration sequence (calibration mode 7) in which the phase shift between excitation current and the field sensitive second harmonics of the excitation frequency can be measured. If this phase shift is known, it can be adjusted by shifting the sampling time of the ADC. Furthermore the sensitivity of the ADC (pT/LSB) can be determined for various phases.

The magnetometer measures in open loop while a test field is generated by the feedback system. In this configuration the ADC sampling time is shift by selectable steps vs excitation. The phase is decoded by 0..255 for 0-180° degree of the second harmonics. Findphase has been performed with two different field settings, 255nT and 510nT. Findphase data recording starts at 7014-16:57:40.31615

4.3.1 IB

In the following plot the measurement results are shown:



The plot shows the sensitivity of the ADC in pT/(2 LSB) in 2048nT range vs phase shift between excitation clock and ADC sampling time. The phase settings are incremented by 10 counts from 4 to 254.

Results are summarized for different phases in the following tables:

Phase 168;170;146 (currently optimum)

LSB-ADC / LSB-DAC measured with +/-4096 LSB-DAC
LSB-ADC / LSB-DAC measured with +/-8192 LSB-DAC
Averaged Result
Field [pT] / LSB-DAC (see startup)
Field [pT] / LSB-ADC in 2048nT range
Field [pT] / LSB-ADC in 8nT range
K1 (sensitivity ADC in processor units, see startup)

	X	Y	Z
LSB-ADC / LSB-DAC measured with +/-4096 LSB-DAC	0,7128	1,2515	0,3021
LSB-ADC / LSB-DAC measured with +/-8192 LSB-DAC	0,7141	1,2501	0,3021
Averaged Result	0,7134	1,2508	0,3021
Field [pT] / LSB-DAC (see startup)	62,49	61,77	62,96
Field [pT] / LSB-ADC in 2048nT range	87,59	49,38	208,43
Field [pT] / LSB-ADC in 8nT range	0,3422	0,1929	0,8142
K1 (sensitivity ADC in processor units, see startup)	22962	12945	54639

The optimum phases during startup were X: 162; Y: 161; Z: 153

Phase 159 (nominal, see startup)

	X	Y	Z
LSB-ADC / LSB-DAC measured with +/-4096 LSB-DAC	0,7043	1,2330	0,2971
LSB-ADC / LSB-DAC measured with +/-8192 LSB-DAC	0,7062	1,2316	0,2972
Averaged Result	0,7053	1,2323	0,2971
Field [pT] / LSB-DAC (see startup)	62,49	61,77	62,96
Field [pT] / LSB-ADC in 2048nT range	88,60	50,12	211,89
Field [pT] / LSB-ADC in 8nT range	0,3461	0,1958	0,8277
K1 (sensitivity ADC in processor units, see startup))	23227	13139	55545

Phase 146 (currently applied)

	X	Y	Z
LSB-ADC / LSB-DAC measured with +/-4096 LSB-DAC	0,6714	1,1705	0,3021
LSB-ADC / LSB-DAC measured with +/-8192 LSB-DAC	0,6737	1,1692	0,3019
Averaged Result	0,6725	1,1698	0,3020
Field [pT] / LSB-DAC (see startup)	62,49	61,77	62,96
Field [pT] / LSB-ADC in 2048nT range	92,92	52,80	208,50
Field [pT] / LSB-ADC in 8nT range	0,3630	0,2062	0,8144
K1 (sensitivity ADC in processor units, see startup)	24358	13841	54656

In the upper three tables the results (grey filled) are summarized. Using the sensitivity of the feedback DAC circuitry measured during the startup procedure (in blue), the sensitivity of the ADC has been calculated. During commissioning the instrument has been operated in 2048nT range. Thus the upper 16 of 24bit are transmitted. The sensitivity of the lowest ADC bit (in red) has been derived by dividing the transmitted value by 8 bit (256). The K1 value is based on the lowest computation unit defined by the processor arithmetic in the FPGA. It has to be calculated by multiplying the lowest ADC resolution bit by 67109 (details see startup procedure).

Currently the magnetometer works with default values programmed before launch. The Phase was set to 146 (accidentally, nominal was 159) and the K1 values are taken from the setup procedure.

The K1 values commanded onboard (taken from the preflight startup procedure) are the following:

	X	Y	Z
Field [pT] / LSB-ADC in 8nT range	0,3714	0,2135	0,8360
K1 (sensitivity ADC in processor units, see startup)	24927	14331	56105

The error, ratio between commanded K1 and currently needed K1 value (for the commanded phase 146) is about 3% (see table below). Assuming a maximum deviation of 100 LSB ADC in close loop mode (control deviation) the maximum error is 2pT.

	X	Y	Z
Ratio between commanded K1 and needed K1 (for phase 146)	1,023	1,035	1,027
Error in pT for 100LSB ADC close loop deviation	0,80	0,68	2,16

In a new setup we have to taken into account, that only one phase can be set for all components. The averaged value of the optimum phases (168, 170, 146) is 159, identical to the nominal phase derived from the preflight tests. In case we adjust the phase only, the errors are as follow:

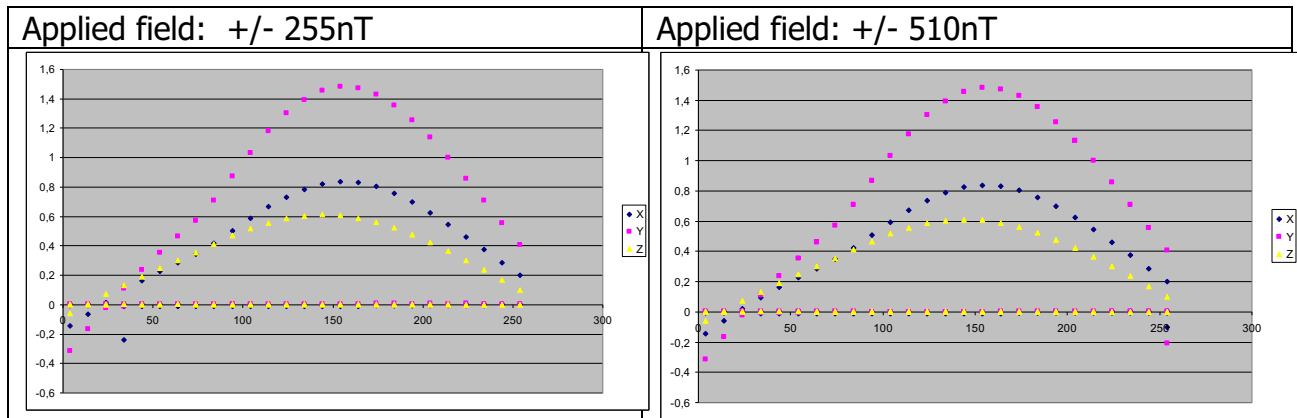
	X	Y	Z
Ratio between commanded K1 and needed K1 (for phase 159)	1,073	1,091	1,010
Error in pT for 100LSB ADC close loop deviation	2,50	1,75	0,82

The optimum settings under the current temperature conditions are:

Phase: 159
K1 X 23227
K1 Y 13139
K1 Z 55545

4.3.2 OB

In the following plot the measurement results are shown:



The plot shows the sensitivity of the ADC in pT/(2 LSB) in 2048nT range vs phase shift between excitation clock and ADC sampling time. The phase settings are incremented by 10 counts from 4 to 254.

Results are summarized for different phases in the following tables:

Phase 158;157;145 (currently optimum)

LSB-ADC / LSB-DAC measured with +/-4096 LSB-DAC
LSB-ADC / LSB-DAC measured with +/-8192 LSB-DAC
Averaged Result
Field [pT] / LSB-DAC (see startup)
Field [pT] / LSB-ADC in 2048nT range
Field [pT] / LSB-ADC in 8nT range
K1 (sensitivity ADC in processor units, see startup)

	X	Y	Z
LSB-ADC / LSB-DAC measured with +/-4096 LSB-DAC	0,4181	0,7415	0,3062
LSB-ADC / LSB-DAC measured with +/-8192 LSB-DAC	0,4194	0,7407	0,3056
Averaged Result	0,4187	0,7411	0,3059
Field [pT] / LSB-DAC (see startup)	62,48	61,76	62,92
Field [pT] / LSB-ADC in 2048nT range	149,20	83,34	205,69
Field [pT] / LSB-ADC in 8nT range	0,5828	0,3255	0,8035
K1 (sensitivity ADC in processor units, see startup)	39113	21846	53920

The optimum phases during startup were X: 162; Y: 161; Z: 153

Phase 159 (nominal)	X	Y	Z
LSB-ADC / LSB-DAC measured with +/-4096 LSB-DAC	0,4165	0,7390	0,2980
LSB-ADC / LSB-DAC measured with +/-8192 LSB-DAC	0,4180	0,7385	0,2985
Averaged Result	0,4173	0,7388	0,2983
Field [pT] / LSB-DAC (see startup)	62,48	61,76	62,92
Field [pT] / LSB-ADC in 2048nT range	149,73	83,60	210,95
Field [pT] / LSB-ADC in 8nT range	0,5849	0,3265	0,8240
K1 (sensitivity ADC in processor units, see startup))	39252	21914	55299

Phase 146 (currently applied)	X	Y	Z
LSB-ADC / LSB-DAC measured with +/-4096 LSB-DAC	0,4100	0,7300	0,3062
LSB-ADC / LSB-DAC measured with +/-8192 LSB-DAC	0,4125	0,7300	0,3056
Averaged Result	0,4113	0,7300	0,3059
Field [pT] / LSB-DAC (see startup)	62,48	61,76	62,92
Field [pT] / LSB-ADC in 2048nT range	151,92	84,60	205,69
Field [pT] / LSB-ADC in 8nT range	0,5934	0,3305	0,8035
K1 (sensitivity ADC in processor units, see startup)	39825	22177	53920

In the upper three tables the results (grey filled) are summarized. Using the sensitivity of the feedback DAC circuitry measured during the startup procedure (in blue), the sensitivity of the ADC has been calculated. During commissioning the instrument has been operated in 2048nT range. Thus the upper 16 of 24bit are transmitted. The sensitivity of the lowest ADC bit (in red) has been derived by dividing the transmitted value by 8 bit (256). The K1 value is based on the lowest computation unit defined by the processor arithmetic in the FPGA. It has to be calculated by multiplying the lowest ADC resolution bit by 67109 (details see startup procedure).

Currently the magnetometer works with default values programmed before launch. The Phase was set to 146 (accidently, nominal was 159) and the K1 values are taken from the setup procedure.

The K1 values commanded onboard (taken from the preflight startup procedure) are the following:

	X	Y	Z
Field [pT] / LSB-ADC in 8nT range	0,60204	0,33782	0,83337
K1 (sensitivity ADC in processor units, see startup)	40402	22671	55926

The error, ratio between commanded K1 and currently needed K1 value (for the commanded phase 146) is about 3% (see table below). Assuming a maximum deviation of 100 LSB ADC in close loop mode (control deviation) the maximum error is 2pT.

	X	Y	Z
Ratio between commanded K1 and needed K1 (for phase 146)	1,015	1,022	1,037
Error in pT for 100LSB ADC close loop deviation	0,85	0,73	2,99

In case that only the phase is changed to the nominal value 159 and the K1 values remains unchanged, the following error has to be taken into account:

	X	Y	Z
Ratio between commanded K1 and needed K1 (for phase 159)	1,029	1,035	1,011
Error in pT for 100LSB ADC close loop deviation	1,71	1,12	0,91

In a new setup we have to taken into account, that only one phase can be set for all components. The averaged value of the optimum phases (158, 157, 145) is 154. This leads to the following settings:

Phase 154 (currently optimum)	X	Y	Z
LSB-ADC / LSB-DAC measured with +/-4096 LSB-DAC	0,4181	0,7415	0,3035
LSB-ADC / LSB-DAC measured with +/-8192 LSB-DAC	0,4194	0,7407	0,3039
Averaged Result	0,4187	0,7411	0,3037
Field [pT] / LSB-DAC (see startup)	62,48	61,76	62,92
Field [pT] / LSB-ADC in 2048nT range	149,20	83,34	207,18
Field [pT] / LSB-ADC in 8nT range	0,5828	0,3255	0,8093
K1 (sensitivity ADC in processor units, see startup)	39113	21846	54311

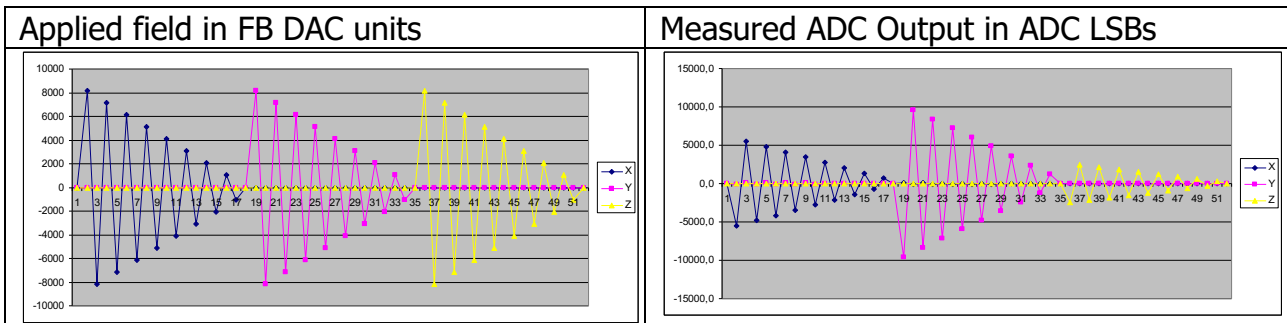
The optimum settings under the current temperature conditions are:

Phase: 154
K1 X 39113
K1 Y 21846
K1 Z 54311

4.4 Meander results (Cal 5)

In the Calibration Mode 5 – Meander – the magnetometer is working in open loop and a meander like field is generated by the feedback system sequentially for the three components. This mode allows the determination of the ADC sensitivity and its linearity. Furthermore, the orientation of the pick-up coils which are perpendicular to the stimulating field axis versus the active feedback coil can be derived. Meander data recording starts at 7014-17:06:44.14242

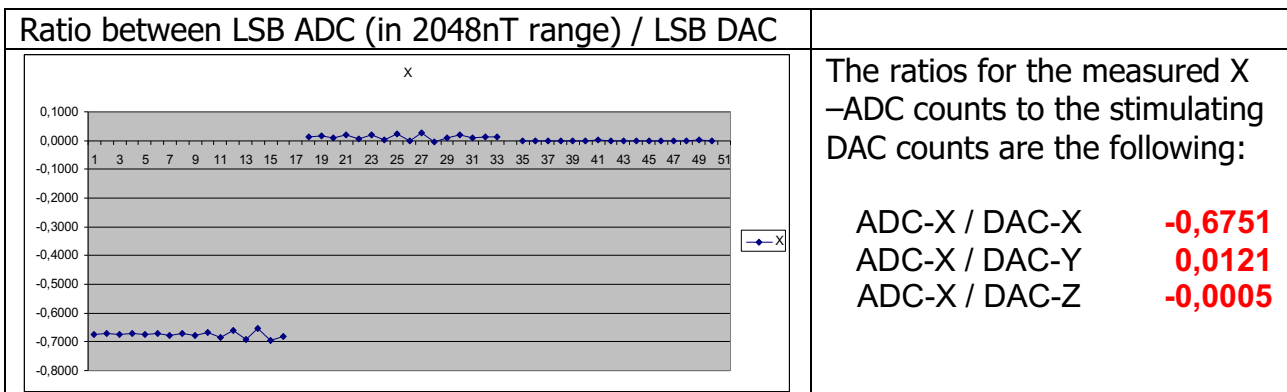
4.4.1 IB

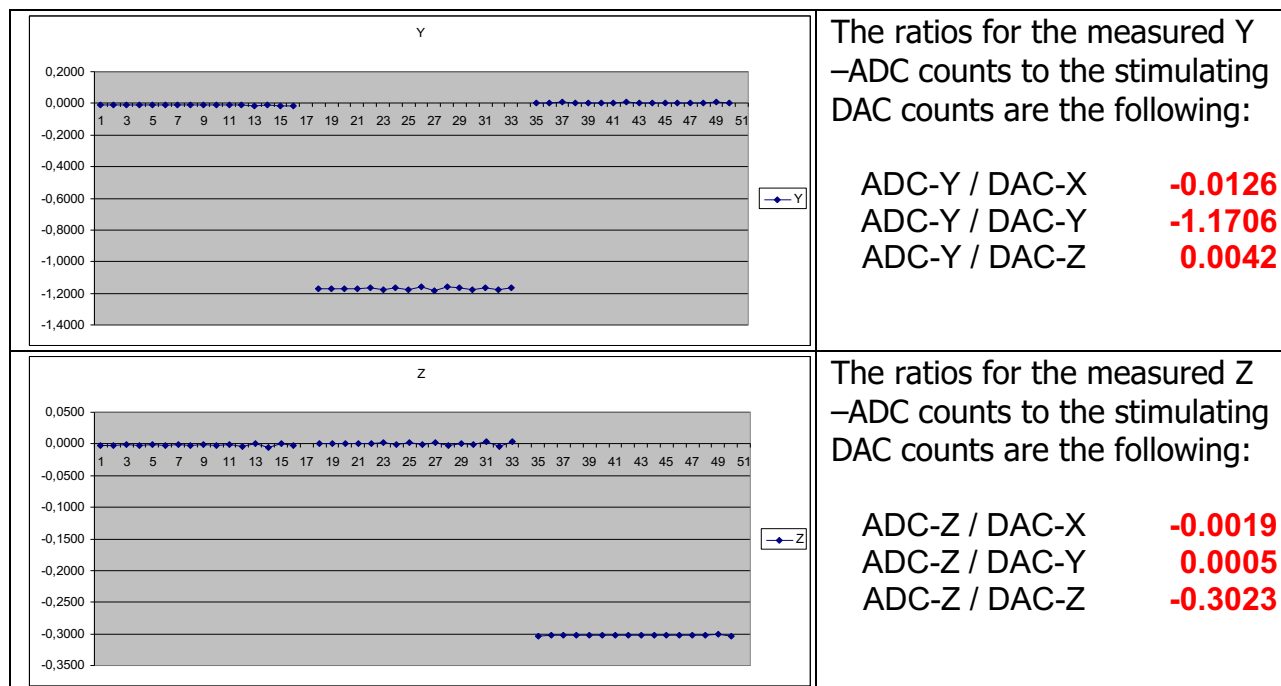


Stimulating FB field and field acquired by the ADC (both in LSB's)

On the left hand side the stimulating field in FB-DAC units is plotted versus measurement steps. The colors indicate the three components. On the right hand side, the response of the ADC is plotted. Also here the colors stand for the three components. In contrast the stimulating field, small variations of the non stimulated components are visible due to the non perfect alignment of pick-up coils and feedback coils.

In the following plots the ratio between ADC response and exciting field is plotted and calculated for each component separately.





Results of the Meander Test Sequence

The field step generates by a feedback coil induces signals in the aligned pickup coil. The feedback coil constant is known, thus the ADC sensitivity and its linearity can be derived;

From the ratio between ADC counts and DAC counts the sensitivity can be calculated:

Meander Results (currently applied phase is 146)

	X	Y	Z
LSB-ADC / LSB-DAC measured	-0,6751	-1,1706	-0,3023
Field [pT] / LSB-DAC (see startup)	62,49	61,77	62,96
Field [pT] / LSB-ADC in 2048nT range	-92,56	-52,76	-208,26
Field [pT] / LSB-ADC in 8nT range	-0,3616	-0,2061	-0,8135
K1 (sensitivity ADC in processor units, see startup)	24264	13832	54595

Findphase Results for Phase 146

Field [pT] / LSB-ADC in 8nT range	0,3630	0,2062	0,8143
K1 (sensitivity ADC in processor units, see startup)	24359	13839	54650

Error

Ratio between Meander and Findphase results	-0,9961	-0,9995	-0,9990
Deviation	0,0039	0,0005	0,0010

The error is in all components less than 0,4%, thus both measurements are consistent.

The field step generates by a feedback coil induces signals in the perpendicular pickup coils. This cross coupling represents the misalignment of feedback and sense coils.

From the ratios of LSB-ADC / LSB DAC (see results meander) and the DAC sensitivity (see blue numbers above) the field measured by the pick up coil can be calculated:

	Bx [pT]	By [pT]	Bz [pT]
LSB DACx	62,49	0,67	0,40
LSB DACy	-1,12	61,77	-0,11
LSB DACz	0,05	-0,22	62,96

Fields measured per DAC step

The cross coupling leads to the following angles of misalignment:

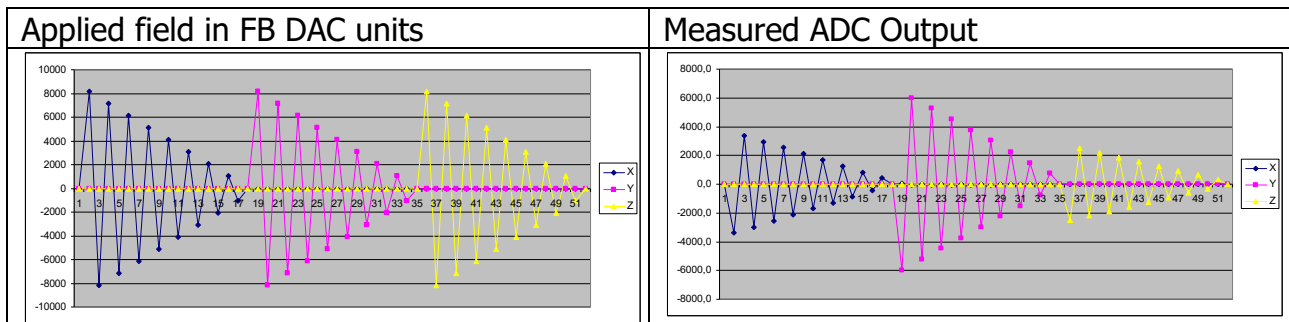
	Sense X	Sense Y	Sense Z
FB x	-	0,61	0,37
FB y	-1,04	-	-0,10
FB z	0,04	-0,20	-

Misalignment between FB coils and sense coils in degree

The misalignment is due to the vector compensation of less importance, however it should be constant of the mission time.

4.4.2 OB

Commissioning Results:

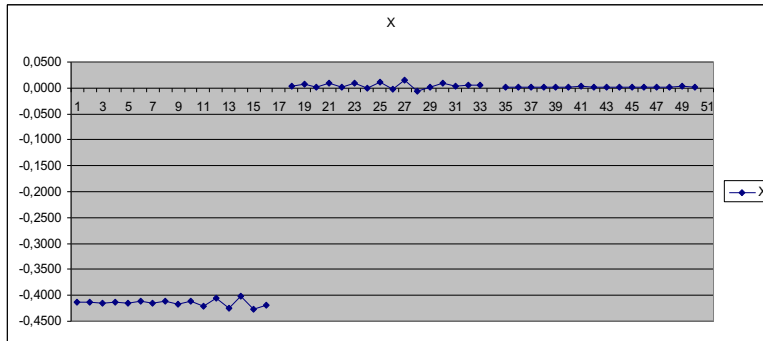


Stimulating FB field and field acquired by the ADC (both in LSB's)

On the left hand side the stimulating field in FB-DAC units is plotted versus measurement steps. The colors indicate the three components. On the right hand side the response of the ADC is plotted. Also here the colors stand for the three components. In contrast the stimulating field, small variations of the non stimulated components are visible due to the non perfect alignment of pick-up coils and feedback coils.

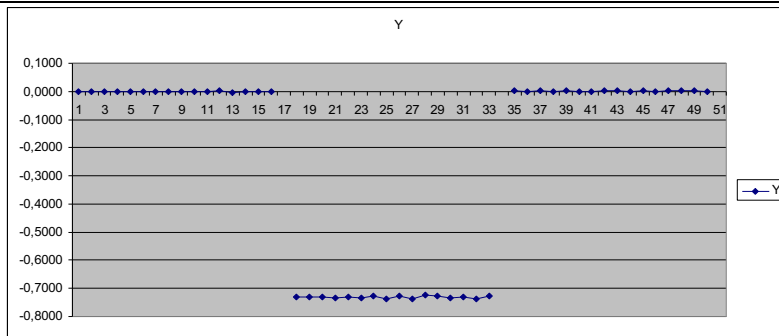
In the following plots the ratio between ADC response and exciting field is plotted and calculated for each component separately.

Ratio between LSB ADC (in 2048nT range) / LSB DAC



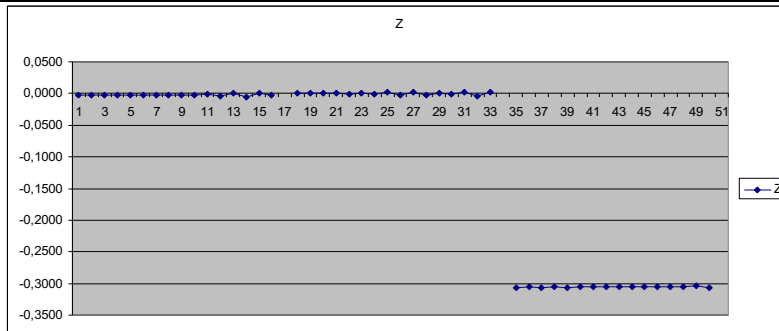
The ratios for the measured X –ADC counts to the stimulating DAC counts are the following:

ADC-X / DAC-X **-0,4146**
ADC-X / DAC-Y **0,0046**
ADC-X / DAC-Z **0,0017**



The ratios for the measured Y –ADC counts to the stimulating DAC counts are the following:

ADC-Y / DAC-X **-0,0008**
ADC-Y / DAC-Y **-0,7313**
ADC-Y / DAC-Z **0,0012**



The ratios for the measured Z –ADC counts to the stimulating DAC counts are the following:

ADC-Z / DAC-X **-0,0023**
ADC-Z / DAC-Y **0,0000**
ADC-Z / DAC-Z **-0,3057**

Results of the Meander Test Sequence

The field step generates by a feedback coil induces signals in the aligned pickup coil. The feedback coil constant is known, thus the ADC sensitivity and its linearity can be derived;

From the ratio between ADC counts and DAC counts the sensitivity can be calculated:

	X	Y	Z
Meander Results (currently applied phase is 146)			
LSB-ADC / LSB-DAC measured	-0,4146	-0,7313	-0,3057
Field [pT] / LSB-DAC (see startup)	62,49	61,77	62,96
Field [pT] / LSB-ADC in 2048nT range	-150,72	-84,46	-205,98
Field [pT] / LSB-ADC in 8nT range	-0,5887	-0,3299	-0,8046
K1 (sensitivity ADC in processor units, see startup)	-39510	-22141	-53997
Findphase Results for Phase 146			
Field [pT] / LSB-ADC in 8nT range	0,59379	0,33046	0,80315
K1 (sensitivity ADC in processor units, see startup)	39849	22177	53899
Error			
Ratio between Meander and Findphase results	-0,9915	-0,9984	-1,0018
Deviation	0,0085	0,0016	-0,0018

The error is in all components less than 0,9%, thus both measurements are consistent.

The field step generates by a feedback coil induces signals in the perpendicular pickup coils. This cross coupling represents the misalignment of feedback and sense coils.

From the ratios of LSB-ADC / LSB DAC (see results meander) and the DAC sensitivity (see blue numbers above) the field measured by the pick-up coil can be calculated:

	Bx [pT]	By [pT]	Bz [pT]
LSB DACx	62,476	0,070	0,481
LSB DACy	-0,698	61,756	-0,005
LSB DACz	-0,251	-0,103	62,915

Fields measured per DAC step

The cross coupling leads to the following angles of misalignment:

	Sense X	Sense Y	Sense Z
FB x	-	0,06	0,44
FB y	-0,65	-	0,00
FB z	-0,23	-0,09	-

Misalignment between FB coils and sense coils in degree

The misalignment is due to the vector compensation of less importance, however it should be constant of the mission time.

4.5 Step Function Results (Cal 1)

Step function data recording starts at 7014-17:12:59.28090

Unfortunately, the function has been commanded by too large steps. Thus, the data are partly saturated. The results obtained so far indicate no problems at the instrument. For completeness, this sub-test may be repeated with smaller steps in a non-interactive manner in the cruise-phase.

4.6 Counter results (Cal 2)

Counter data recording starts at 7014-17:20:02.28630

The counter function has been commanded in 2048nT. Thus only the upper 16 of 24 bits are transmitted. The intention was to check telemetry by increment in a counter. For that the lower bits are needed. The data obtained so far indicate no problem with the telemetry. Thus, for completeness, this sub-test may be repeated with the correct range in a non-interactive manner in the cruise-phase.

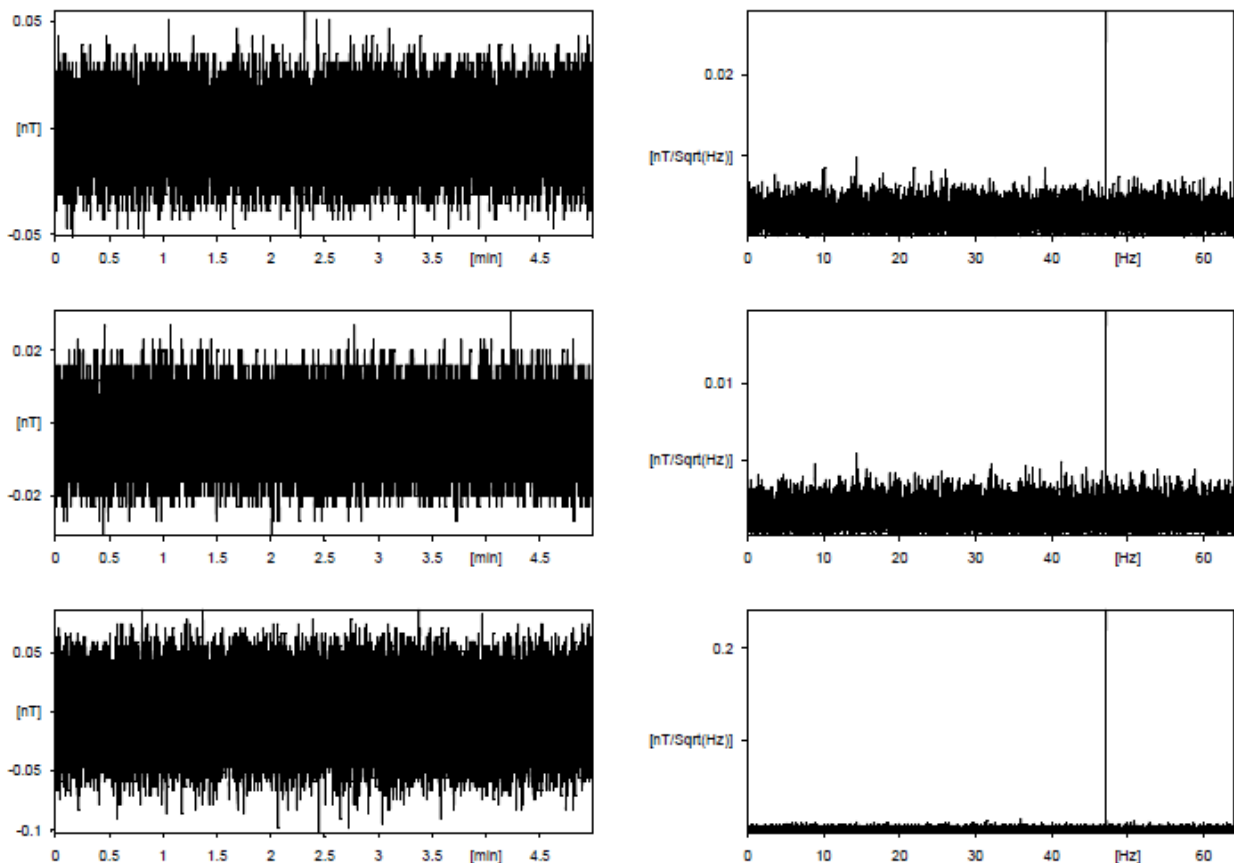
4.7 ADC noise test

The magnetometer is commanded in open loop and the excitation clock is switched off. Thus the fluxgate sensor is a passive coil system, however the ADC is working nominal. This allows to check out the noise of the ADC circuitry which should in the ideal case less than the noise of the sensor itself.

Excitation off data recording starts at 7014-16:48:04.25433

4.7.1 IB

Time series and FFT are plotted below:



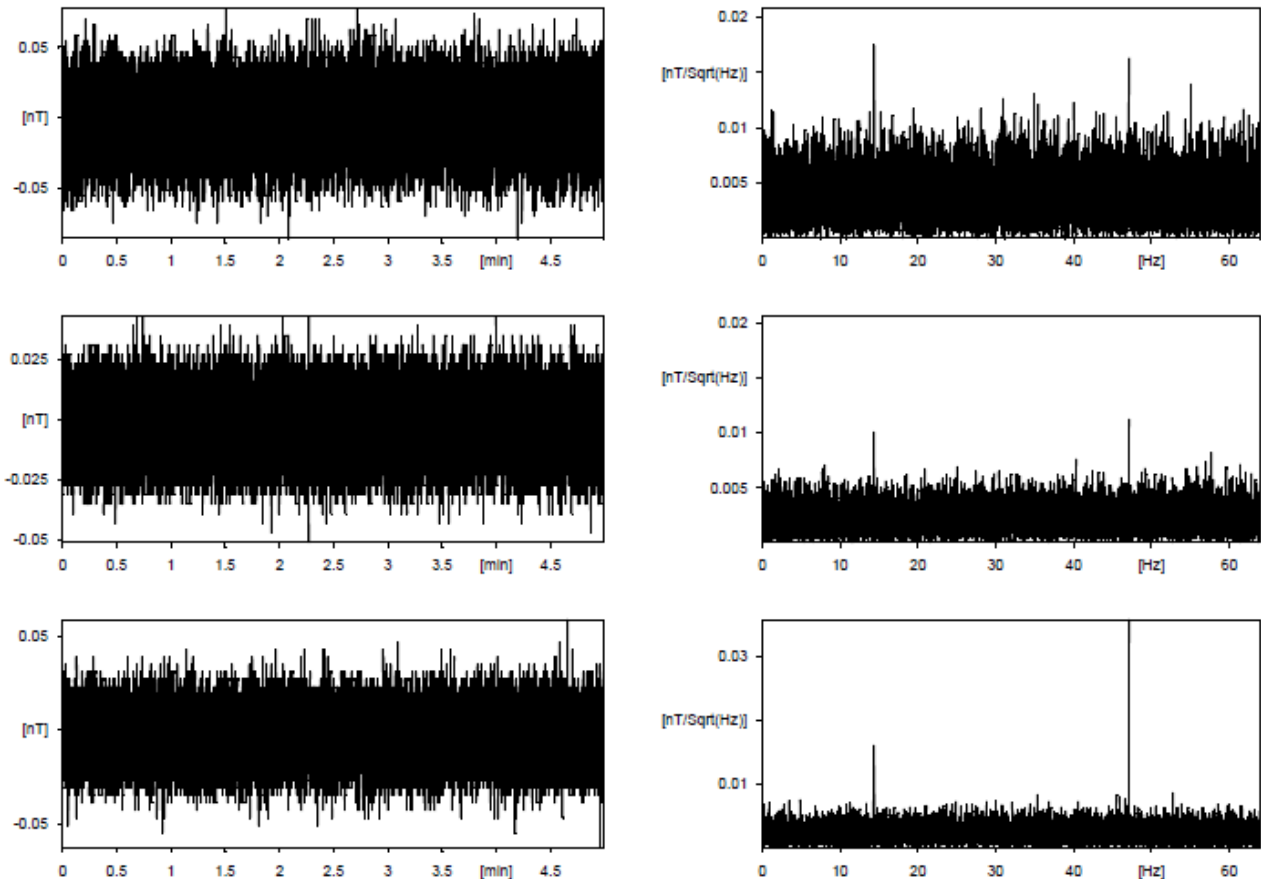
The noise is white (in contrast to the 1/f behavior of the sensor noise) and at the following levels:

X	2.5 pT/Sqrt(Hz)
Y	1.4 pT/Sqrt(Hz)
Z	3.4 pT/Sqrt(Hz)

The noise level is below the noise level of the fluxgate sensor. Thus the ADC sampling doesn't contribute to the overall noise. Interferences are visible at 47,24Hz.

4.7.2 OB

Time series and FFT are plotted below:



The noise is white (in contrast to the 1/f behavior of the sensor noise) and at the following levels:

X	3.9 pT/Sqrt(Hz)
Y	2.2 pT/Sqrt(Hz)
Z	2.3 pT/Sqrt(Hz)

The noise level is below the noise level of the fluxgate sensor. Thus the ADC sampling doesn't contribute to the overall noise. Interferences are visible at 14.45 and 47.24Hz. The amplitude of the 47Hz interference is lower as the interference at IB

4.8 Rate Test

On 4/11/2018 a rate test was performed. For this purpose, the instrument was set in every possible sampling rate. For comparison the various field amplitude spectra were computed and are compared here. The data has been pre-calibrated against ground calibration before

entering the spectral analysis. For the spectra, a hamming window was used as window function. The data was not de-trended before the spectral analysis. The data was checked for unusual data signatures such as jumps or strong unknown interference.

Instrument Boot: 2018.298.17.27.12. using nominal PSU (LCL B)

Rate Test Start:
2018-11-04T18:44:07

Rate Test End:
2018-11-04T19:29:36

Sampling rate	Start UTC	End UTC
1	2018-11-04T18:44:07	2018-11-04T18:48:39
2	2018-11-04T18:48:39	2018-11-04T18:53:38
3	2018-11-04T18:53:39	2018-11-04T18:58:38
4	2018-11-04T18:58:39	2018-11-04T19:03:38
5	2018-11-04T19:03:39	2018-11-04T19:08:38
6	2018-11-04T19:08:39	2018-11-04T19:13:39
7	2018-11-04T19:13:39	2018-11-04T19:18:39
8	2018-11-04T19:18:39	2018-11-04T19:23:39
9	2018-11-04T19:27:22	2018-11-04T19:29:36

The instrument returned data in all sampling rates with correct time separation (checked by computing the mean time separation between samples).

Figure 1 shows the reaction wheel frequencies for the duration of the rate test. All the frequencies were in the range 700...880 rpm (11.67...14.67 Hz).



Figure 1 : Reaction wheel frequencies vs. time during the time of the rate test.

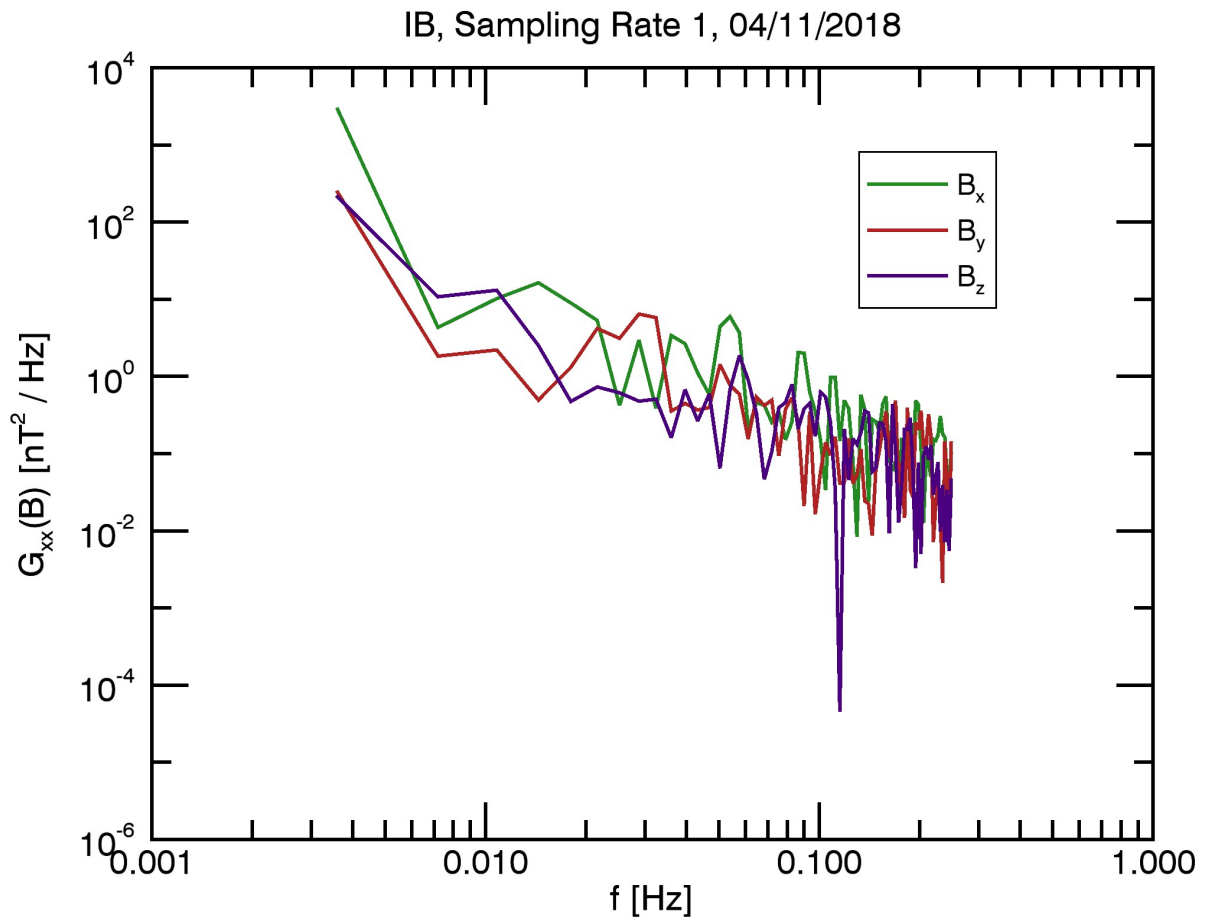


Figure 2 : Amplitude spectrum for the data with a sampling rate of 0.5 Hz

Figure 2 shows the spectrum for the lowest sampling rate. Figure 3 and Figure 4 show the spectra for the two highest sampling rates (64Hz and 128Hz). In all spectras, the spectral value at 0.1 Hz is about 1 nT²/Hz. So, the spectral slopes are expected to be the same for the low frequency range. The PSU probably induces an artificial spectral peak at 8 Hz. The corresponding peak amplitudes may be found in Table 1. It is evident, that this artificial peak is not present in the B_y-component. The spectral power in the B_x and B_z component show different amplitudes depending on the sampling rate but remain in the same order of magnitude.

Figure 5 shows the detail of the spectra for the two highest sampling rates. There, the reaction wheel frequencies are at the same frequencies (only the one at ca. 13 Hz is a bit shifted) and have roughly the same amplitude. There is a sharp peak at 16 Hz that which could be a harmonic of the previously identified 8 Hz peak from the PSU. This remains to be analyzed. It should be noted, that the spectra are flat for frequencies higher than 10 Hz suggesting that the instrument's noise has a flat noise component with an amplitude of 10⁻⁴ nT² / Hz. This refers to an amplitude of the order of 10⁻⁶ nT which is orders of magnitudes below expected scientific signals.

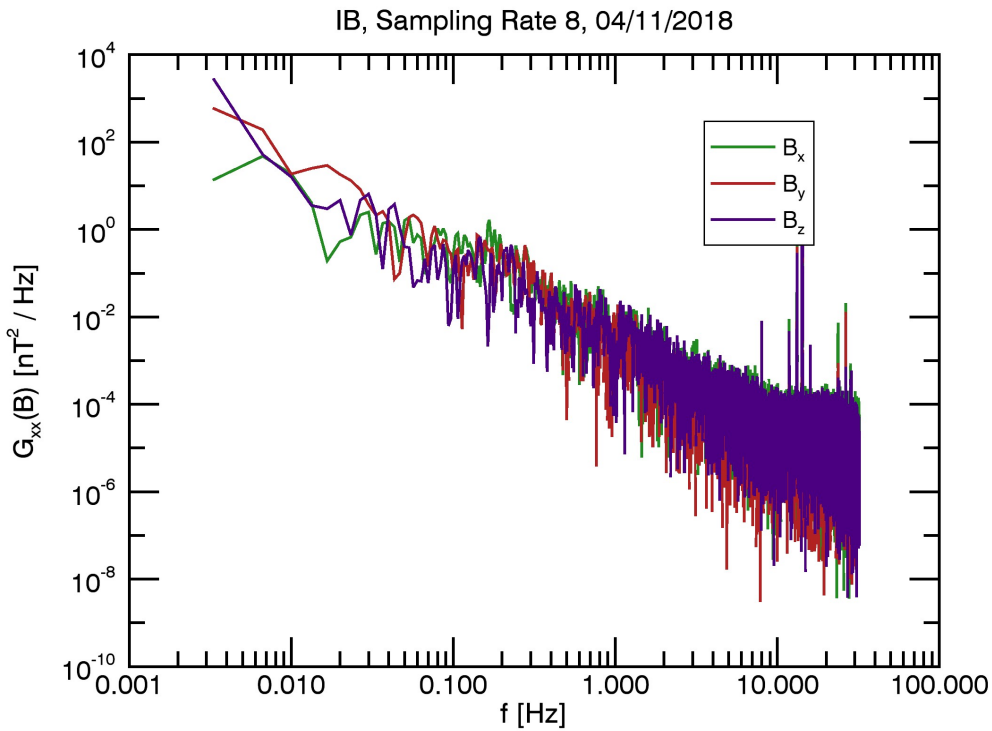


Figure 3 : Amplitude spectrum for magnetic field data recorded at 64Hz.

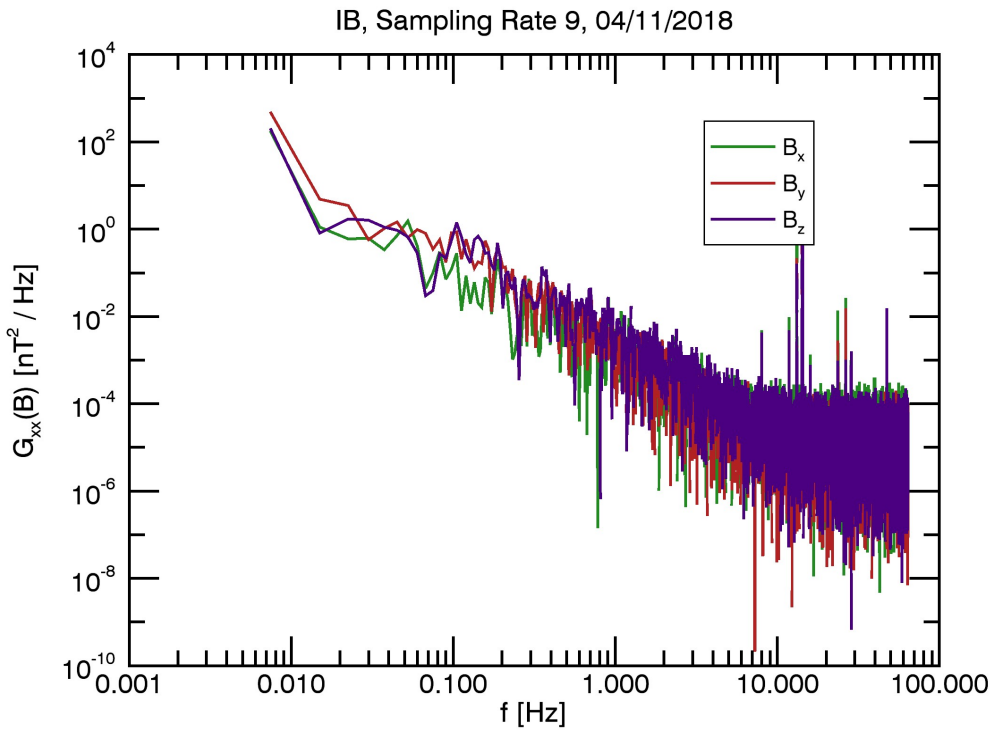


Figure 4 : Amplitude spectrum for magnetic field data recorded at 128 Hz (burst mode).

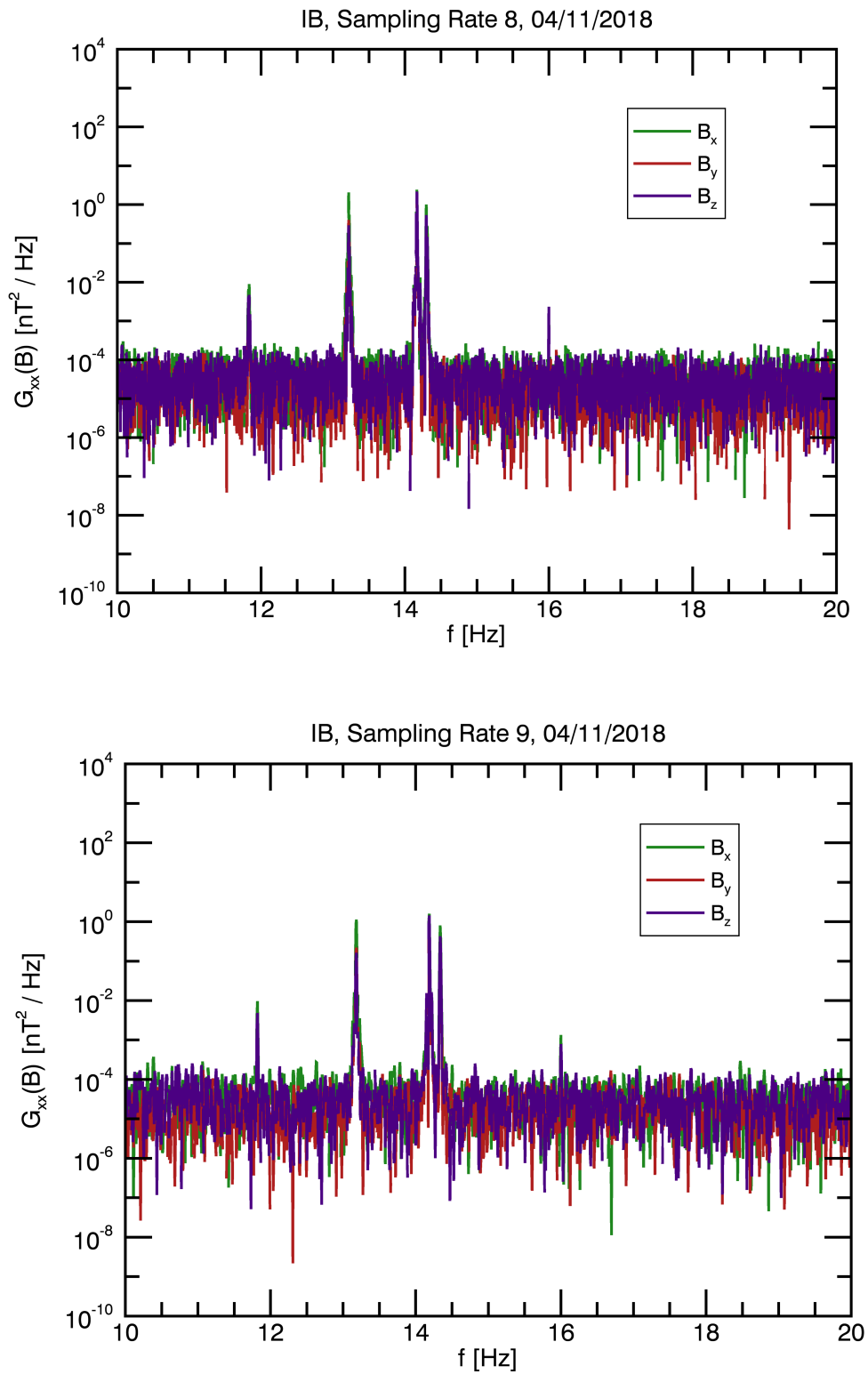


Figure 5 : Detail of the spectra at the highest sampling rates.

Table 1 : Comparison of the 8Hz (PSU-induced?) spektral peak amplitude.

Sampling Rate [Hz]	Gxx,x [nT²/Hz]	Gxx,y [nT²/Hz]	Gxx,z [nT²/Hz]
128	0.00389	0.00010	0.00389
64	0.00790	0.00010	0.00790
32	0.00248	0.00010	0.00248
16	0.00200	0.00010	0.00200

Conclusion of the Rate Test

The instrument provides all data rates and the spectral characteristics show expected behavior.

Results of HK Measurements

4.9 Temperature of Sensor and Electronics

Sensor temperature:

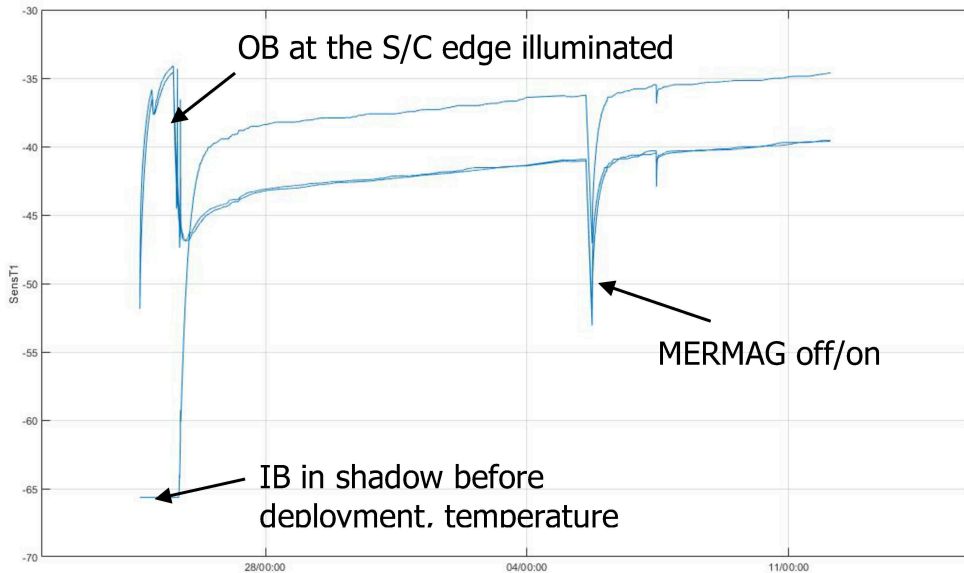
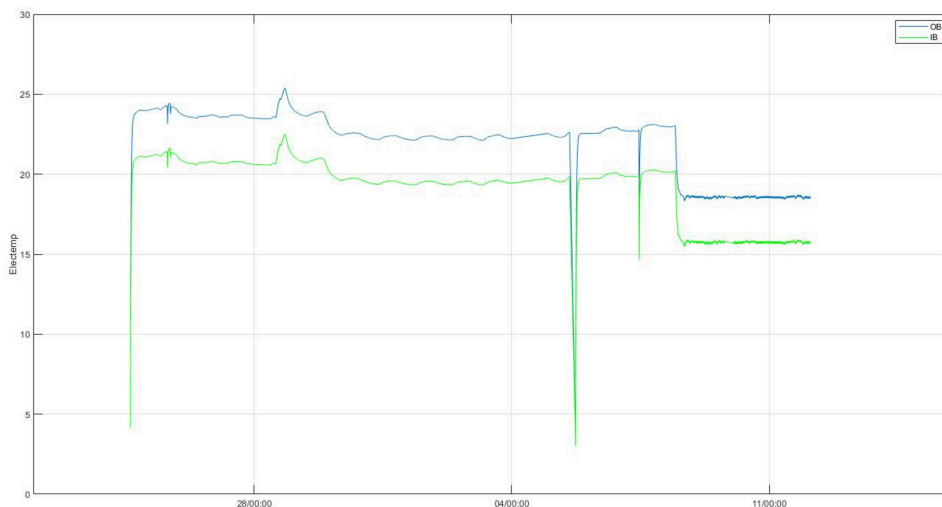


Figure 6 : Sensor temperature vs. time. Time range: 24/10/2018-11/11/2018. The s/c flipping started at 29/10/2018. The s/c is flipped twice per day.

Influence of flipping is not visible, illumination at both position seems to be similar

Electronics temperature:



4.10 Heater operation

Thermal modelling and heater strategy will not be discussed now. Shall be done after Venus flyby because at that time due to different distances of BepiColombo to the Sun more input will be available.

4.11 Voltages / Currents

The instrument voltages and currents are as expected and stable over time. Figure 7 and Figure 8 show the respective time series for one particular day.

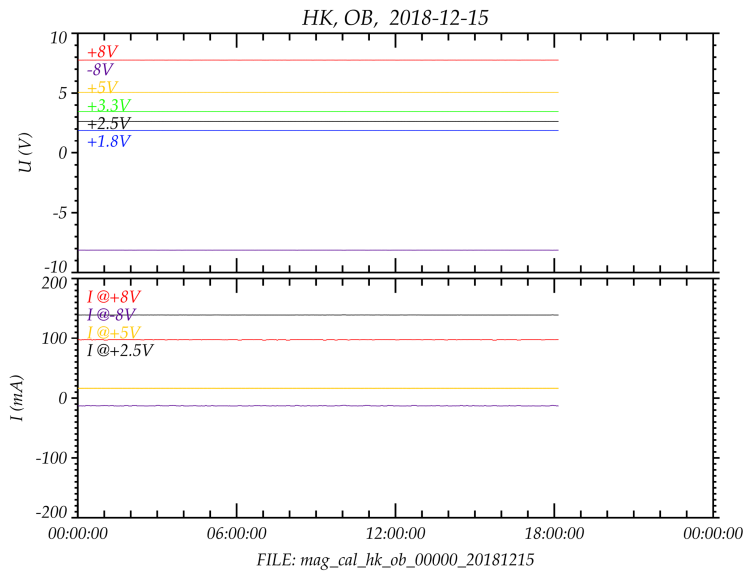


Figure 7 : Voltages and currents of the OB-sensor for 05/12/2018.

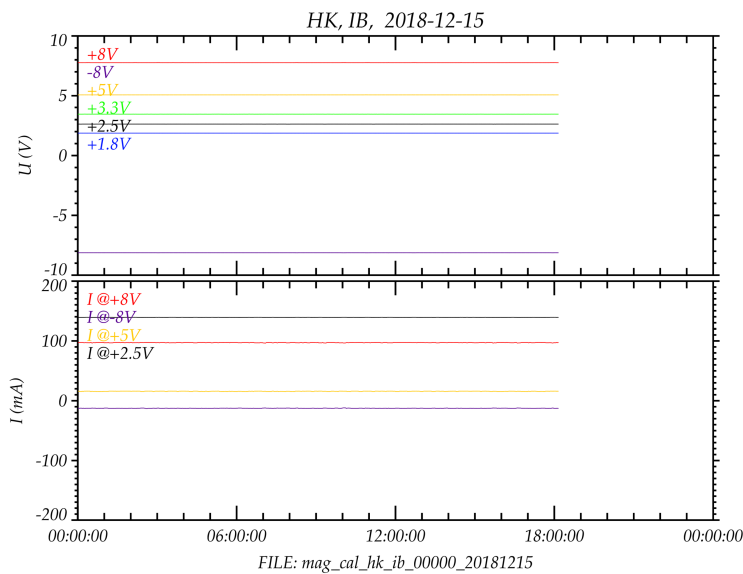


Figure 8 : Voltages and currents of the IB-sensor for 05/12/2018.

5 Results Offset Calibration

The available 1 Hz data intervals are calibrated using the Hedgecock-method, more precisely the Davis-Smith method, which is based on minimization of the variance of the squared magnitude of the magnetic field recorded during free solar wind measurements. The data is not preselected.

A time window of five minutes is shifted over the data and the offset is calculated for each section. If the minimization process is not successful or the calculated offsets exceed some threshold, the result for the corresponding time window is discarded.

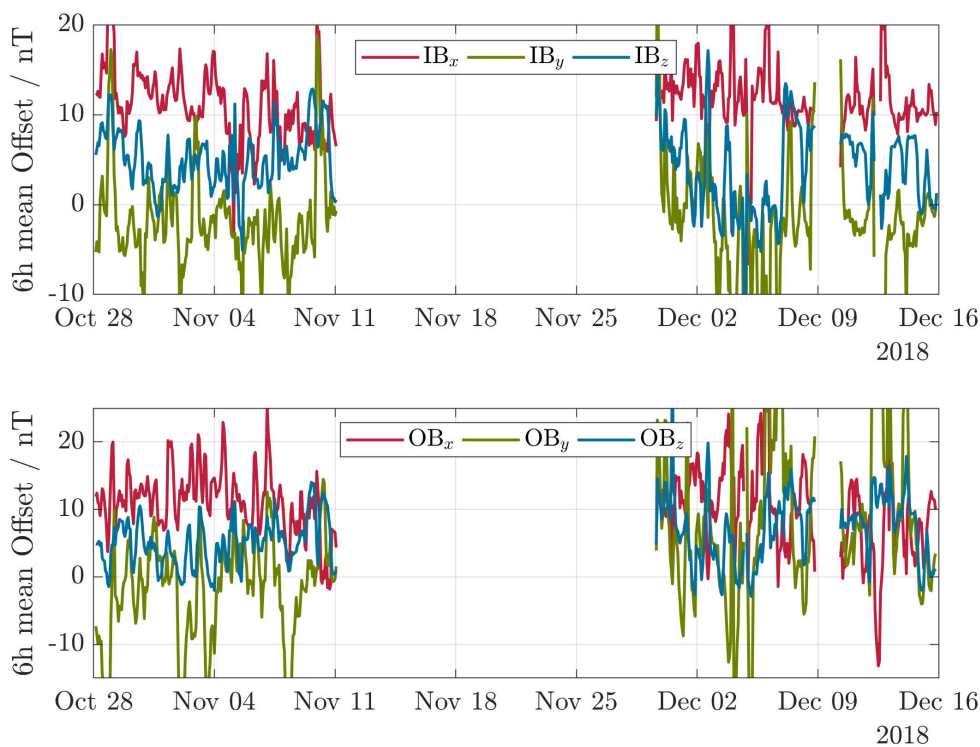


Figure 9 : Offsets for 3 sensor components (xyz) for inboard (IB) and outboard (OB) sensors. All offsets are calculated within a 6h time window. This window is stepped through time by steps of 1.3 h (for easy display).

Figure 9 shows 6h-averaged offsets of IB and OB for the available 1 Hz data. As no preselection is made these offsets are highly variable.

Three long data intervals are available as seen in Figure 9. For each of the intervals Figure 10 to Figure 15 show the distribution of the offset for the x, y and z component. In- and outbound sensor are separately displayed.

The necessity of a preselection is further illustrated by the partially existing bimodal structure, e.g. z-component in Figure 12.

Although the offset distributions are broad, preliminary offset values can be deduced with an approximate accuracy of about ± 1 nT, except for the IB and OB z-components. These are:

IB [10nT; -3nT; ~]

OB [9.5nT; -4nT; ~].

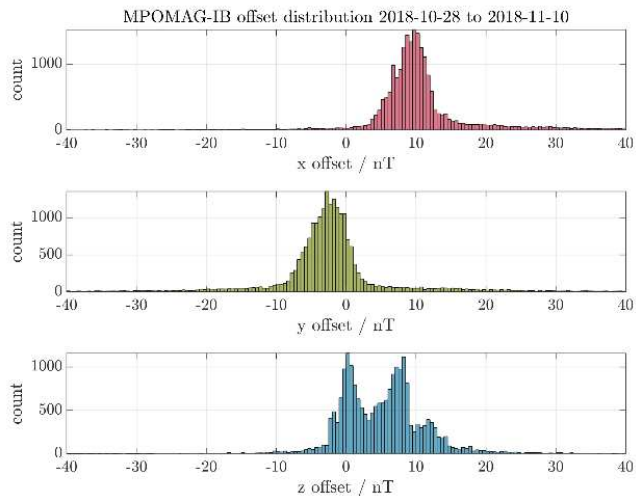


Figure 10 IB offset distribution 28 October to 10 November 2018.

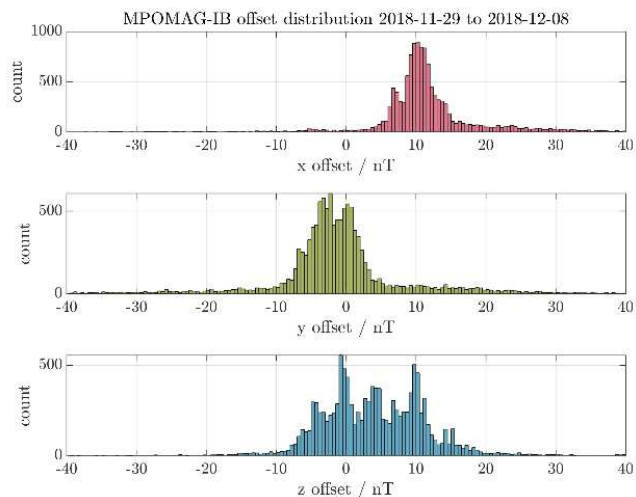


Figure 11 IB offset distribution 29 November to 8 December 2018.

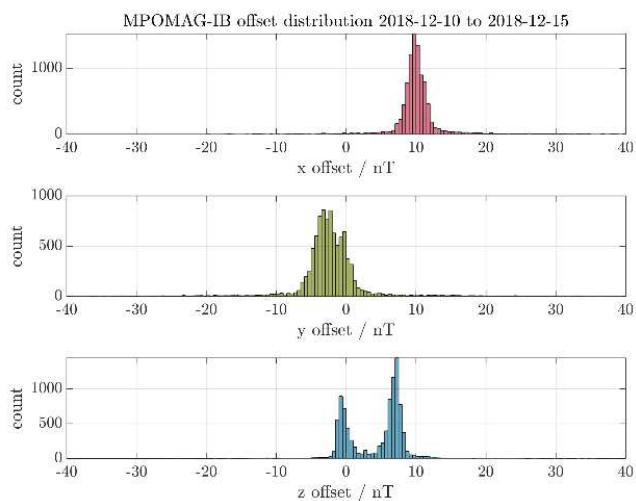


Figure 12 IB offset distribution 10 December to 15 December 2018.

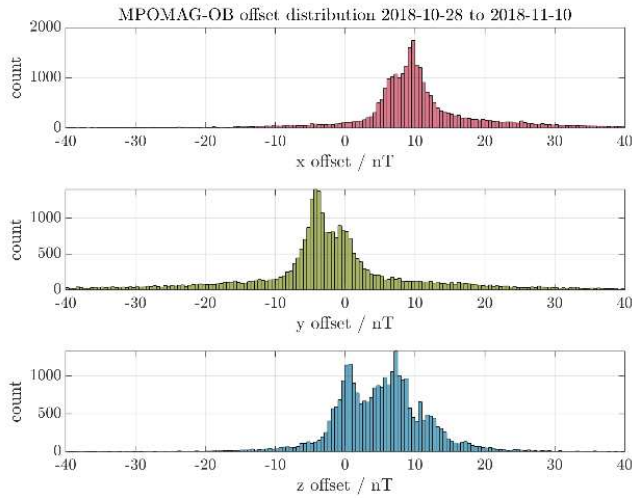


Figure 13 OB offset distribution 28 October to 10 November 2018.

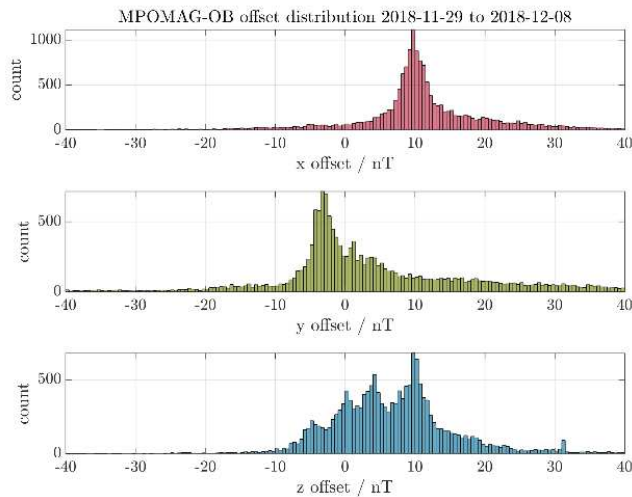


Figure 14 OB offset distribution 29 November to 8 December 2018.

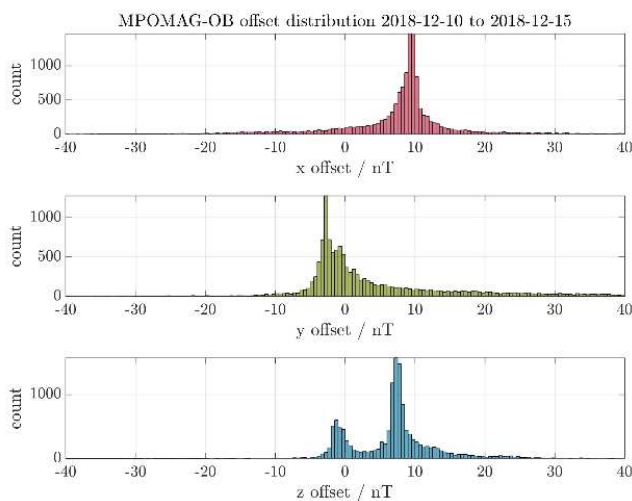


Figure 15 OB offset distribution 10 December to 15 December 2018.

6 Investigation of S/C Interferences

For the science goal of mapping the Hermean magnetic field with a high precision, the s/c induced magnetic interferences must be filtered from the data. Therefore, several magnetic tests were performed on ground with the aim to characterize individual disturbers. In addition, during the near-Earth commissioning phase the MPO-MAG remained on for several intervals to monitor the commissioning activities of several other instruments as well as s/c subsystems. Because not all instruments are fully operational, MPO-MAG did not monitor all subsystems and instruments, the investigation for magnetic disturbers is not yet complete. Also, the environmental conditions will change once in orbit around Mercury. Along with this, magnetic moments of the disturbers will also change.

As BepiColombo has left the terrestrial magnetosphere early in the mission, the measured magnetic field is the sum of the natural interplanetary field (IMF) and fields from s/c subsystems or instruments. In order to separate these magnetic field sources, the MPO-MAG instrument consists of two sensors (inboard (IB) and outboard (OB) sensor). The IMF is assumed to be constant across IB and OB. Thus, by taking the difference by components ($\Delta B_x = B_{OBx} - B_{IBx}$, etc.) the IMF part drops out and only the s/c part remains – i.e. if one sees a signature in the difference of the components it has to be s/c induced. Ideally, if there is no s/c induced disturbance, one only would see straight lines (not 0 as the instrument offsets have not been calibrated in this data). If a signature appears in all 3 difference components without a phase shift, it is usually due to an electrical current signature. If there is a phase shift in the signature, it is usually due to something magnetic that rotates. For example, it has been established (from earlier measurements) that the MTM solar array induces magnetic disturbances depending on both the rotational position as well as the power extracted from the arrays.

In order to correlate magnetic disturbances seen in MPO-MAG data to a physical source, the WebMUST tool provided by ESAC has been proven extremely valuable as HK-parameters may be easily visualized and compared to MPO-MAG data.

6.1 PSU

On ground, the magnetometer was tested against the noise induced by the MPO-MAG power supply. It has been found that the redundant PSU (LCL B) is actually performing better than the nominal PSU (LCL A). More precisely, the redundant PSU induces a weaker disturbance at a single frequency line than the nominal one. The disturbance frequency is strongly temperature dependant.

The MPO-MAG team therefore asked to be switched on with LCL B as default rather than LCL A. ESA then defined a nominal switch-on with LCL B and a redundant switch-on with LCL A.

This is reflected in the PKK00021 parameter in the command log.

In order to verify this behaviour in space, we must analyse data measured with at least 32 Hz in a quiet environment (no commissioning activity from us and low activity on the s/c as well as quiet solar wind conditions) and also in a period after boom deployment (in order to naturally suppress s/c induced noise).

From the command log, we identified the following periods

nominal (ESA): 25/10/2018 : 14.049 – 14.064 h
redundant (ESA): 25/10/2018 : 15.655 – 15.675 h

2018 – DOY 298 = 25/10/2018

At these time periods, the instrument was still in a Calibration -Mode. Thus, no data is fed to the SGS science data pipeline and we performed the following analysis on magnetic field data in counts rather than in Nanotesla.

Figure 16 and Figure 17 show the time series of the magnetic field for the selected time periods. They show relatively quiet periods. Figure 18 displays the flywheel speed in the time range 14:00 to 16:00 on 25/10/2018. Two out of four wheels are driven in at a frequency of about 18.3 Hz (1100 rpm).

Figure 4 to Figure 9 show the amplitude spectra in different scalings. This is to show that the expected 8 Hz spectral peak is indeed slightly lower (even vanishing for the By-component) if the magnetometer is run with the nominal PSU (LCL B). The higher noise at lower frequencies for the nominal PSU is probably due to noisier magnetic field background.

This analysis has to be repeated for the OB sensor. Furthermore, the temperature dependence has to be verified for a longer measurement time interval in space.

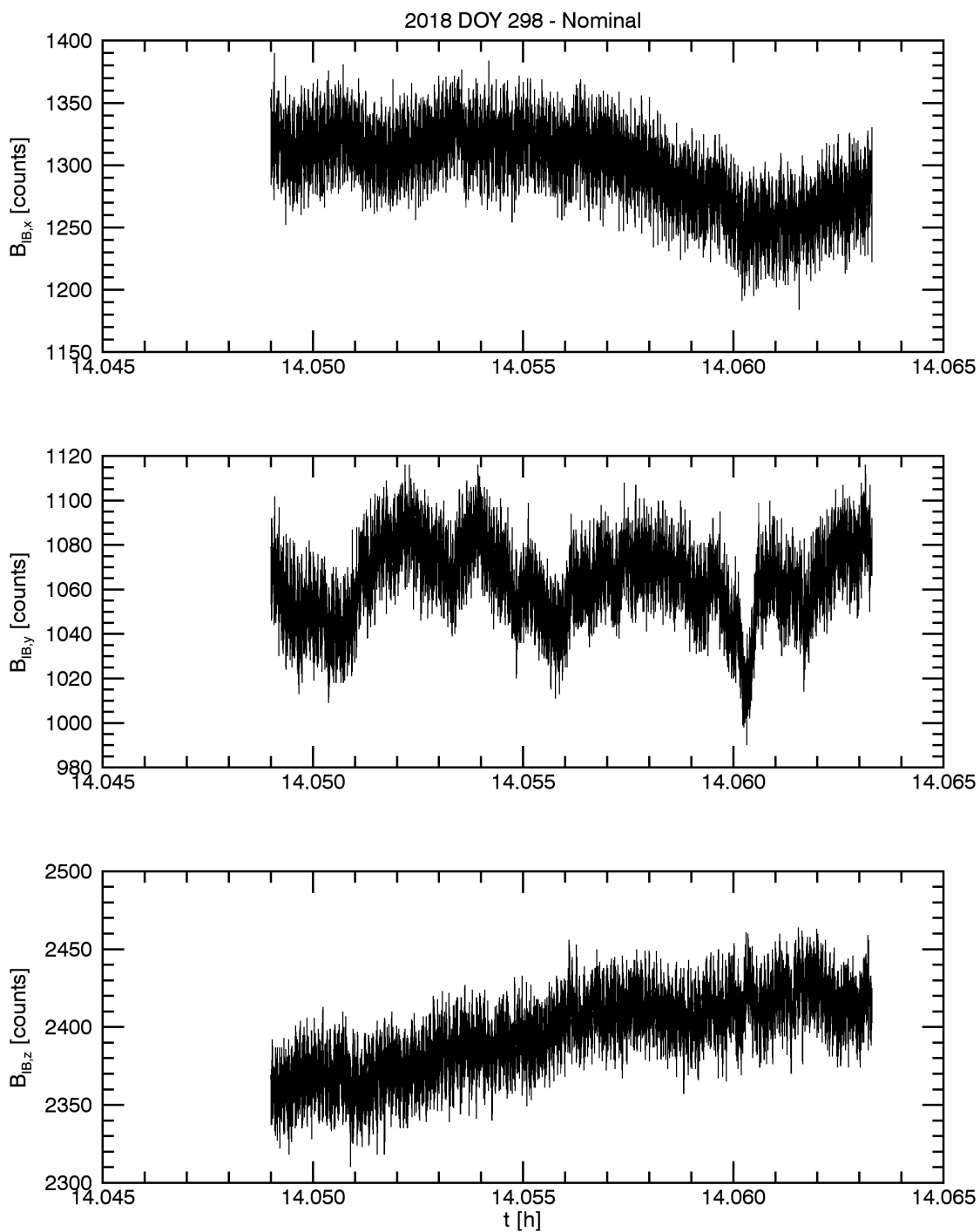


Figure 16 : Magnetic field time series measured using nominal PSU (LCL B).

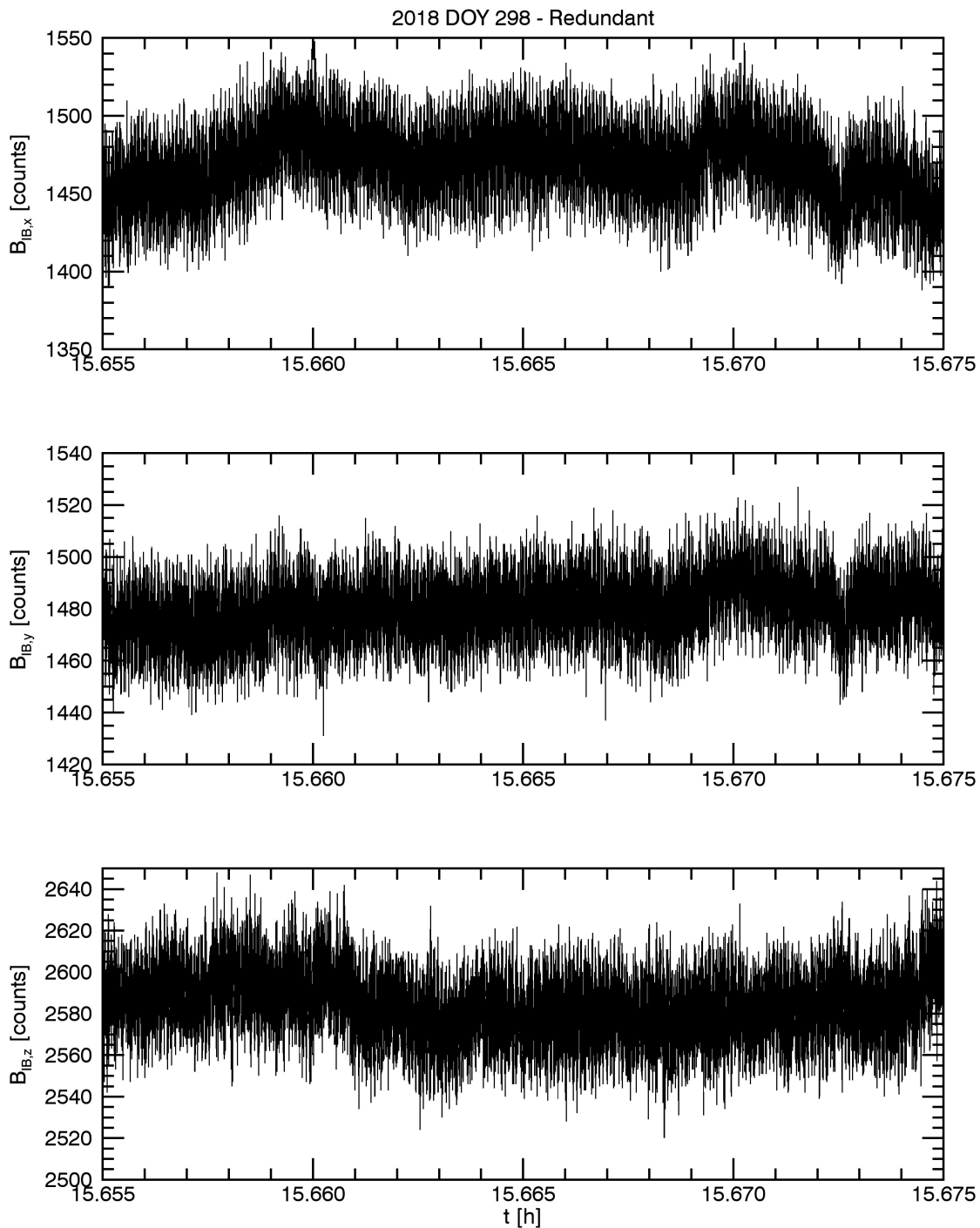


Figure 17 : Magnetic field time series measured using redundant PSU (LCL A).

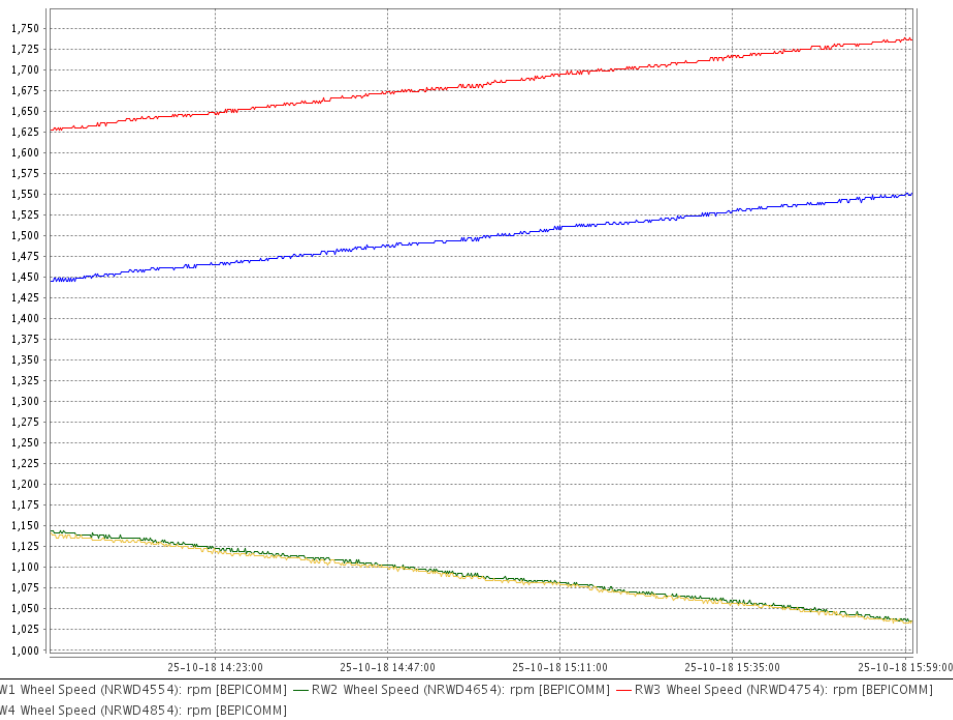


Figure 18 : Time Series for flywheel frequencies in rpm at 25/10/2018 in the time range 14:00-16:00. 1100 rpm correspond to 18.3 Hz.

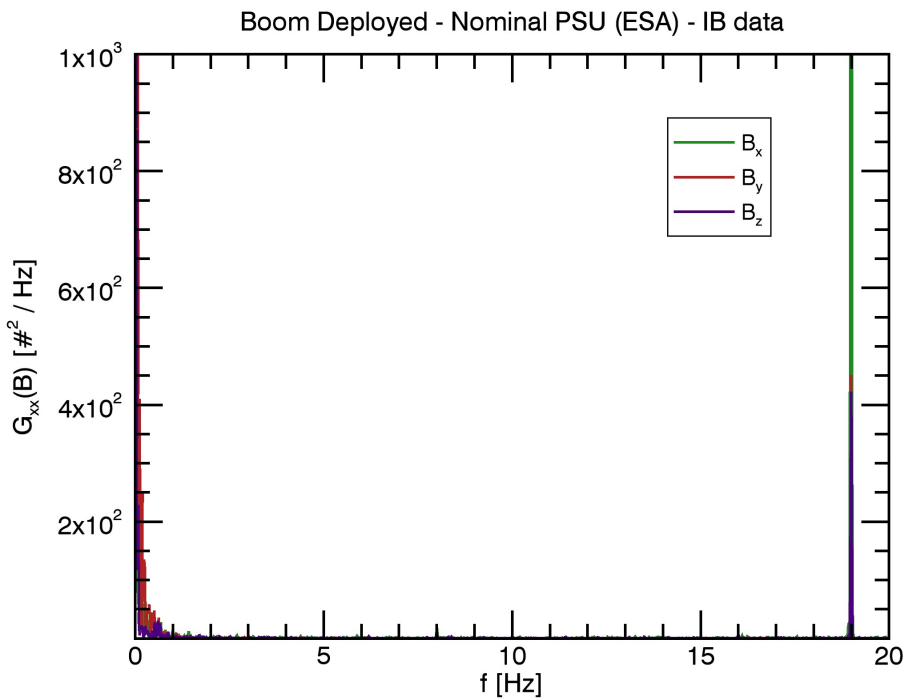


Figure 19 : Spectrum of magnetic field for nominal PSU. The frequency range is reduced to 0-20 Hz.

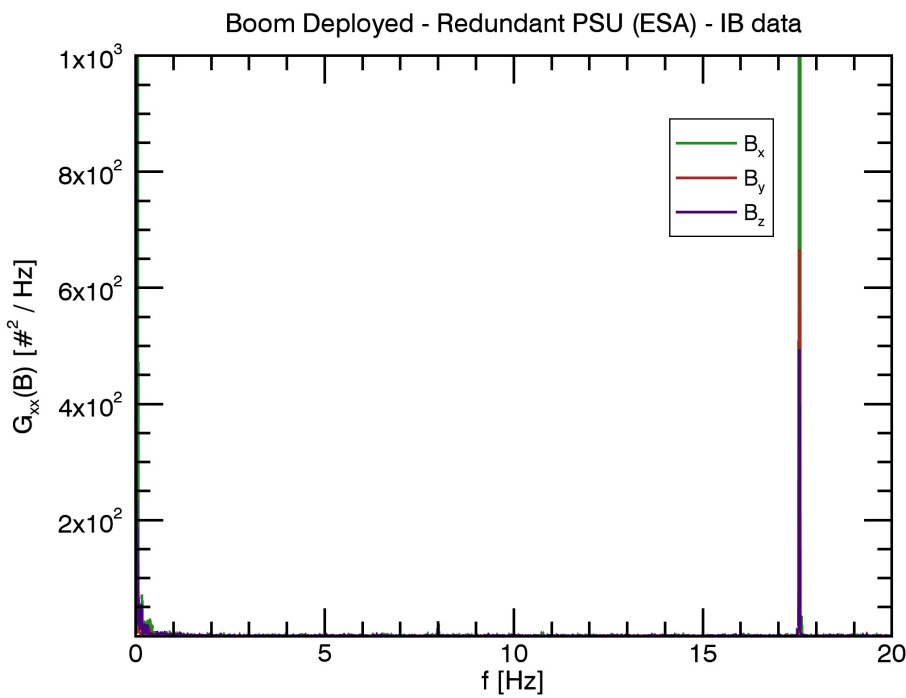


Figure 20 : Spectrum of magnetic field for redundant PSU. The frequency range is reduced to 0-20 Hz. The spectral peak at about 17Hz corresponds to 2 flywheels.

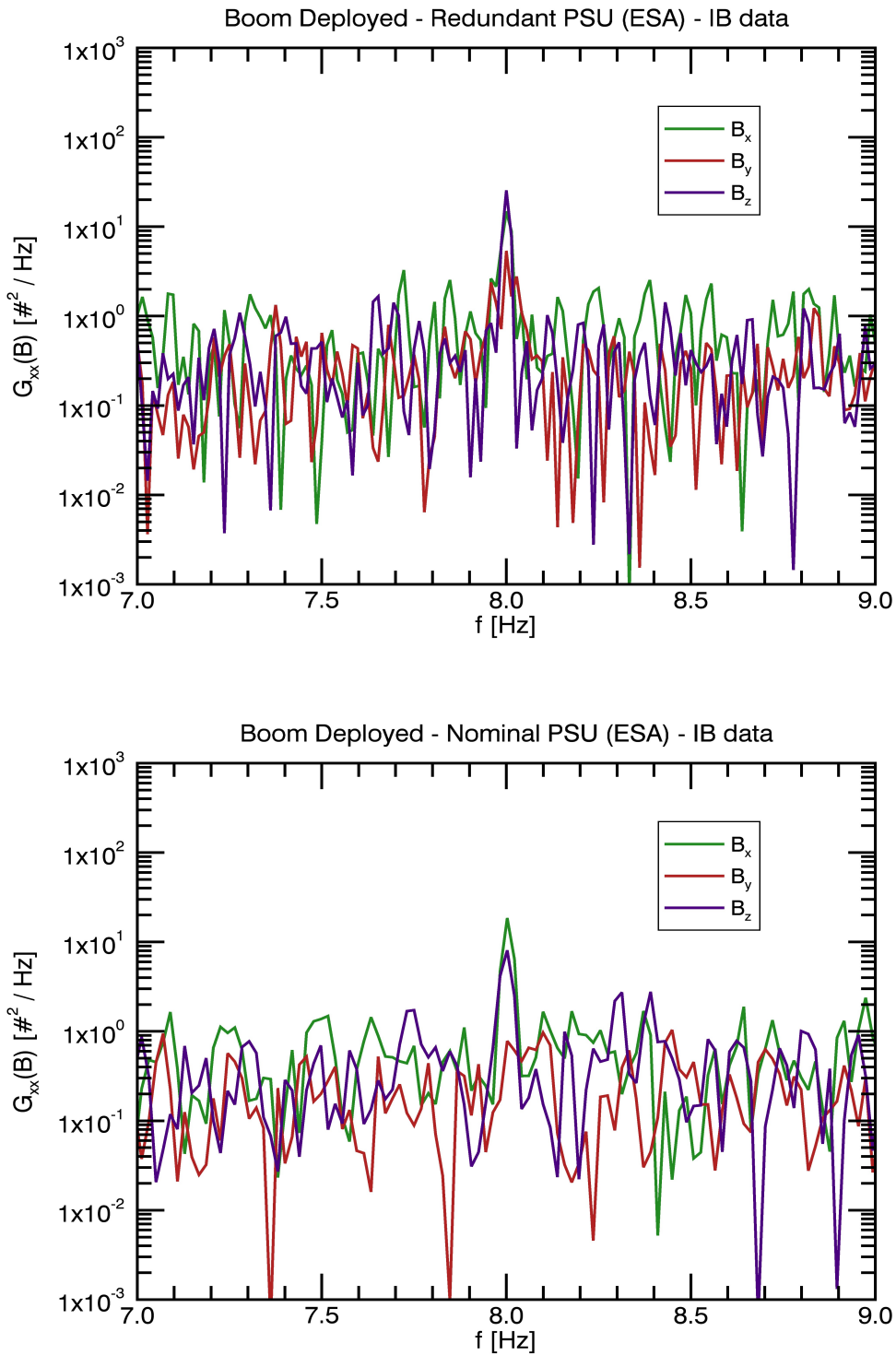


Figure 21 : Detail of spectra around 8 Hz.

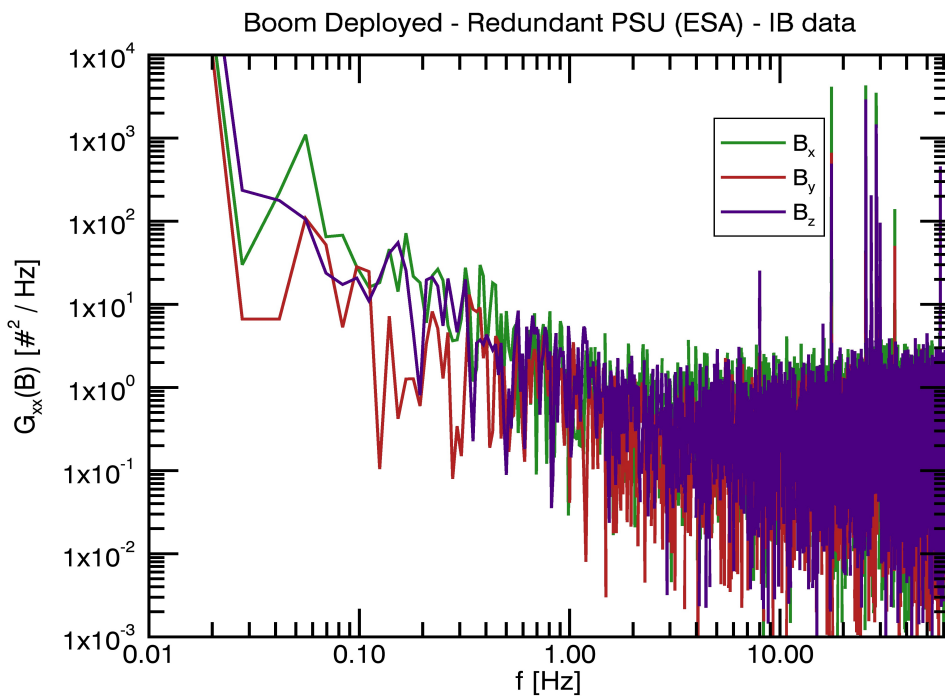
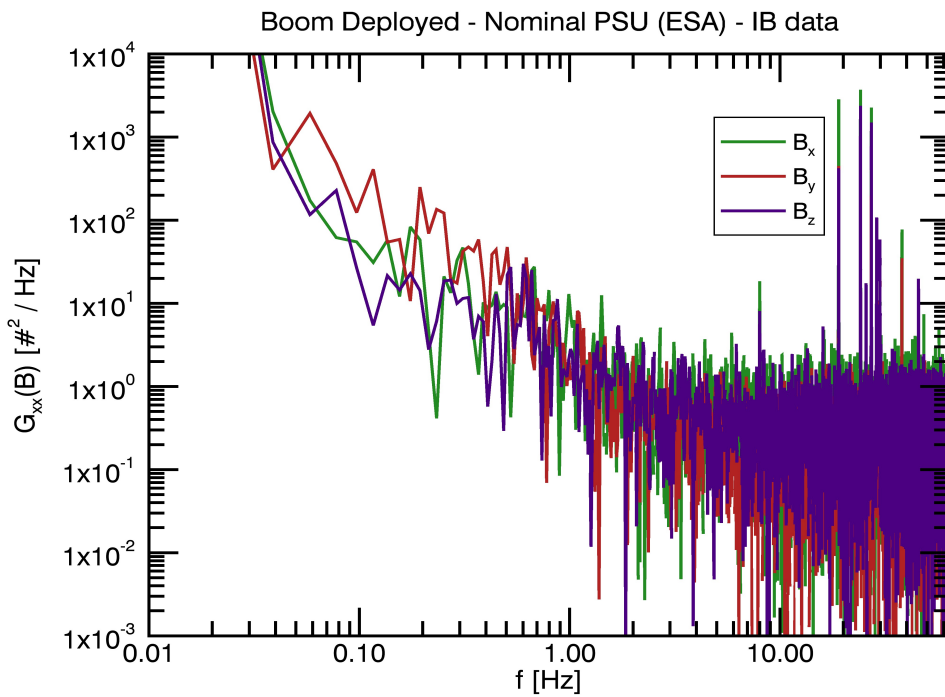


Figure 22 : Full spectra in double-logarithmic scaling.

6.2 Boom Deployment

On 25/10/2018 the magnetometer boom has been deployed. Figure 23 shows the time series of magnetic field data recorded during the deployment. The decrease seen in all magnetic field components clearly shows the successful deployment and the weakness of the s/c induced static magnetic field after deployment. A detailed analysis of the s/c magnetic moment is TBW. Also, the variations in the magnetic field are decreased with a deployed boom as shown in Figure 24. The average fluctuations between 0.1Hz and 1 Hz have an approximate amplitude of less than 22pT (in the IB-x component). Thus, the sensor noise must be lower than that.

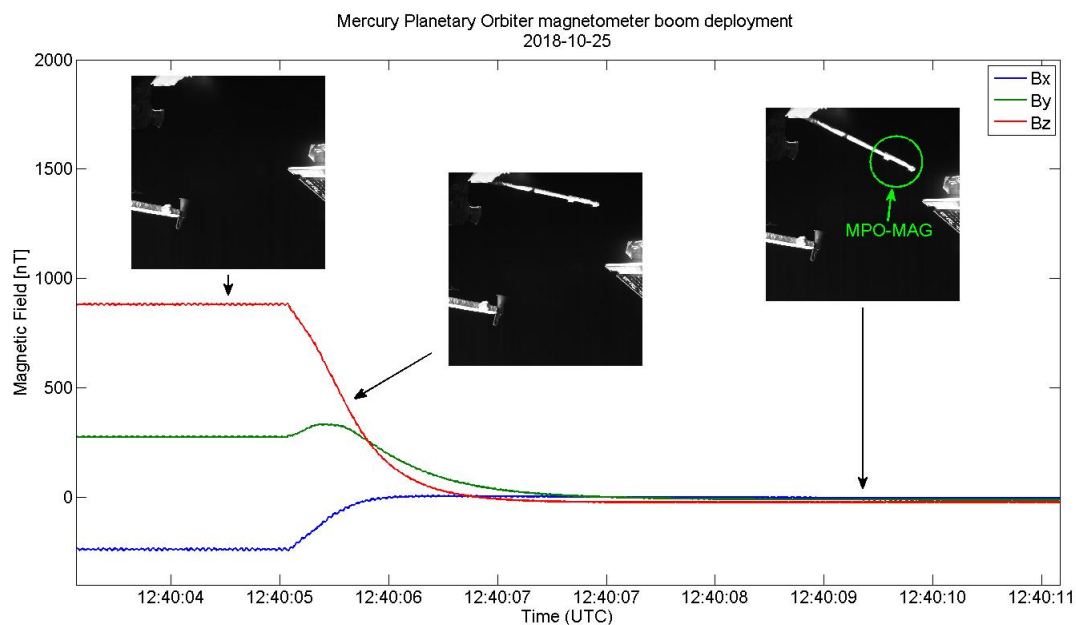


Figure 23 : Time series of magnetic field data during boom deployment.

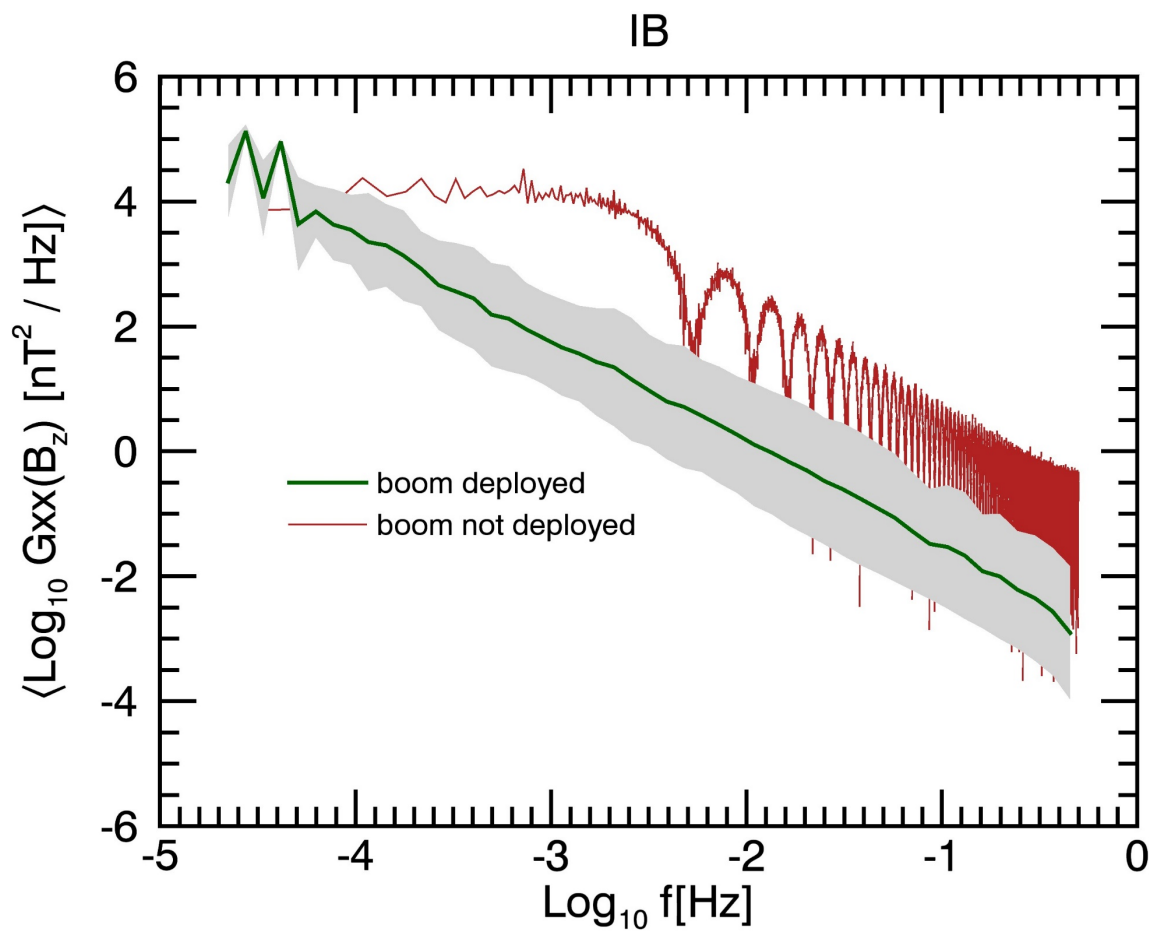


Figure 24 : Magnetic power spectra for the IB sensor. In red the spectrum for the measurements with a still undeployed boom are shown. In green the average spectrum with a deployed boom is shown.

6.3 Reaction Wheels

Reaction wheels are known to produce strong time-dependent and geometrically complex magnetic signatures. The MMO-MGF sensors are able to monitor the reaction wheels easily as the MAST remains undeployed. The MPO s/c is equipped with 4 (2 pairs) reaction wheels. These are continuously operated. During the commissioning phase, events such as wheel off-loadings and s/c flips occurred often.

Location of Reaction wheels:

MPO drawing:
 RW1 and RW2 are located in about 1m distance, see drawing.

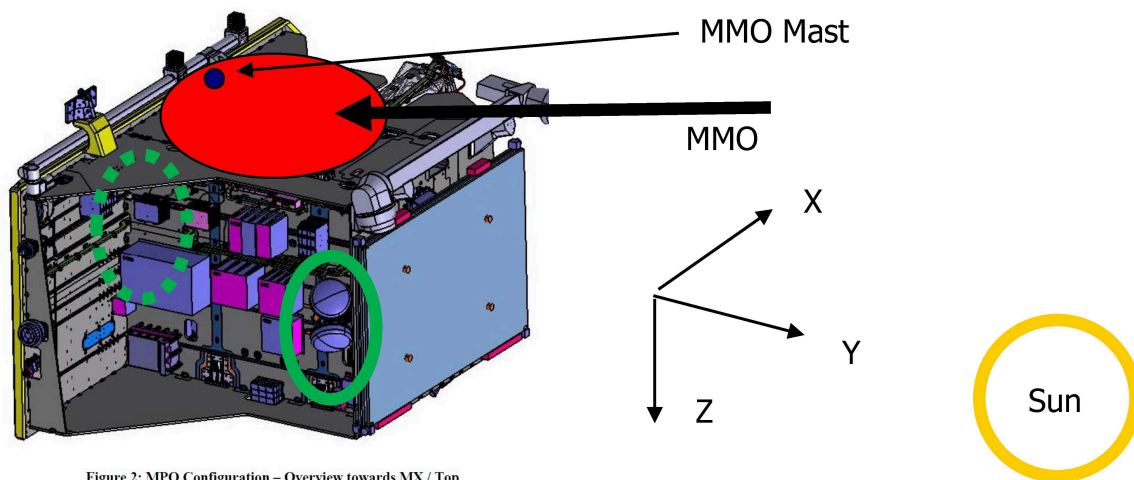
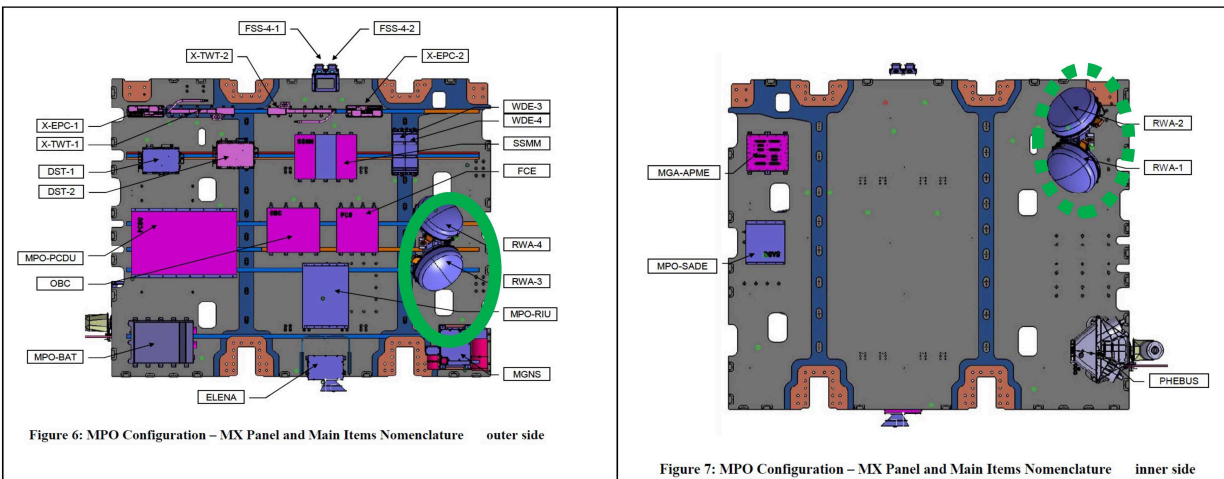


Figure 2: MPO Configuration – Overview towards MX / Top

Y is flip axis

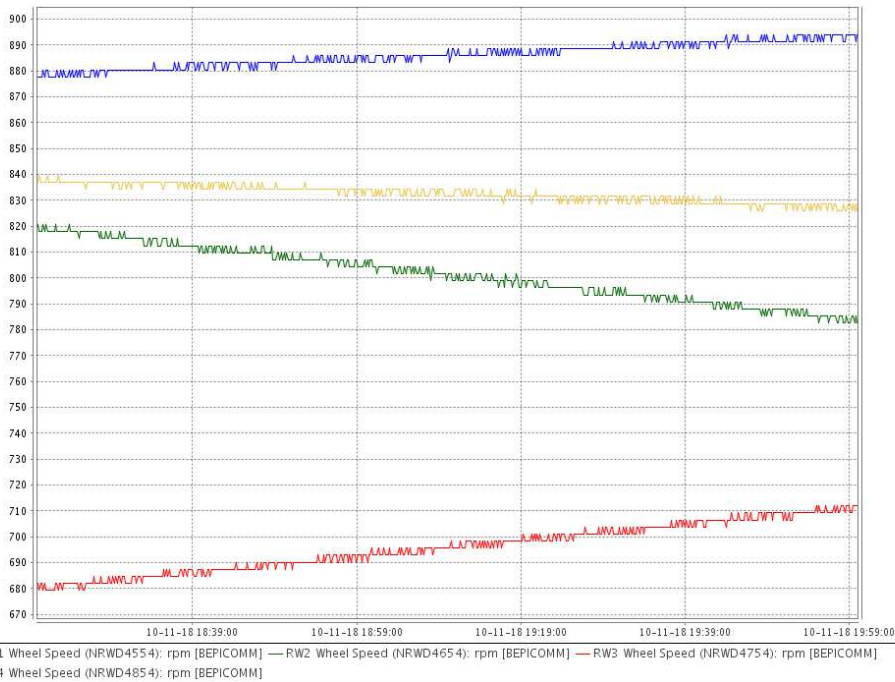
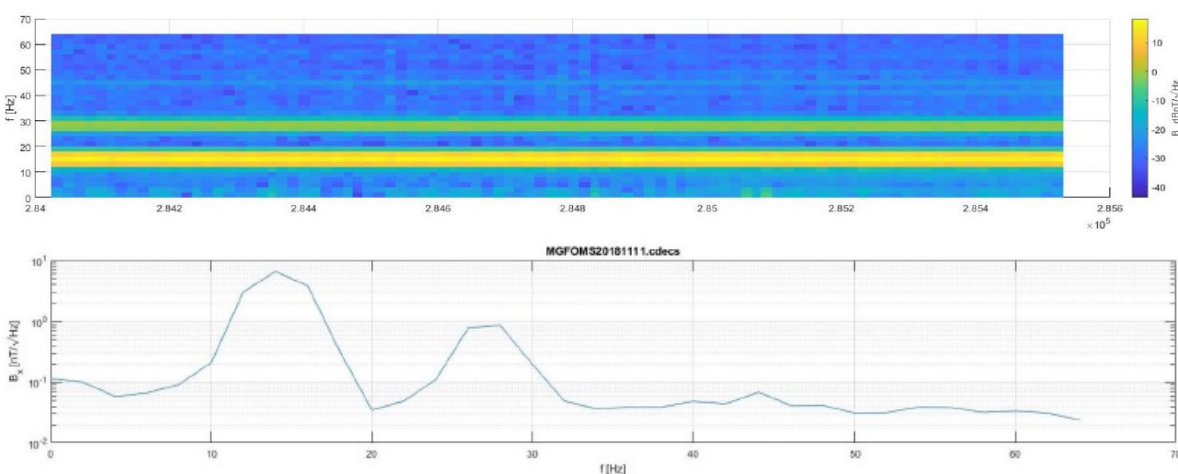


Figure 25 : Frequency behaviour of reaction wheels.

Reaction wheel signature measured by MMO MGF:

45nT measured at 13Hz by both sensors in 128Hz mode
 MMO OB: X 20nTpp, Y: 45nTpp, Z: 45nTpp
 MMO IB: X: 40nTpp, Y: 35nTpp, Z: 40nTpp



Reaction wheels have equivalent magnetic moment of 200mAm² (see report from Anita Przyklenk, BC-MAG-MC-00532). This results in a 1m distance between MMO sensors and wheels

Reaction wheel signature during flips:

During flips the RW signal is visible in 1Hz data, if spin rate is crossing zero:

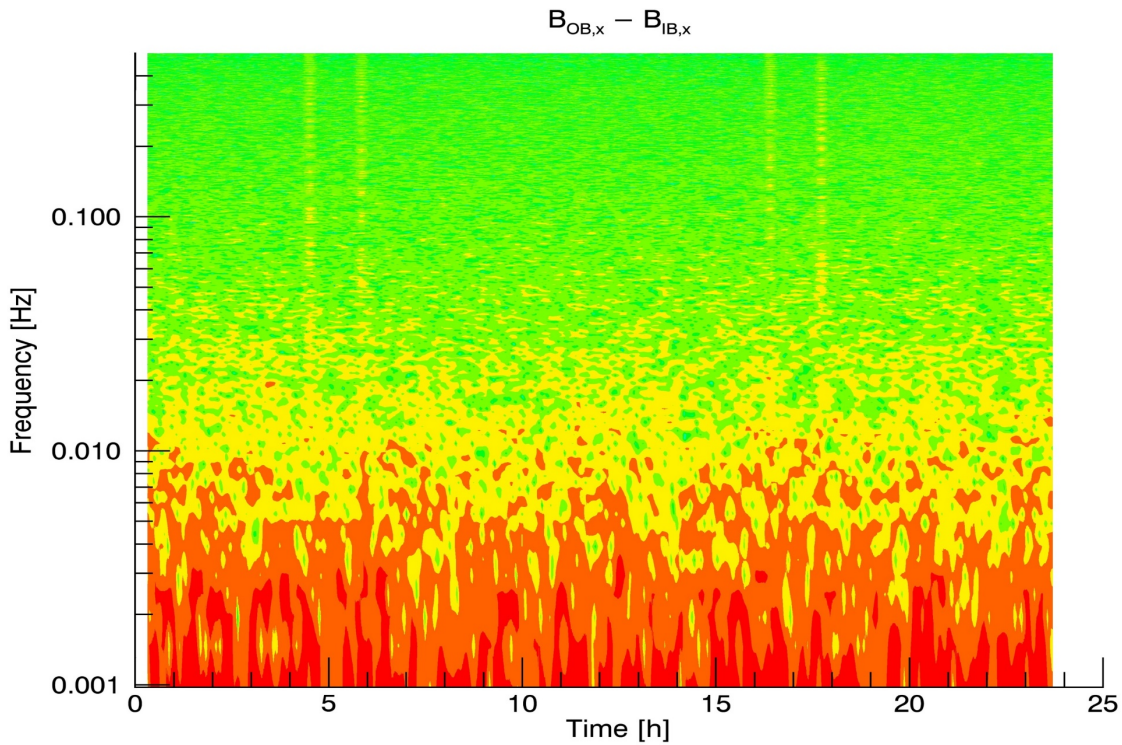
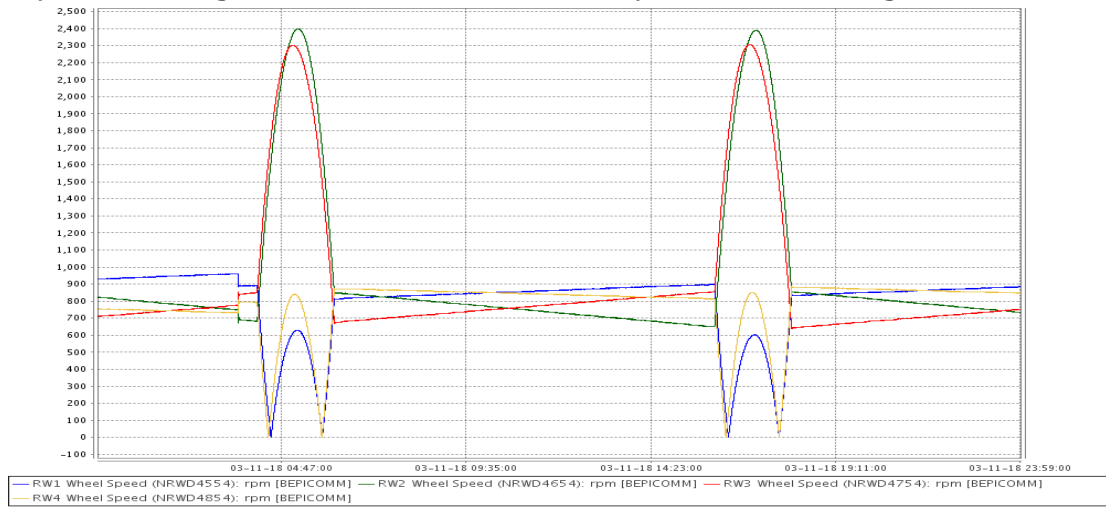
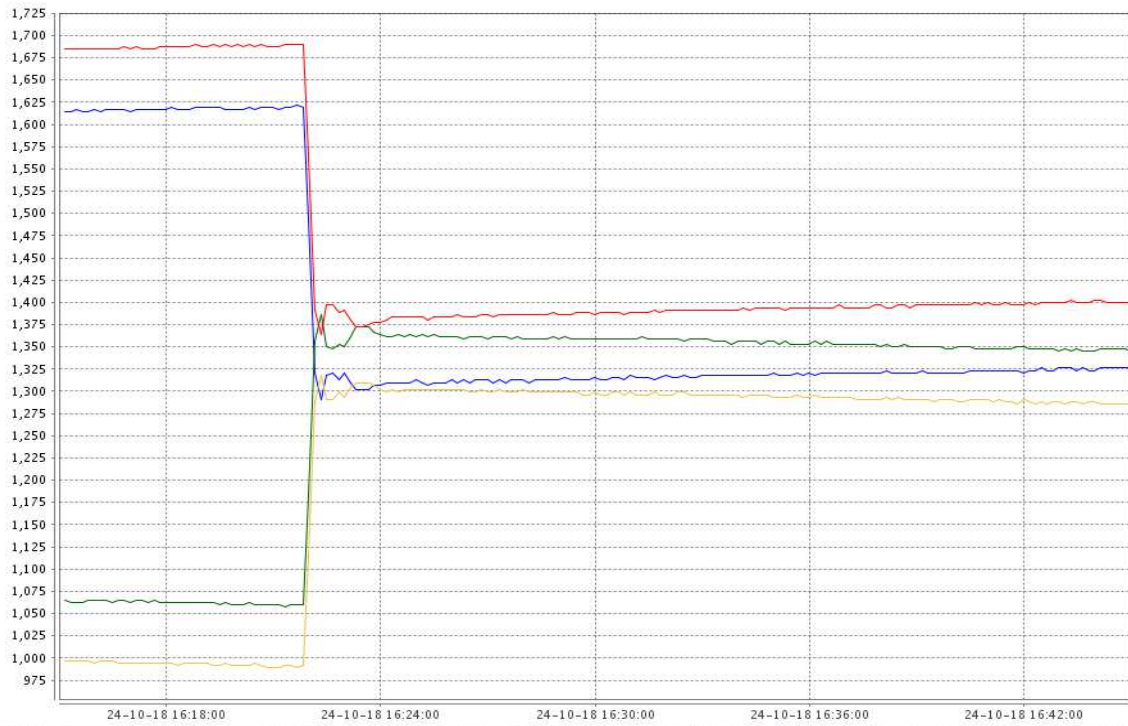


Figure 26 : Dynamic spectrum of the difference in the x-components during two s/c flips.

Figure 27 shows the reaction wheel speed with the magnetometer boom still stowed and the magnetometer was set to a high sampling rate (128 Hz). Figure 28 shows the dynamic spectra of the OB sensor during this wheel off-loading event.



— RW1 Wheel Speed (NRWD4554): rpm [BEPICOMM] — RW2 Wheel Speed (NRWD4654): rpm [BEPICOMM] — RW3 Wheel Speed (NRWD4754): rpm [BEPICOMM]
 — RW4 Wheel Speed (NRWD4854): rpm [BEPICOMM]

Figure 27 : Reaction wheel speed during wheel off-loading event.

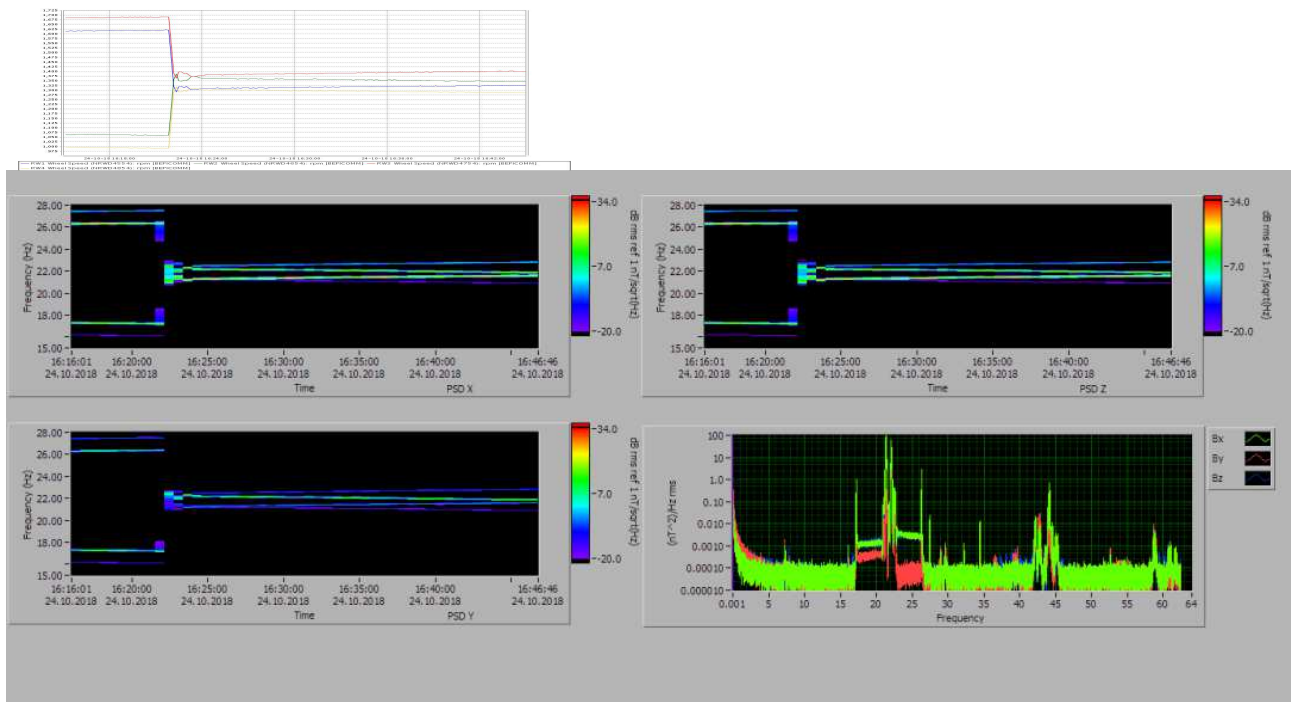


Figure 28 : Fourier spectra of magnetic field time series during WOL event.

Conclusion of Reaction wheel monitoring

MPO-MAG as well as MMO-MGF are able to monitor the reaction wheels. As these wheels are continuously operated even in the orbital phase, this signature deserves major

attendance of the MERMAG team. An algorithm to clean this disturbance appropriately is still under development.

6.4 MTM solar panel currents

On 4/11/2018, the MTM solar array was moved in identical sequences. This was recorded by MPO-MAG (Figure 29 shows the rotation angle and the OB magnetic field data). It was found that the magnetic disturbance is stronger on the OB sensor than on the IB sensor, which indicates a current loop located at the entire solar array. The center of the solar array (and with that also of the current loop) is closer to the OB sensor (cf. Figure 30) – which explains the observed signature.

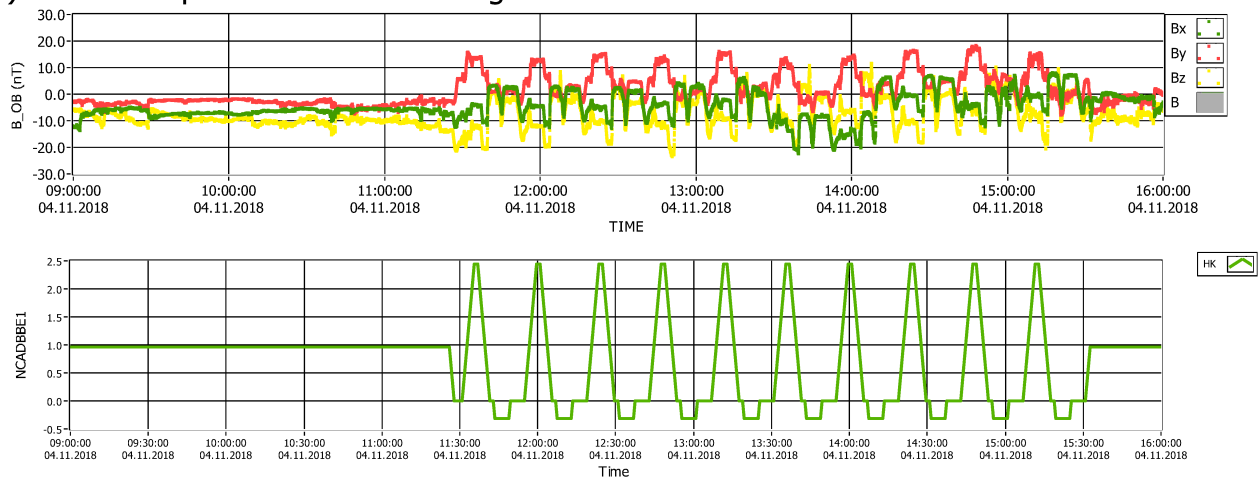


Figure 29 : Comparison of OB magnetic field data with the rotation angle of the MTM solar array.

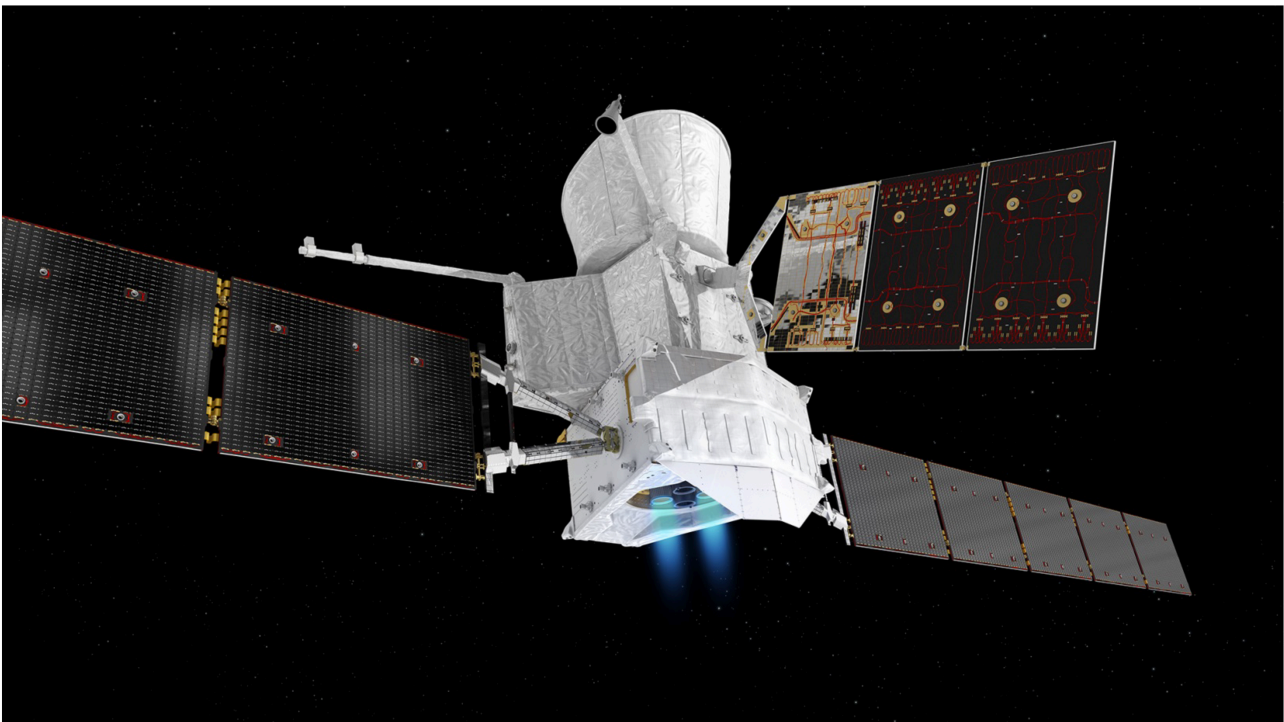


Figure 30 : Artistic sketch of the MPO-MAG location w.r.t. the MTM solar array.

Conclusion of MTM solar array monitoring

The MTM solar array causes a strong magnetic signature on both MPO-MAG sensors. A correlation with the solar array power (HK parameter: NZWSY110) including the rotation angle of the solar array is still to be done. The priority of this is not the highest as the MTM will not be present in the orbit phase.

6.5 MPO solar panel currents

On 07/12/2018, the MPO solar arrays were nudged by 2°. MPO-MAG monitored this activity. Figure 31 shows the respective difference time series during this event.

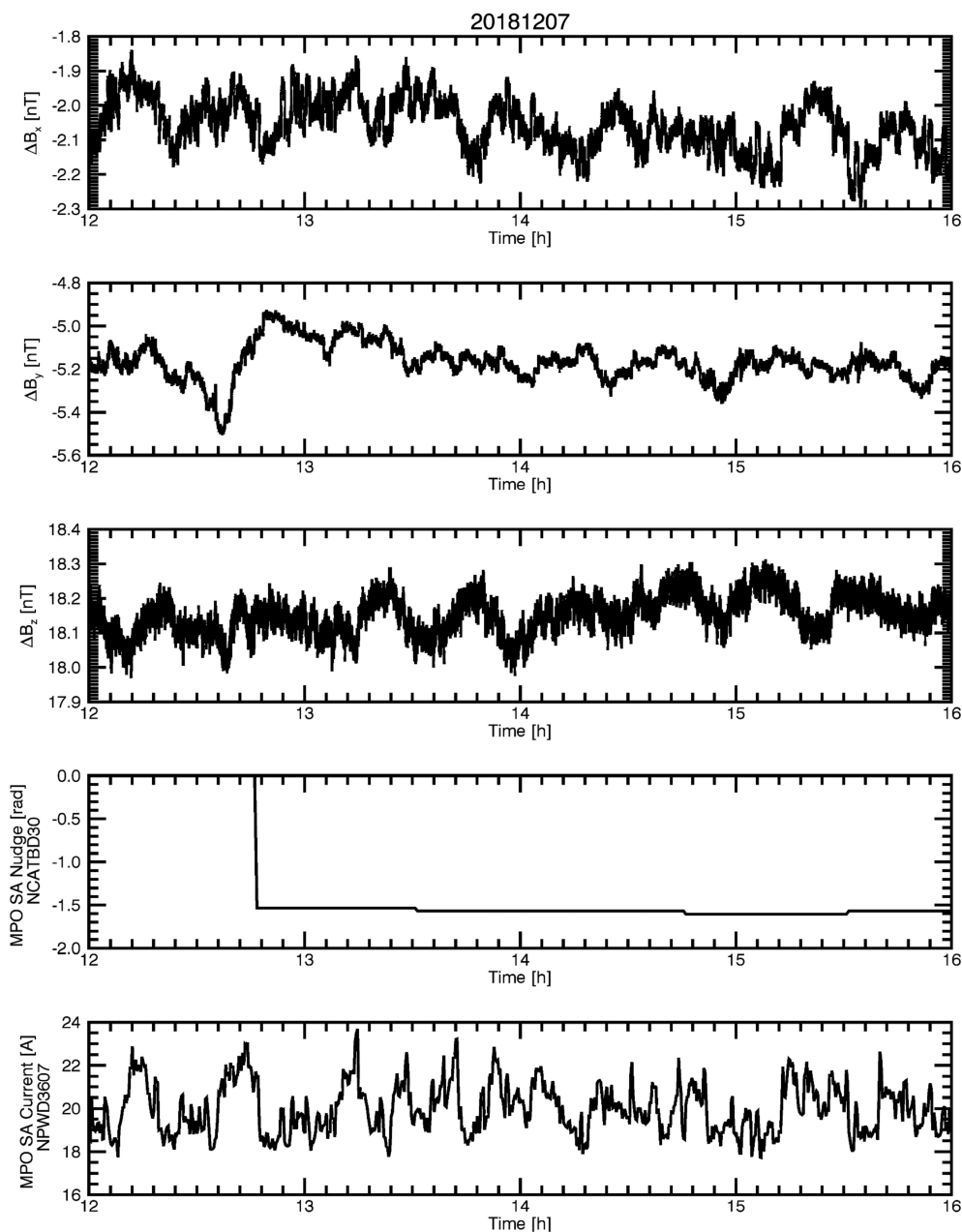


Figure 31 : Time series of magnetic field differences compared to MPO solar array nudging and MPO solar array current.

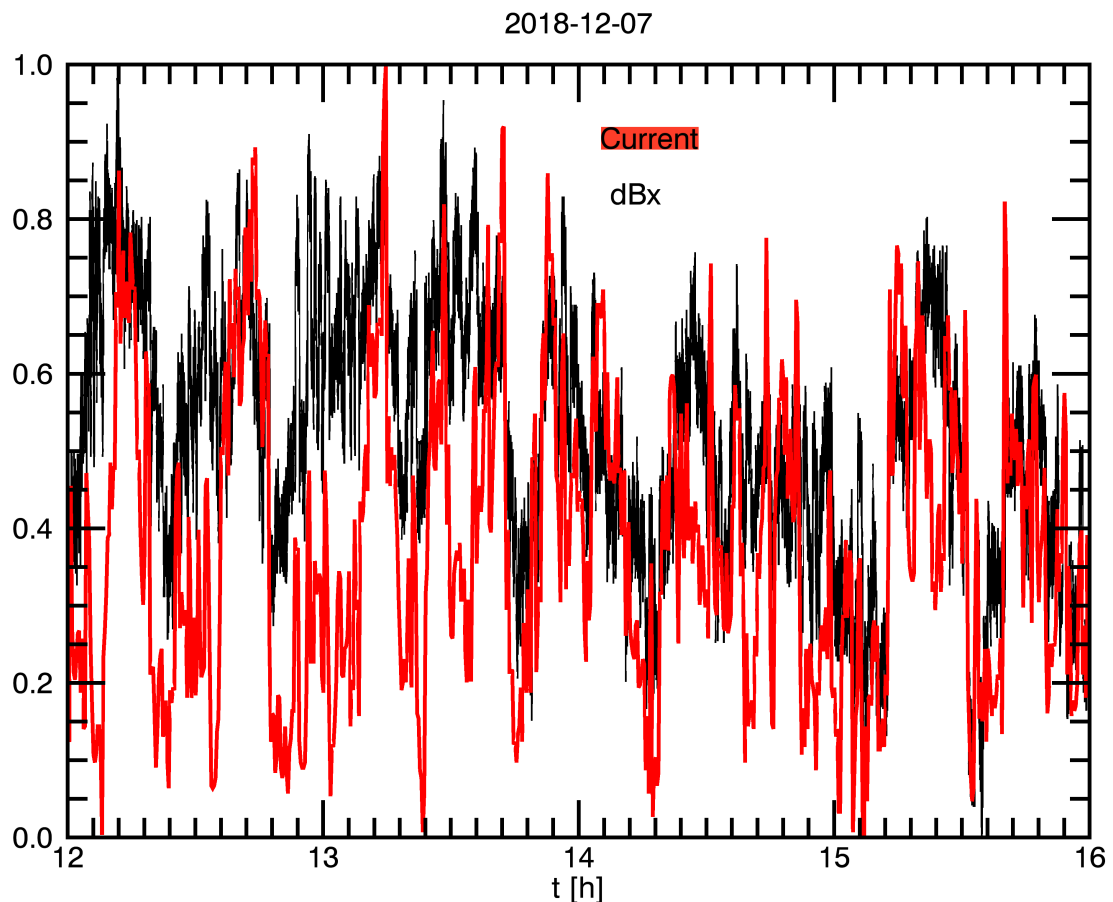


Figure 32 : Normalized time series of MPO solar array current and magnetic field difference in the x-component.

Conclusion of MPO solar panel monitoring

A correlation with the solar array angle is not evident from this event. The amplitude of the nudging might be too small to definitely tell. A correlation with the current with the magnetic field data seems too weak. As the solar panel is active during the orbit phase, this potential magnetic disturber should be further monitored.

6.6 Phebus

On ground measurements showed a strong magnetic moment associated with the Phebus baffle. It was found that a magnet is installed on the baffle for angle measurement. A compensation magnet was installed to decrease the far-field. In order to evaluate the successful compensation, the Phebus commissioning was monitored by MPO-MAG. Figure 33 shows the baffle rotation during the Phebus commissioning.

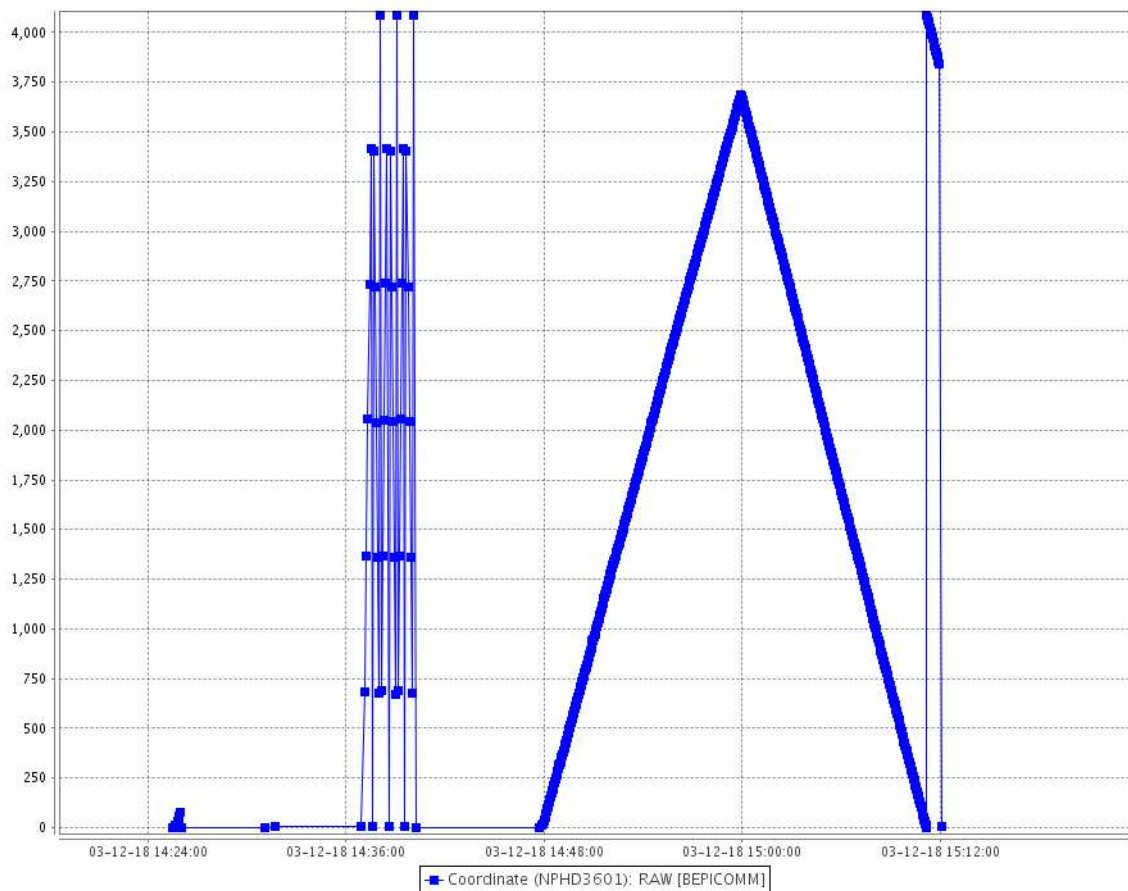


Figure 33 : Time series of Phebus baffle rotations. The triangular signature is centred around 15:00. Therefore, any magnetic signature from the baffle rotation should also be symmetric around 15:00.

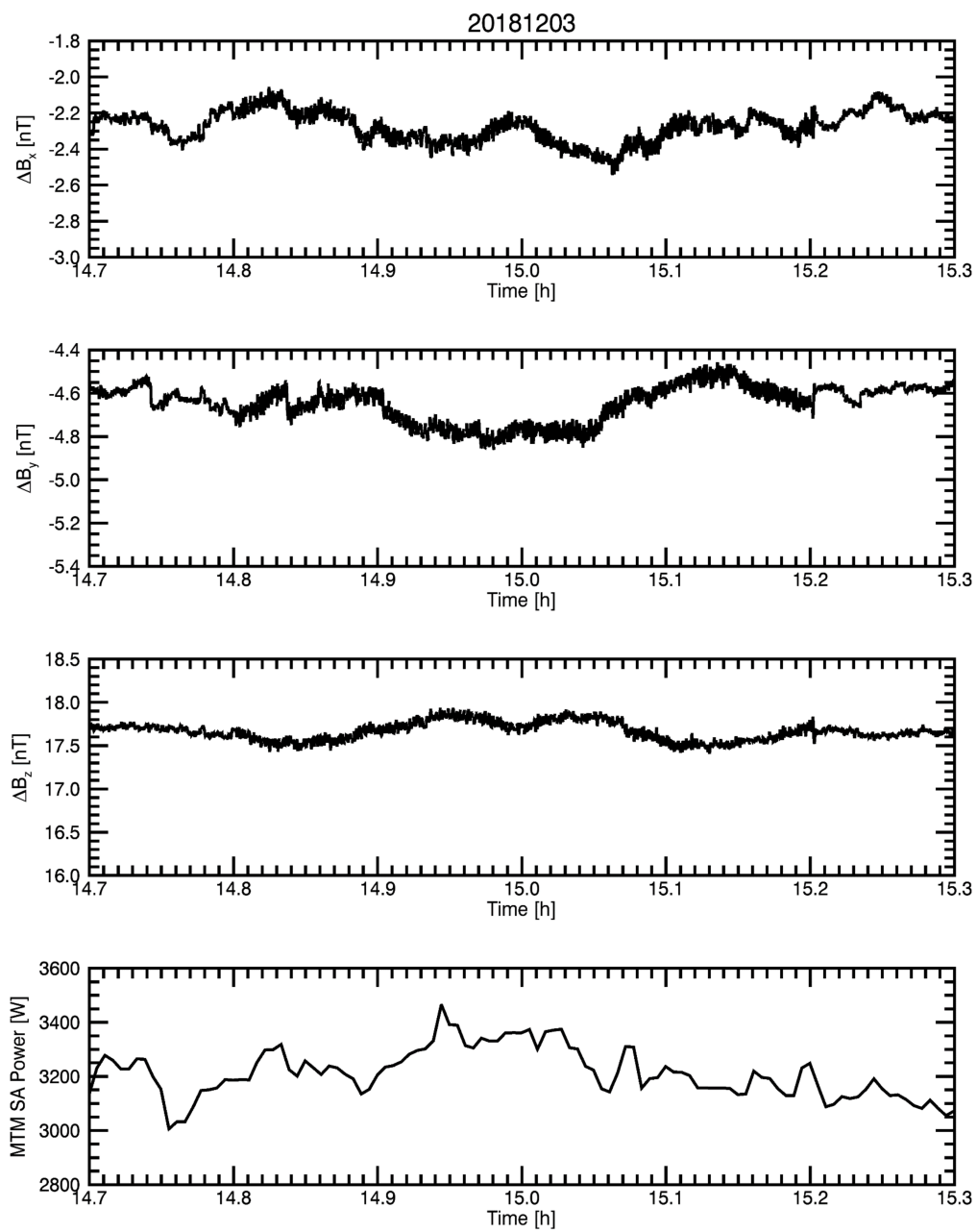


Figure 34 : Time series of magnetic field differences during the slow Phebus baffle rotation.

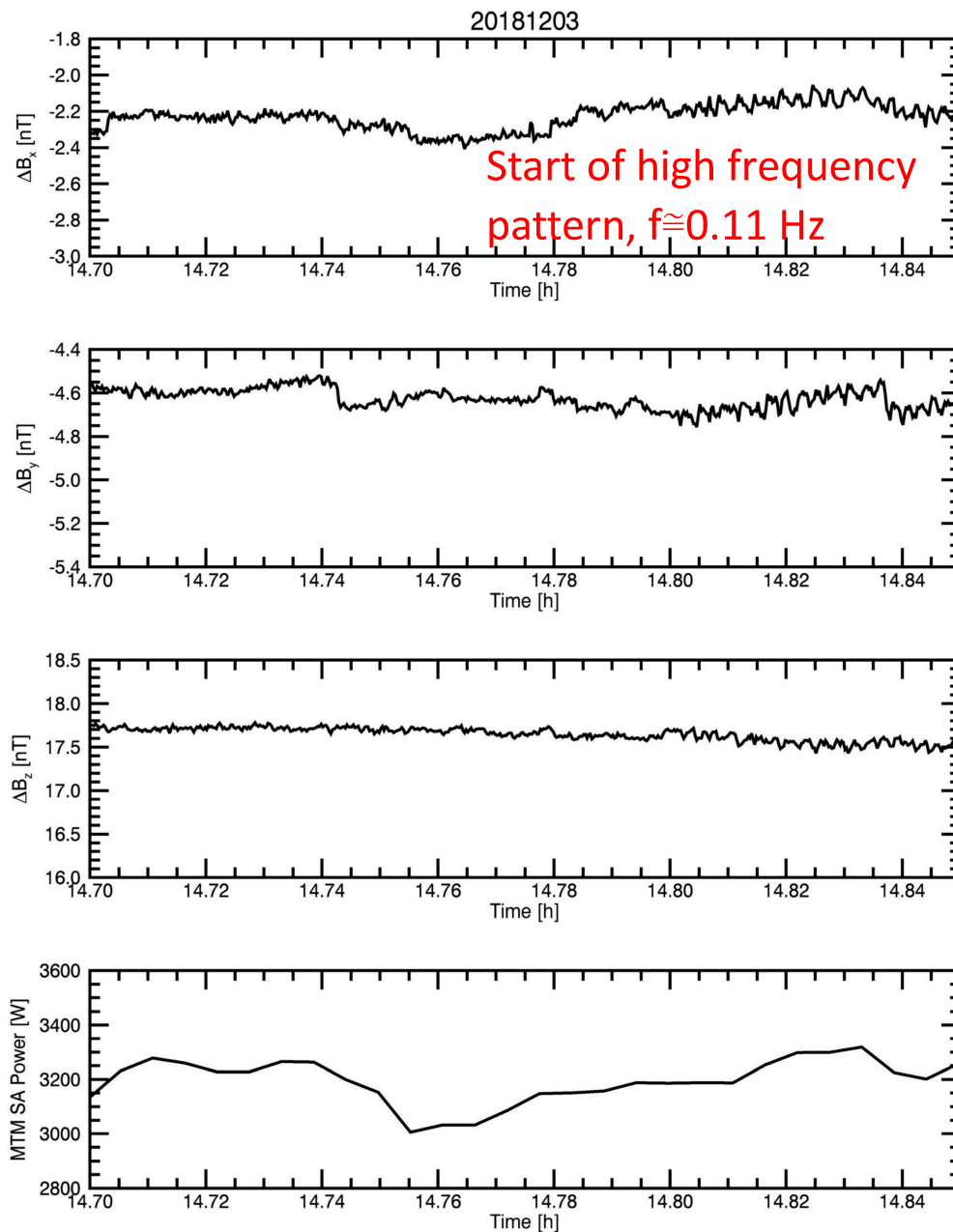


Figure 35 : Detailed time series of the beginning of the baffle rotation.

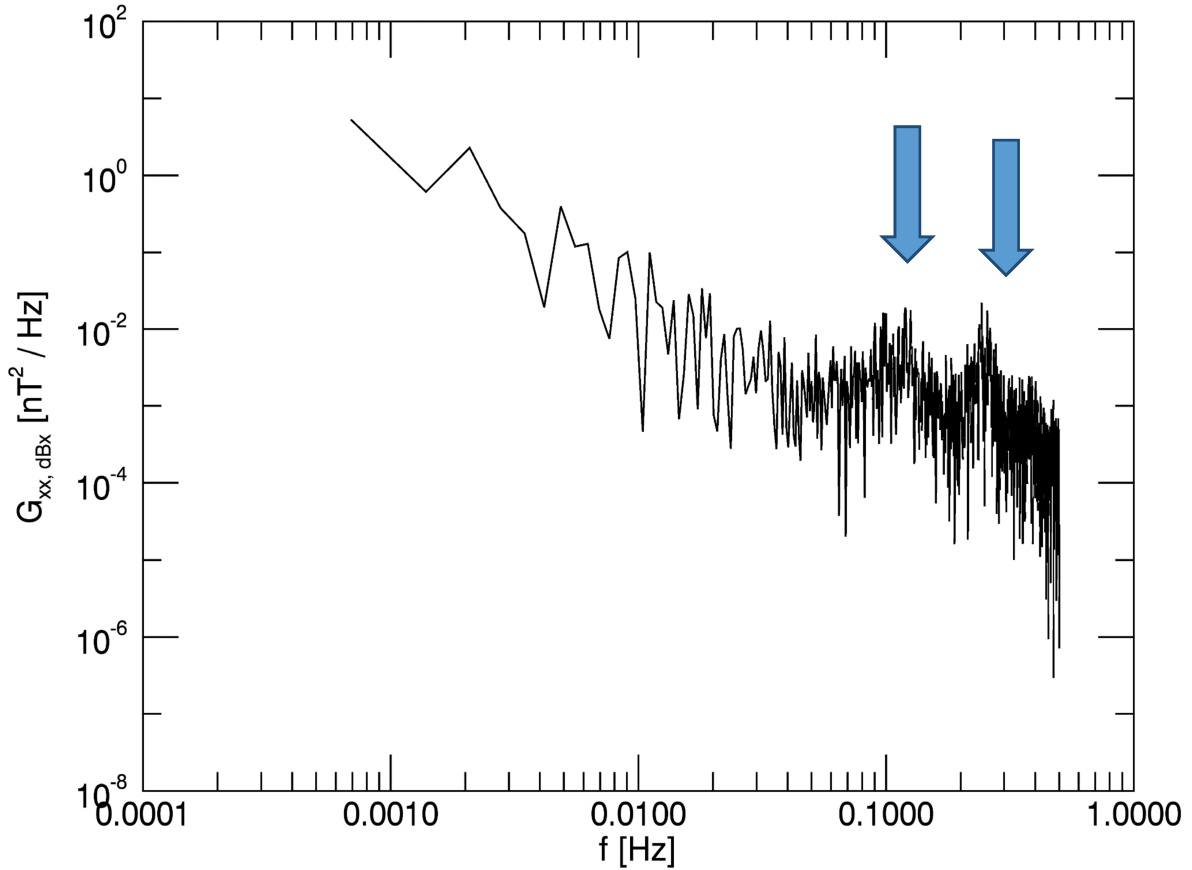


Figure 36 : Fourier-Spectrum of the magnetic field differences in the x-component with spectral peaks induced by the step motor driving the Phebus baffle.

Conclusion of Phebus monitoring

Step motor induces a app. 0.1 Hz signature. The signature of the baffle rotation is weak but noticeable. Further modelling/monitoring suggested.

6.7 SEPS

The ion engine accelerates the BepiColombo stacked s/c towards Mercury. The MPO-MAG team indicated the unique scientific opportunity to take measurements during the cruise to Mercury. Therefore, the magnetic disturbance from the SEPS (solar electric propulsion system) must become known, modelled and eventually removed from the magnetic field data. Furthermore, the monitoring of the SEPS activities by MPO-MAG provides an independent tool to verify operations and settings of the SEPS, not only when there is an anomaly.

2018-12-2T08:33 Set Range: 512nT
2018-12-2T19:05 Set Range: 128nT

NECP Timeline excerpt for SEPS activities:

2018-11-29: MEPS commissioning - EPCM on SEPT1
2018-11-30: MEPS commissioning - EPCM on SEPT2
2018-12-01: MEPS commissioning - Hybrid dual EPCM SEPT1/4
2018-12-02: MEPS commissioning - Routine EPCM with SEPT 1/4 on same thrust level

In the following, daily time series of field differences are shown to give a general overview about the measurements. Detailed signatures are discussed in the next sections.

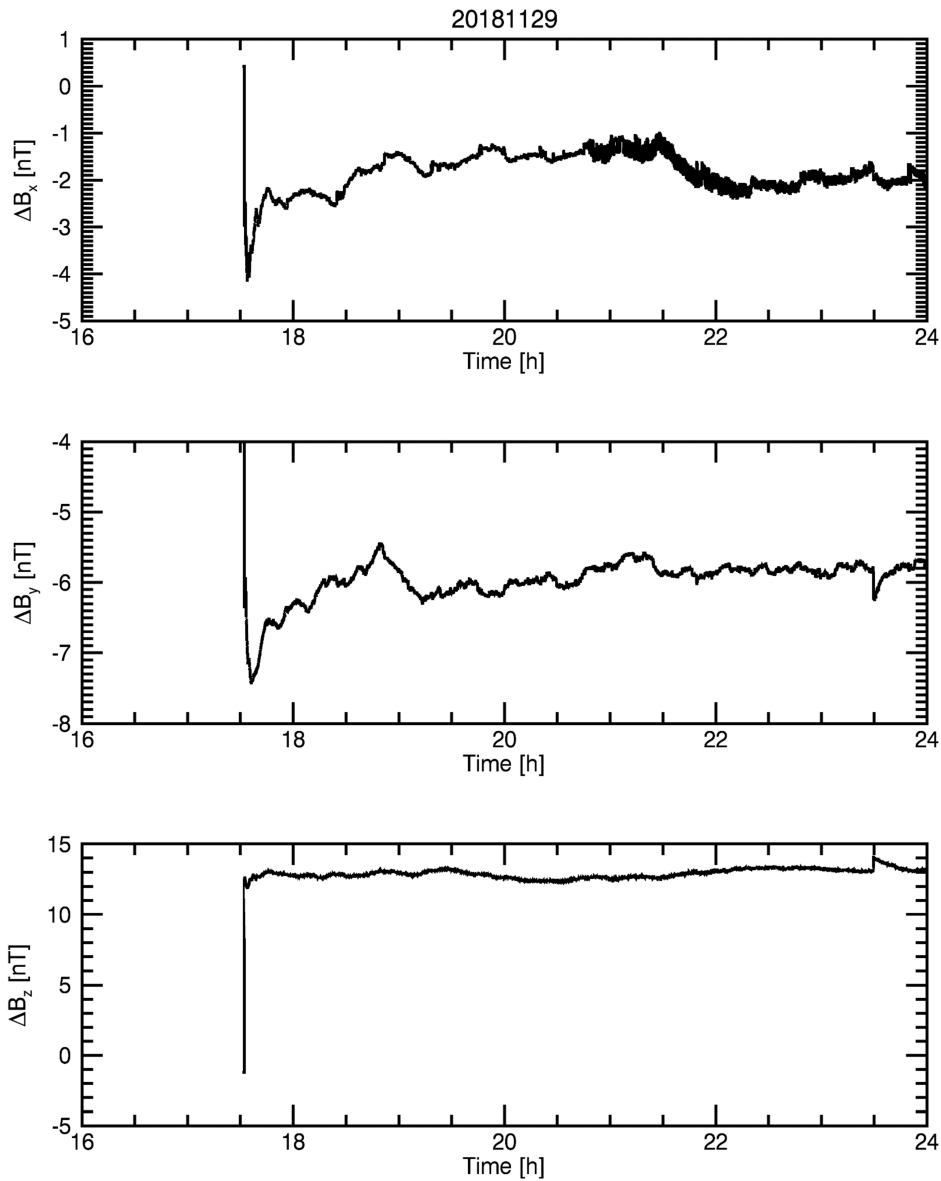


Figure 37: Time series of differences in the magnetic field (OB-IB) for 29/11/2018. The drastic change after switch-on is expected to be due to warming-up of the sensors and instrument electronics [TBC].

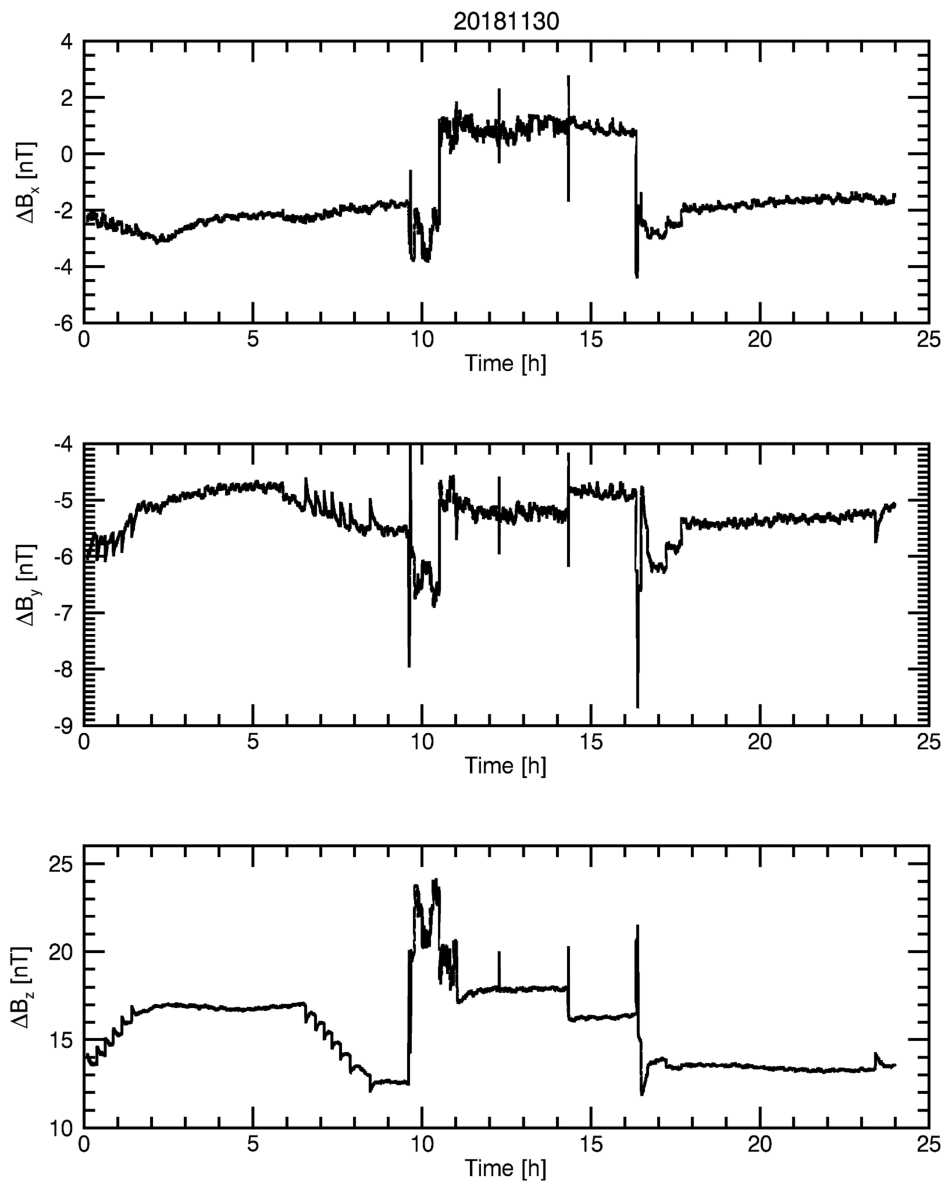


Figure 38: Time series of differences in the magnetic field (OB-IB) for 30/11/2018.

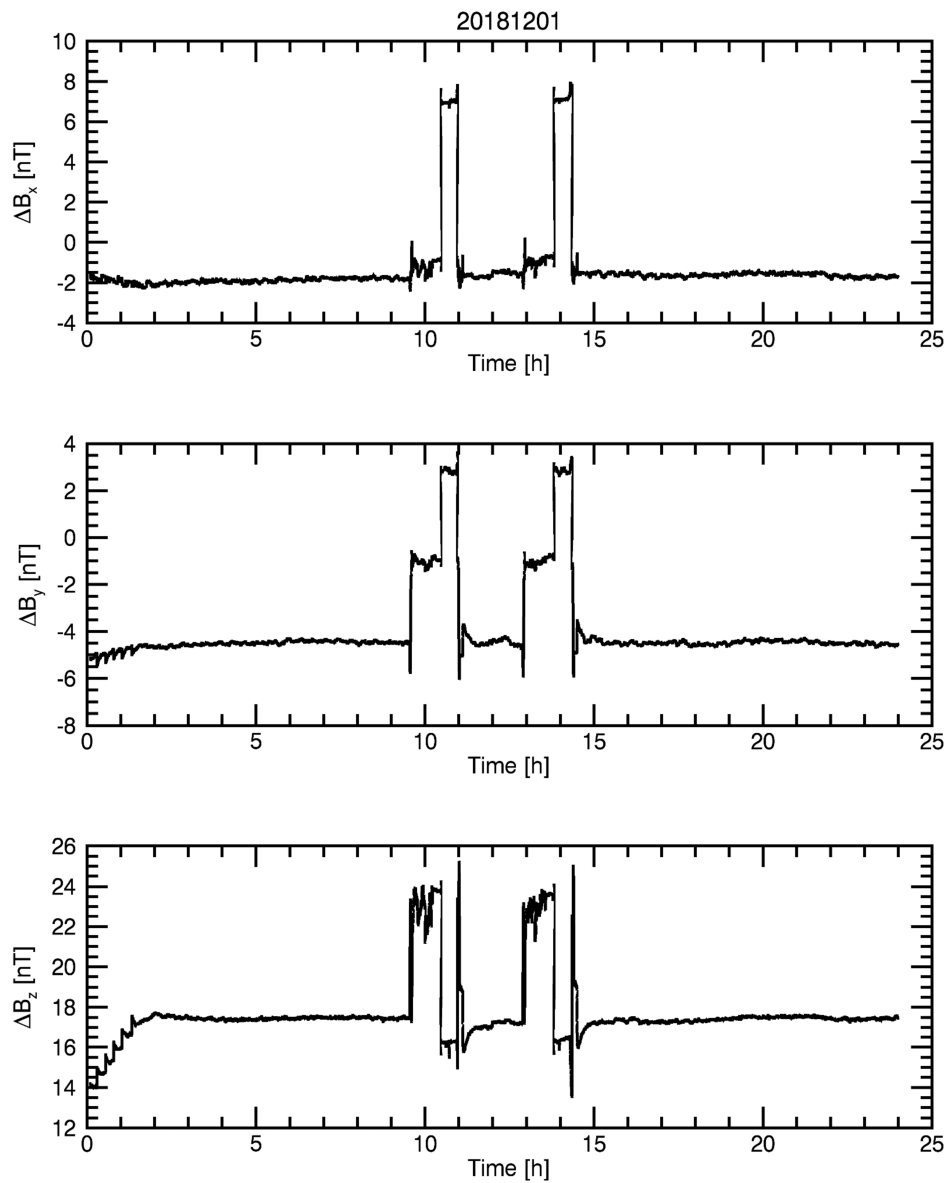


Figure 39: Time series of differences in the magnetic field (OB-IB) for 01/12/2018.

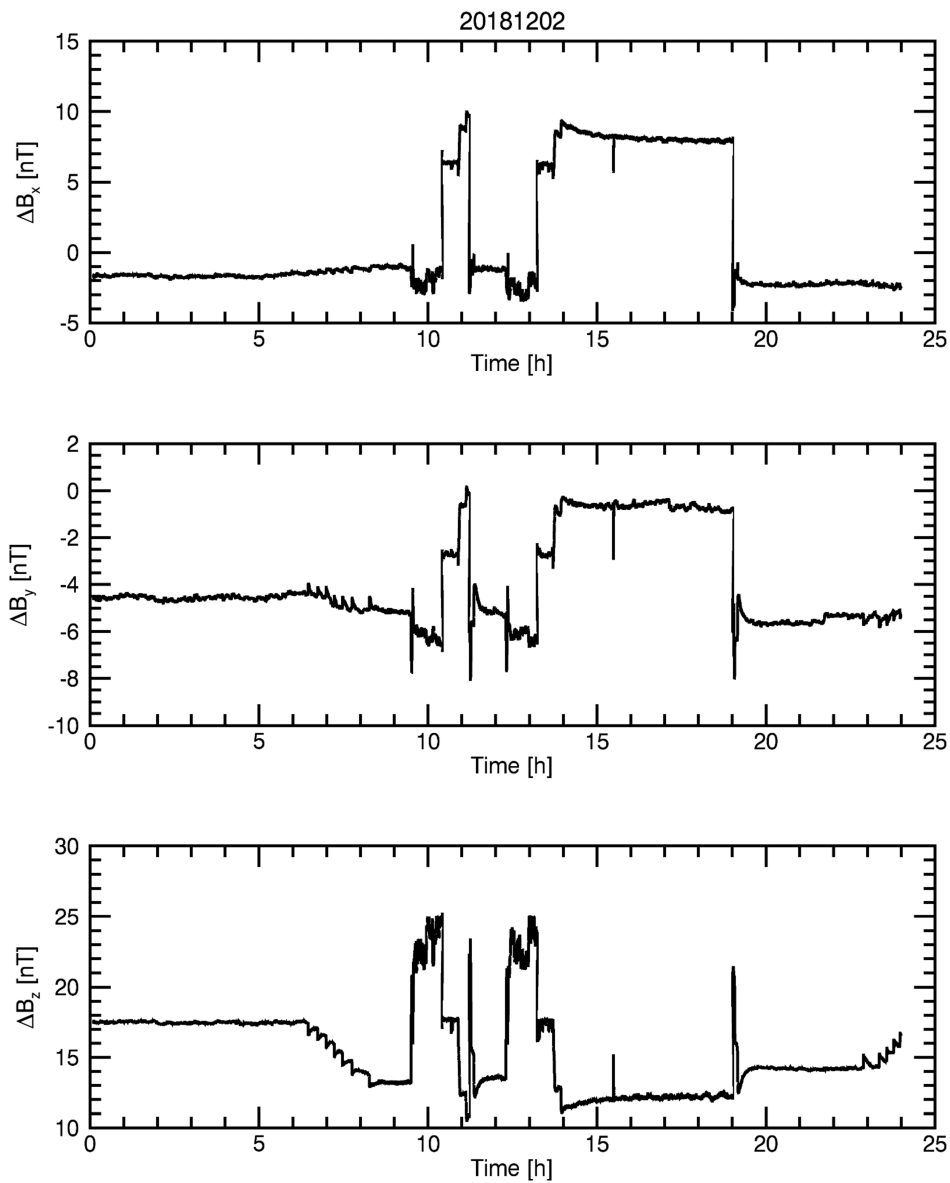


Figure 40: Time series of differences in the magnetic field (OB-IB) for 02/12/2018.

Detailed Signatures

01/12/2018

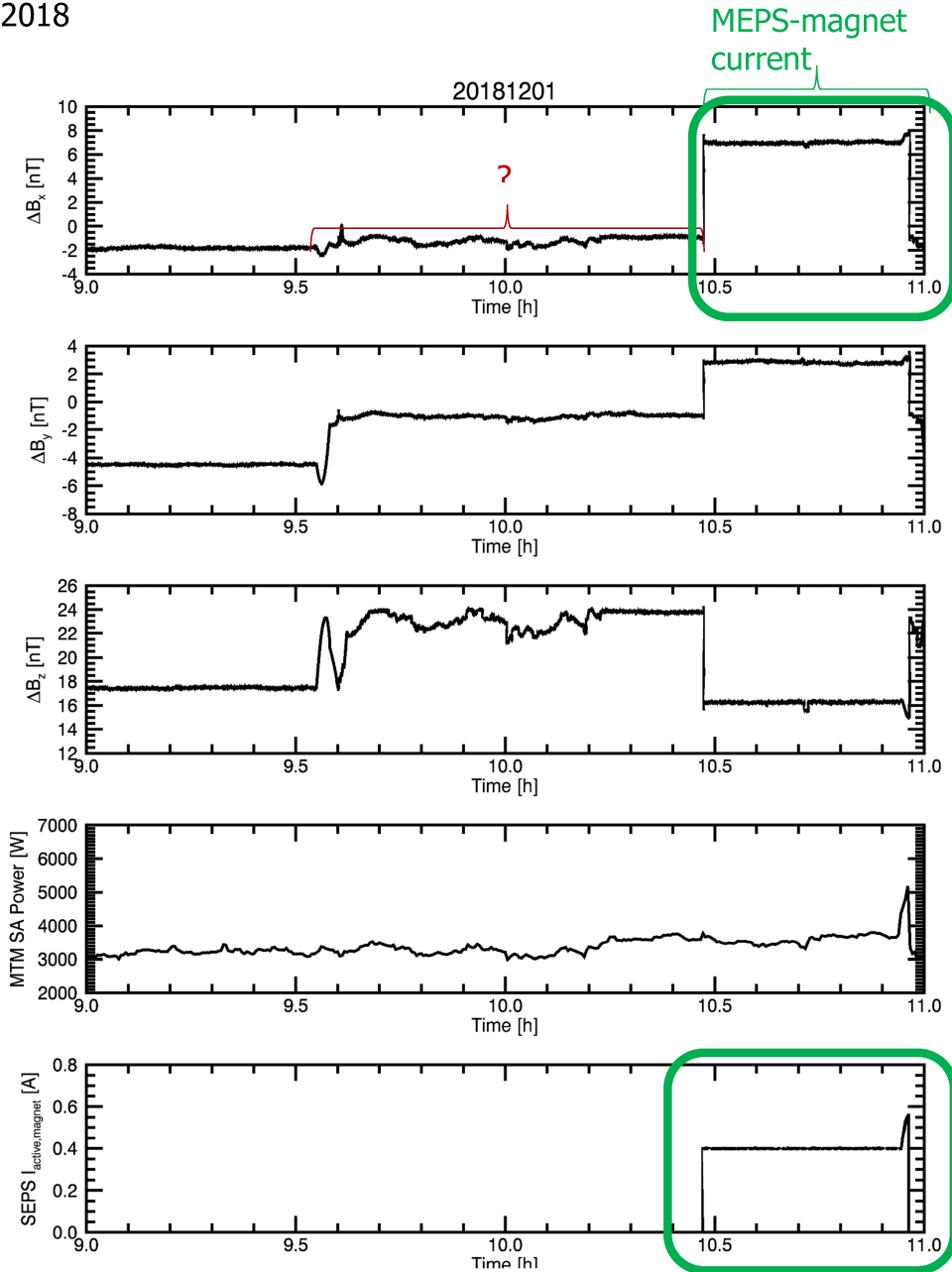


Figure 41: Detail of measurements taken on 01/12/2018. The signature at 10.5 h is strongly correlated to changes in the MEPS current to a magnetic relay and weakly correlated to MTM solar array power. The source of the signature between 9.5h and 10.5h remains to be determined. MTM SA Power refers to the NZWSY110 parameter. SEPS $I_{active,magnet}$ refers to the product $NZMD1402 * NZMD0161(0,1) * NZMD0160(0,1)$ – i.e. the current to the relay magnet if the supply is activated (1) and the thruster function is in magnet mode (1). If the supply is not activated or the thruster function is in heater mode, the current is set to 0 by the multiplication operation.

02/12/2018

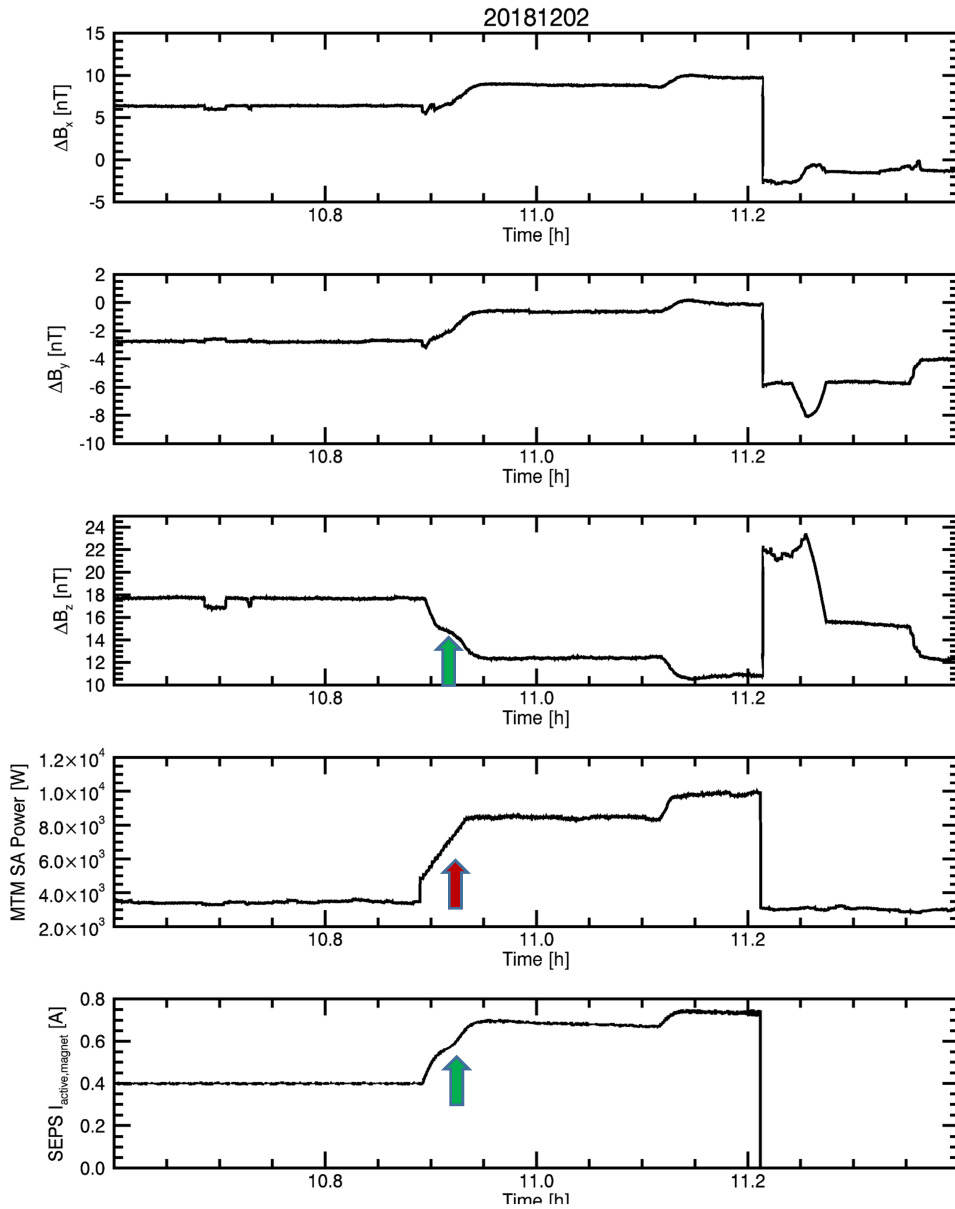


Figure 42 : Detail of measurements taken on 02/12/2018. The signature that starts at ca. 10.9 h and ends at ca.11.2h is clearly correlated to changes in the MEPS current to a magnetic relay and MTM solar array power. Observe the small bulge at 10.92h in the SEPS current that is visible in the magnetic field but not in the MTM solar array power (arrows).

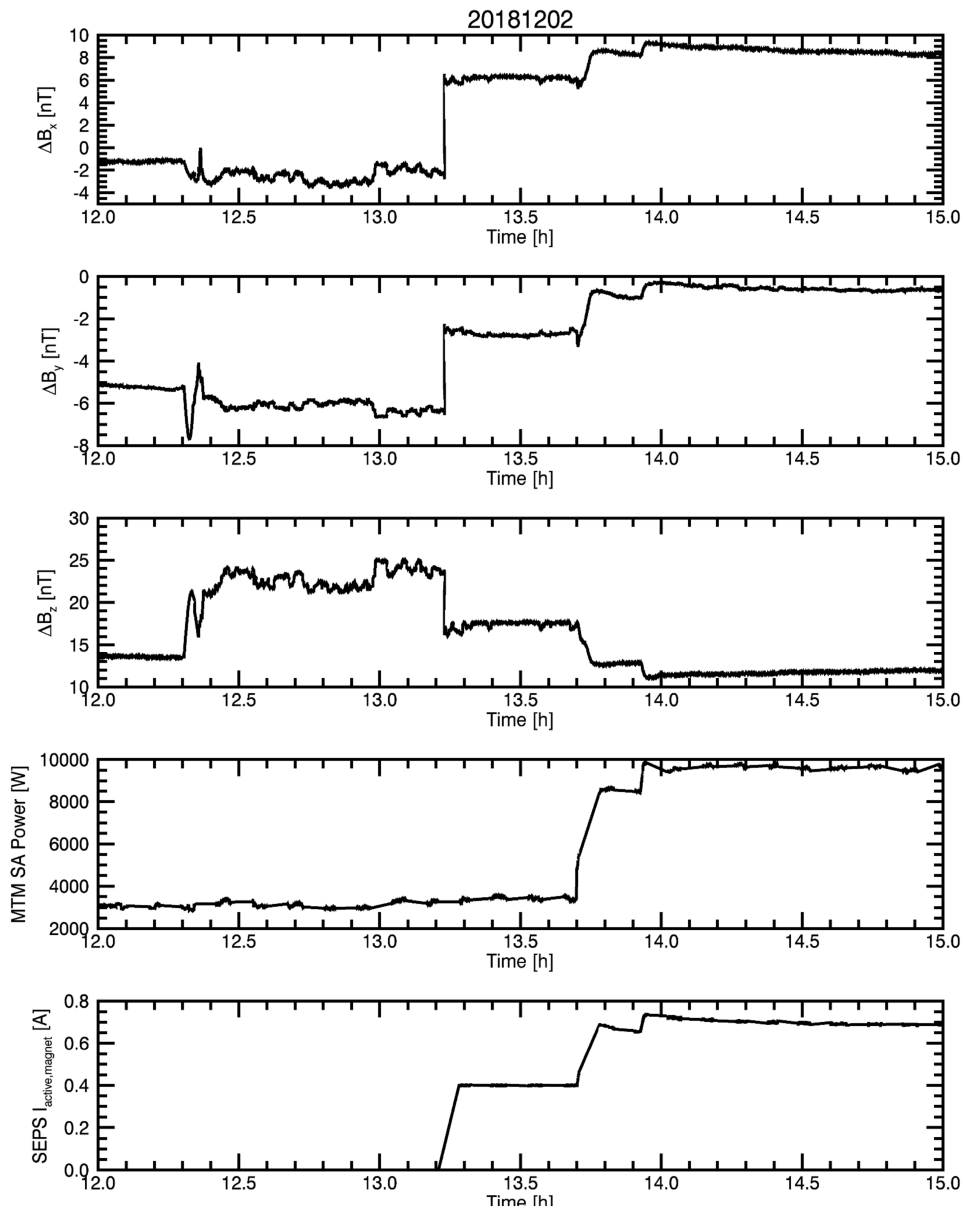


Figure 43 : Detail of measurements taken on 02/12/2018.

Conclusions of Monitoring SEPS Activities

The commissioning activities of the SEPS are clearly seen in the magnetic field data – proving the monitoring ability of the magnetometers. The operations of the SEPS have not driven the magnetometers into saturation. Thus, only fields less than 512 nT have been measured. For the future, a range setting of 256 nT could be commanded. The range change itself has not introduced a jump in the magnetic field data. The sampling frequency of 1 Hz also seems sufficient. It is seen that the correlation between the SEPS relay current with the magnetic field is stronger than the correlation from the MTM solar array power. Detailed analysis to relate magnetic signatures to individual SEPS operations is ongoing.

6.8 HGA

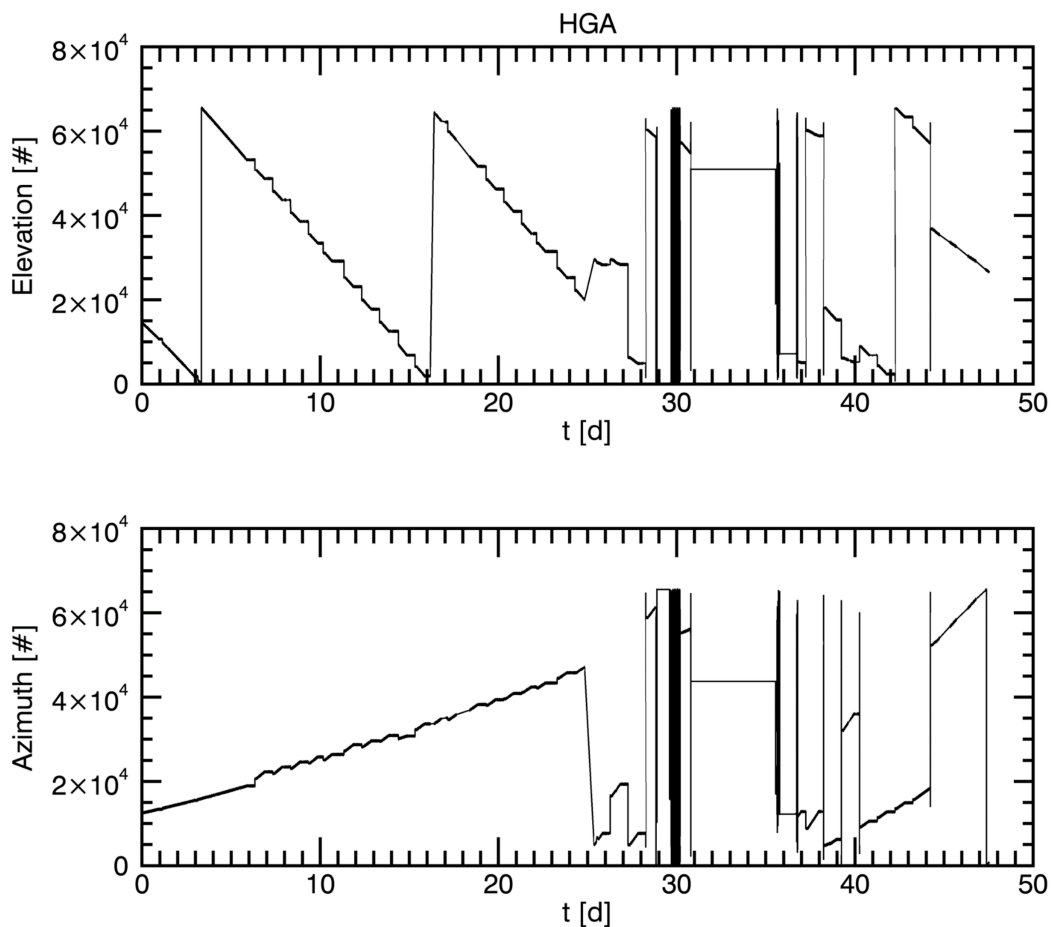


Figure 44 : HGA movements over a long time interval during the commissioning. Azimuth and elevation parameters are still in counts.

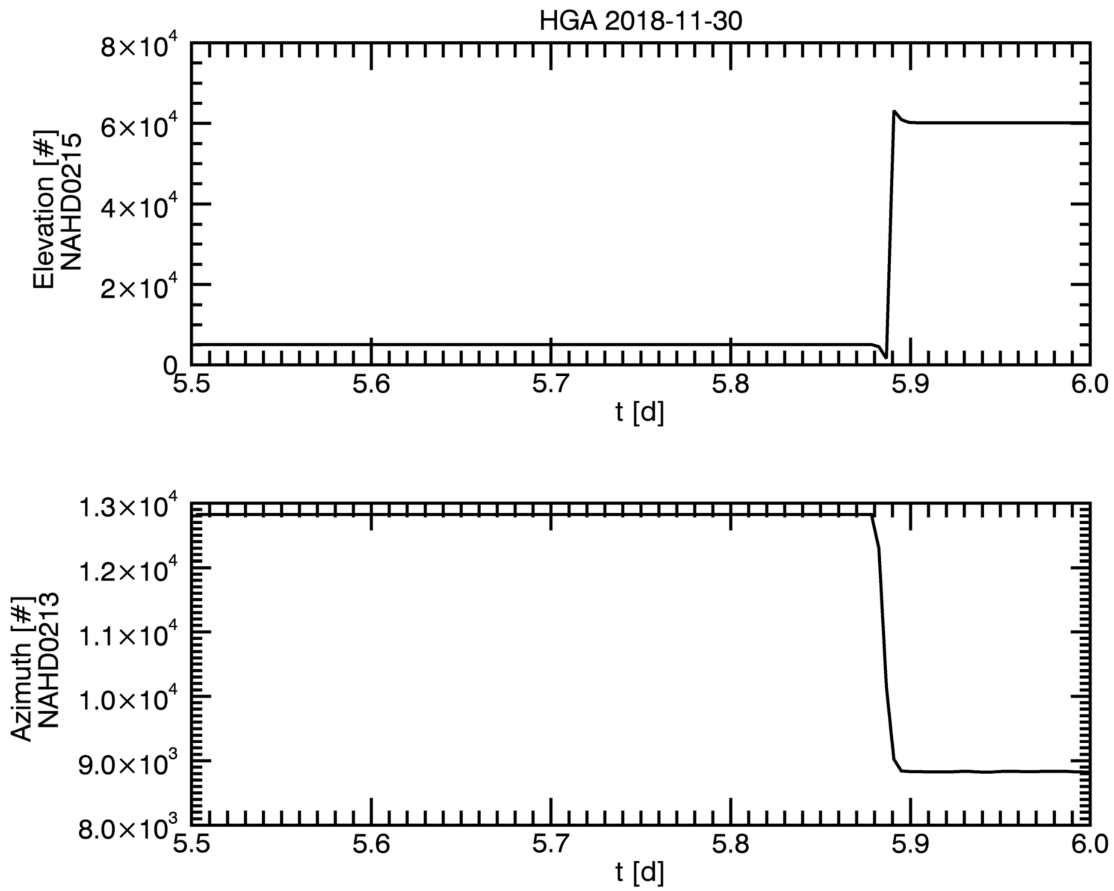


Figure 45 : Detailed time series of HGA movement on 30/11/2018.

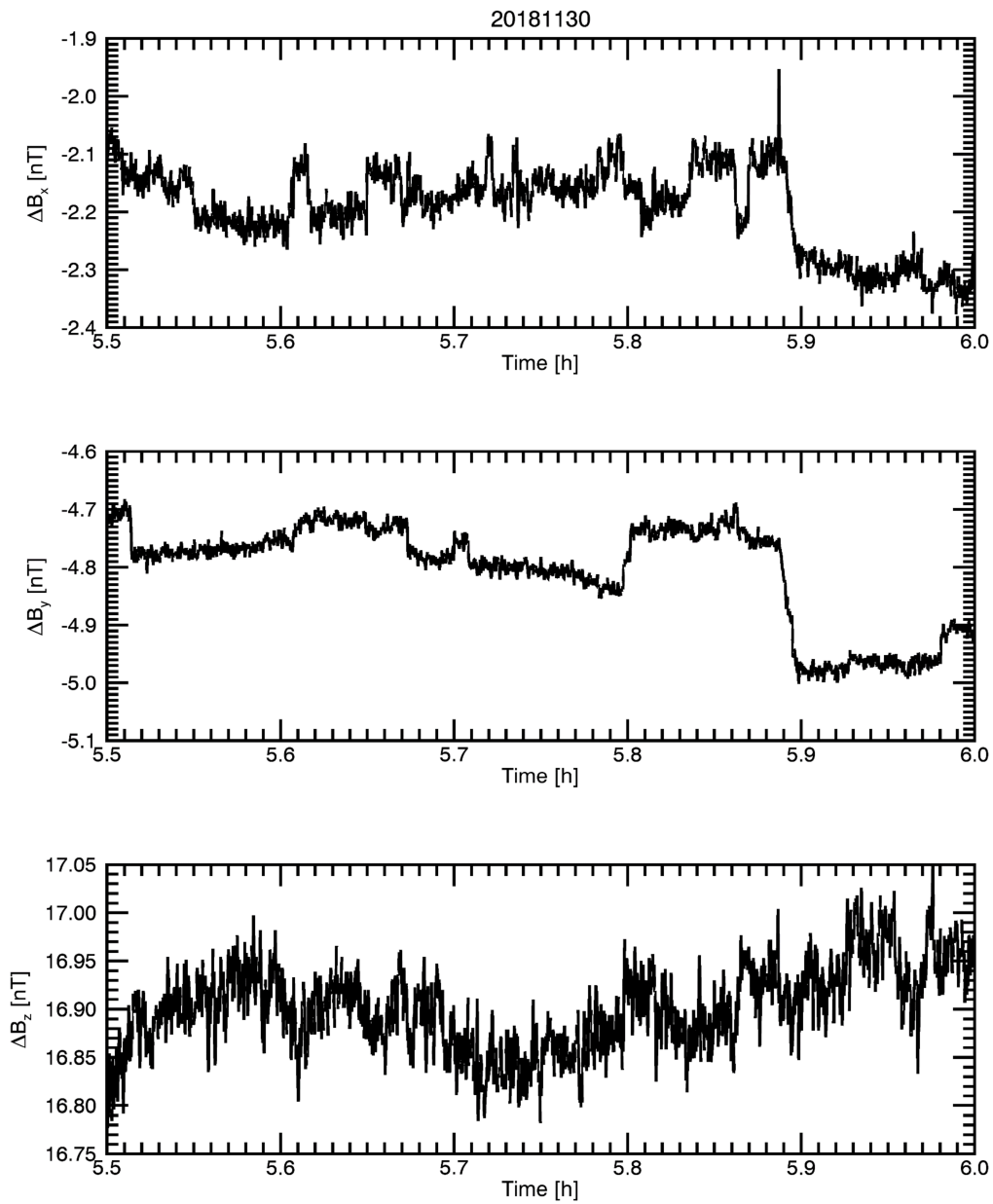


Figure 46 : Time series of magnetic field differences on 30/11/2018. The discontinuity at t=5.9h could be correlated to the HGA movement.

Conclusion of HGA monitoring

There could be a correlation between HGA movement and the magnetic field. Signal is expected to be weak but more statistics is need for verification.

7 Common measurement with MMO

Alignment of MMO Sensors and MPO IB sensor to MPO OB sensor

Johannes has derived the rotation matrices for MMO IB, OB and MPO IB for reorienting the sensors into the MPO OB sensor system by the field variation measured by all sensors.

Rotation Matrix between different magnetometer sensors and the MPO OB sensor coordinate system.

MMO IB to MPO OB

-1.2547556e-01	-4.5428481e-03	-9.9208631e-01
-9.8362969e-01	-1.2979813e-01	1.2500035e-01
-1.2933880e-01	9.9153003e-01	1.1818012e-02

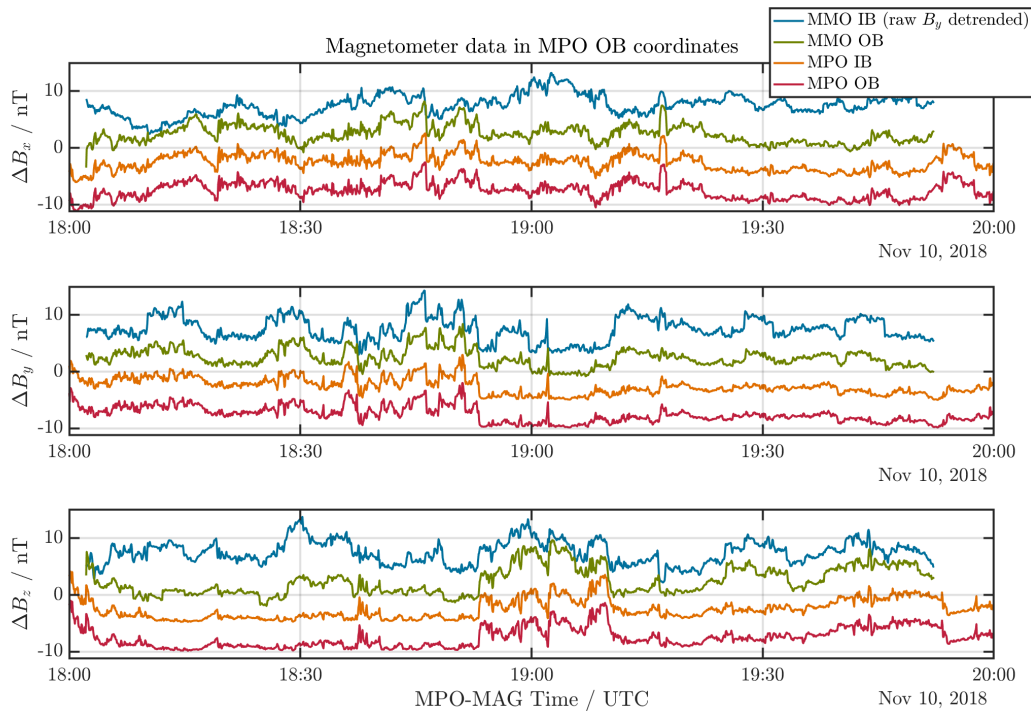
MMO OB to MPO OB

4.0198766e-01	8.5606931e-01	-3.2488653e-01
-1.1834270e-01	-3.0326658e-01	-9.4552863e-01
-9.0796527e-01	4.1853879e-01	-2.0599873e-02

MPO IB to MPO OB

9.9983383e-01	1.8194685e-02	1.1217374e-03
-1.8171746e-02	9.9967514e-01	-1.7871783e-02
-1.4465445e-03	1.7848430e-02	9.9983966e-01

The following plot shows the comparison of the components in MPO OB system. Offsets and the trend of the MMO IB sensor (still stowed and next to MMO S/C) is subtracted. Artificial offset is added to separate plot lines.



8 Agenda for Future Activities

- **Extended compression test:** one Earth-day at 128Hz sampling rate (dual) in the lowest range. Half day with and the other half day without compression. Remaining data volume to be expected in the range 35%-60%.
- **Extended heater test:**
App. Sequence:
 1. Switch-on
 2. 5 min sampling in dual science mode (rate and range TBD)
 3. switch-on heater (duty cycle TBD)
 4. switch-off and switch-on heater several times (TBD)
- **Extended Counter Sequence Test**
- **Software update:**
Upload optimized amplifier phases and K1 values.
- **Reaction wheel test:**
Run a reaction wheels with more separate frequencies (only if s/c safety allows, sequence TBD)
- **Selective Downlink Test**

9 Appendix 1 – Commissioning sequence:

ZME02705 MERM Set Instr Sci Mode AMET003A BC 2018.308.15.54.35.102916 2018.308.16.00.00.000000
 PME02104 New Science Mode Eng Dec CalScience
 ZME02614 MERMSensorSetAutoHeater AMET003A BC 2018.308.15.54.35.102918 2018.308.16.00.01.000000
 PME02078 OBSensAutoHeaterEnable Eng Dec Off
 PME02096 IBsensAutoHeaterEnable Eng Dec Off
 PME02094 OBHeaterTargetTemp Eng Dec 0.0
 PME02095 IBHeaterTargetTemp Eng Dec 0.0
 ZME02616 MERMSensorSetHeaterValue AMET003A BC 2018.308.15.54.35.102920 2018.308.16.00.02.000000
 PME02030 Sensor ID Eng Dec BothSensors
 PME02081 Sensor Heater Value Raw Dec 0
 ZME02701 MERMSetMeasurementRate AMET003A BC 2018.308.15.54.35.102922 2018.308.16.00.03.000000
 PME08005 PID Eng Dec ScienceX
 PME02030 Sensor ID Eng Dec BothSensors
 PME02100 Measurement Rate Eng Dec 128
 ZME02612 MERMSensorSingleAutoComp AMET003A BC 2018.308.15.54.35.102924 2018.308.16.00.04.000000
 PME02030 Sensor ID Eng Dec BothSensors
 ZME02611 MERMSensorSetCompVal AMET004A BC 2018.308.15.54.35.102926 2018.308.16.00.11.000000
 PME02030 Sensor ID Eng Dec MAGIB
 PME02059 SensManualCompValX Raw Dec 0
 PME02060 SensManualCompValY Raw Dec 0
 PME02061 SensManualCompValZ Raw Dec 0
 ZME02611 MERMSensorSetCompVal AMET004A BC 2018.308.15.54.35.102928 2018.308.16.00.12.000000
 PME02030 Sensor ID Eng Dec MAGOB
 PME02059 SensManualCompValX Raw Dec 0
 PME02060 SensManualCompValY Raw Dec 0
 PME02061 SensManualCompValZ Raw Dec 0
 ZME02704 MERMSetMeasurementRange AMET004A BC 2018.308.15.54.35.102930 2018.308.16.00.13.000000
 PME02030 Sensor ID Eng Dec BothSensors
 PME02103 Measurement Range Eng Dec 0128

ZME02611 MERMSensorSetCompVal	AMET004A BC	2018.308.15.54.35.102932	2018.308.16.10.13.000000
PME02030 Sensor ID	Eng Dec	MAGIB	
PME02059 SensManualCompValX	Raw Dec	-300	
PME02060 SensManualCompValY	Raw Dec	-300	
PME02061 SensManualCompValZ	Raw Dec	-300	
ZME02611 MERMSensorSetCompVal	AMET004A BC	2018.308.15.54.35.102934	2018.308.16.10.14.000000
PME02030 Sensor ID	Eng Dec	MAGOB	
PME02059 SensManualCompValX	Raw Dec	-300	
PME02060 SensManualCompValY	Raw Dec	-300	
PME02061 SensManualCompValZ	Raw Dec	-300	
ZME02611 MERMSensorSetCompVal	AMET004A BC	2018.308.15.54.35.102936	2018.308.16.11.14.000000
PME02030 Sensor ID	Eng Dec	MAGIB	
PME02059 SensManualCompValX	Raw Dec	300	
PME02060 SensManualCompValY	Raw Dec	300	
PME02061 SensManualCompValZ	Raw Dec	300	
ZME02611 MERMSensorSetCompVal	AMET004A BC	2018.308.15.54.35.102938	2018.308.16.11.15.000000
PME02030 Sensor ID	Eng Dec	MAGOB	
PME02059 SensManualCompValX	Raw Dec	300	
PME02060 SensManualCompValY	Raw Dec	300	
PME02061 SensManualCompValZ	Raw Dec	300	
ZME02611 MERMSensorSetCompVal	AMET004A BC	2018.308.15.54.35.102940	2018.308.16.12.15.000000
PME02030 Sensor ID	Eng Dec	MAGIB	
PME02059 SensManualCompValX	Raw Dec	0	
PME02060 SensManualCompValY	Raw Dec	0	
PME02061 SensManualCompValZ	Raw Dec	0	
ZME02611 MERMSensorSetCompVal	AMET004A BC	2018.308.15.54.35.102942	2018.308.16.12.16.000000
PME02030 Sensor ID	Eng Dec	MAGOB	
PME02059 SensManualCompValX	Raw Dec	0	
PME02060 SensManualCompValY	Raw Dec	0	
PME02061 SensManualCompValZ	Raw Dec	0	
ZME02705 MERM Set Instr Sci Mode	AMET005A BC	2018.308.15.54.35.102944	2018.308.16.14.10.000000
PME02104 New Science Mode	Eng Dec	CalScience	
ZME02702 MERMSetCalibrationMode	AMET005A BC	2018.308.15.54.35.102946	2018.308.16.14.11.000000

PME02030 Sensor ID	Eng	Dec	BothSensors		
PME02101 Calibration Mode	Eng	Dec	Cal4OL		
ZME02608 MERMSensorSetCalFBDAC	AMET005A	BC		2018.308.15.54.35.102948	2018.308.16.14.12.000000
PME02030 Sensor ID	Eng	Dec	MAGIB		
PME02056 Sensor Feedback DAC X	Raw	Dec	0		
PME02057 Sensor Feedback DAC Y	Raw	Dec	0		
PME02058 Sensor Feedback DAC Z	Raw	Dec	0		
ZME02608 MERMSensorSetCalFBDAC	AMET005A	BC		2018.308.15.54.35.102950	2018.308.16.14.13.000000
PME02030 Sensor ID	Eng	Dec	MAGOB		
PME02056 Sensor Feedback DAC X	Raw	Dec	0		
PME02057 Sensor Feedback DAC Y	Raw	Dec	0		
PME02058 Sensor Feedback DAC Z	Raw	Dec	0		
ZME02602 MERMSensorSetDACWeights	AMET005A	BC		2018.308.15.54.35.102952	2018.308.16.14.14.000000
PME02030 Sensor ID	Eng	Dec	BothSensors		
PME02053 Sensor K2 X DAC	Raw	Dec	0		
PME02054 Sensor K2 Y DAC	Raw	Dec	0		
PME02055 Sensor K2 Z DAC	Raw	Dec	0		
ZME02704 MERMSetMeasurementRange	AMET005A	BC		2018.308.15.54.35.102954	2018.308.16.14.15.000000
PME02030 Sensor ID	Eng	Dec	BothSensors		
PME02103 Measurement Range	Eng	Dec	0128		
ZME02611 MERMSensorSetCompVal	AMET004A	BC		2018.308.15.54.35.102956	2018.308.16.14.21.000000
PME02030 Sensor ID	Eng	Dec	MAGIB		
PME02059 SensManualCompValX	Raw	Dec	0		
PME02060 SensManualCompValY	Raw	Dec	0		
PME02061 SensManualCompValZ	Raw	Dec	0		
ZME02611 MERMSensorSetCompVal	AMET004A	BC		2018.308.15.54.35.102958	2018.308.16.14.22.000000
PME02030 Sensor ID	Eng	Dec	MAGOB		
PME02059 SensManualCompValX	Raw	Dec	0		
PME02060 SensManualCompValY	Raw	Dec	0		
PME02061 SensManualCompValZ	Raw	Dec	0		
ZME02704 MERMSetMeasurementRange	AMET004A	BC		2018.308.15.54.35.102960	2018.308.16.14.23.000000
PME02030 Sensor ID	Eng	Dec	BothSensors		
PME02103 Measurement Range	Eng	Dec	0128		

ZME02611 MERMSensorSetCompVal	AMET004A BC	2018.308.15.54.35.102962	2018.308.16.24.23.000000
PME02030 Sensor ID	Eng Dec	MAGIB	
PME02059 SensManualCompValX	Raw Dec	-300	
PME02060 SensManualCompValY	Raw Dec	-300	
PME02061 SensManualCompValZ	Raw Dec	-300	
ZME02611 MERMSensorSetCompVal	AMET004A BC	2018.308.15.54.35.102964	2018.308.16.24.24.000000
PME02030 Sensor ID	Eng Dec	MAGOB	
PME02059 SensManualCompValX	Raw Dec	-300	
PME02060 SensManualCompValY	Raw Dec	-300	
PME02061 SensManualCompValZ	Raw Dec	-300	
ZME02611 MERMSensorSetCompVal	AMET004A BC	2018.308.15.54.35.102966	2018.308.16.25.24.000000
PME02030 Sensor ID	Eng Dec	MAGIB	
PME02059 SensManualCompValX	Raw Dec	300	
PME02060 SensManualCompValY	Raw Dec	300	
PME02061 SensManualCompValZ	Raw Dec	300	
ZME02611 MERMSensorSetCompVal	AMET004A BC	2018.308.15.54.35.102968	2018.308.16.25.25.000000
PME02030 Sensor ID	Eng Dec	MAGOB	
PME02059 SensManualCompValX	Raw Dec	300	
PME02060 SensManualCompValY	Raw Dec	300	
PME02061 SensManualCompValZ	Raw Dec	300	
ZME02611 MERMSensorSetCompVal	AMET004A BC	2018.308.15.54.35.102970	2018.308.16.26.25.000000
PME02030 Sensor ID	Eng Dec	MAGIB	
PME02059 SensManualCompValX	Raw Dec	0	
PME02060 SensManualCompValY	Raw Dec	0	
PME02061 SensManualCompValZ	Raw Dec	0	
ZME02611 MERMSensorSetCompVal	AMET004A BC	2018.308.15.54.35.102972	2018.308.16.26.26.000000
PME02030 Sensor ID	Eng Dec	MAGOB	
PME02059 SensManualCompValX	Raw Dec	0	
PME02060 SensManualCompValY	Raw Dec	0	
PME02061 SensManualCompValZ	Raw Dec	0	
ZME02606 MERM Sensor Set FB Relay	AMET006A BC	2018.308.15.54.35.102974	2018.308.16.28.20.000000
PME02030 Sensor ID	Eng Dec	BothSensors	
PME02073 SensFeedbackRelayEnable	Eng Dec	Off	

ZME02606 MERM Sensor Set FB Relay AMET006A BC 2018.308.15.54.35.102976 2018.308.16.38.20.000000
PME02030 Sensor ID Eng Dec BothSensors
PME02073 SensFeedbackRelayEnable Eng Dec On
ZME02607 MERM Sensor Set Excite AMET007A BC 2018.308.15.54.35.102978 2018.308.16.48.20.000000
PME02030 Sensor ID Eng Dec BothSensors
PME02074 SensorExcitationEnable Eng Dec Off
ZME02606 MERM Sensor Set FB Relay AMET007A BC 2018.308.15.54.35.102980 2018.308.16.48.21.000000
PME02030 Sensor ID Eng Dec BothSensors
PME02073 SensFeedbackRelayEnable Eng Dec Off
ZME02607 MERM Sensor Set Excite AMET007A BC 2018.308.15.54.35.102982 2018.308.16.53.21.000000
PME02030 Sensor ID Eng Dec BothSensors
PME02074 SensorExcitationEnable Eng Dec On
ZME02705 MERM Set Instr Sci Mode AMET008A BC 2018.308.15.54.35.102984 2018.308.16.54.20.000000
PME02104 New Science Mode Eng Dec CalScience
ZME02701 MERMSetMeasurementRate AMET008A BC 2018.308.15.54.35.102986 2018.308.16.54.21.000000
PME08005 PID Eng Dec ScienceX
PME02030 Sensor ID Eng Dec BothSensors
PME02100 Measurement Rate Eng Dec 128
ZME02704 MERMSetMeasurementRange AMET008A BC 2018.308.15.54.35.102988 2018.308.16.54.22.000000
PME02030 Sensor ID Eng Dec BothSensors
PME02103 Measurement Range Eng Dec 0128
ZME02612 MERMSensorSingleAutoComp AMET008A BC 2018.308.15.54.35.102990 2018.308.16.55.22.000000
PME02030 Sensor ID Eng Dec BothSensors
ZME02611 MERMSensorSetCompVal AMET009A BC 2018.308.15.54.35.102992 2018.308.16.55.30.000000
PME02030 Sensor ID Eng Dec MAGIB
PME02059 SensManualCompValX Raw Dec 0
PME02060 SensManualCompValY Raw Dec 0
PME02061 SensManualCompValZ Raw Dec 0
ZME02611 MERMSensorSetCompVal AMET009A BC 2018.308.15.54.35.102994 2018.308.16.55.31.000000
PME02030 Sensor ID Eng Dec MAGOB
PME02059 SensManualCompValX Raw Dec 0
PME02060 SensManualCompValY Raw Dec 0
PME02061 SensManualCompValZ Raw Dec 0

ZME02702	MERMSSetCalibrationMode	AMET009A	BC	2018.308.15.54.35.102996	2018.308.16.55.32.000000
PME02030	Sensor ID	Eng	Dec	BothSensors	
PME02101	Calibration Mode	Eng	Dec	Cal3ADAC	
ZME02702	MERMSSetCalibrationMode	AMET014A	BC	2018.308.15.54.35.102998	2018.308.16.57.41.000000
PME02030	Sensor ID	Eng	Dec	BothSensors	
PME02101	Calibration Mode	Eng	Dec	Cal7Findphase	
ZME02704	MERMSSetMeasurementRange	AMET014A	BC	2018.308.15.54.35.103000	2018.308.16.57.42.000000
PME02030	Sensor ID	Eng	Dec	BothSensors	
PME02103	Measurement Range	Eng	Dec	2048	
ZME02611	MERMSensorSetCompVal	AMET014A	BC	2018.308.15.54.35.103002	2018.308.16.57.43.000000
PME02030	Sensor ID	Eng	Dec	MAGIB	
PME02059	SensManualCompValX	Raw	Dec	0	
PME02060	SensManualCompValY	Raw	Dec	0	
PME02061	SensManualCompValZ	Raw	Dec	0	
ZME02611	MERMSensorSetCompVal	AMET014A	BC	2018.308.15.54.35.103004	2018.308.16.57.44.000000
PME02030	Sensor ID	Eng	Dec	MAGOB	
PME02059	SensManualCompValX	Raw	Dec	0	
PME02060	SensManualCompValY	Raw	Dec	0	
PME02061	SensManualCompValZ	Raw	Dec	0	
ZME02620	MERMSensorSetFindPhase	AMET014A	BC	2018.308.15.54.35.103006	2018.308.16.57.45.000000
PME02083	Sensor Cal StartPhase	Raw	Dec	4	
PME02084	Sensor Cal EndPhase	Raw	Dec	255	
PME02085	Sensor Cal PhaseStep	Raw	Dec	10	
PME02086	Sensor Cal JumpSize	Raw	Dec	4096	
PME02087	Sensor Cal Waitsamples	Raw	Dec	1	
ZME02620	MERMSensorSetFindPhase		BC	2018.308.15.54.35.103008	2018.308.17.01.45.000000
PME02083	Sensor Cal StartPhase	Raw	Dec	4	
PME02084	Sensor Cal EndPhase	Raw	Dec	255	
PME02085	Sensor Cal PhaseStep	Raw	Dec	10	
PME02086	Sensor Cal JumpSize	Raw	Dec	8192	
PME02087	Sensor Cal Waitsamples	Raw	Dec	1	
ZME02704	MERMSSetMeasurementRange	AMET015A	BC	2018.308.15.54.35.103010	2018.308.17.05.51.000000
PME02030	Sensor ID	Eng	Dec	BothSensors	

PME02103 Measurement Range	Eng	Dec	2048		
ZME02702 MERMSSetCalibrationMode	AMET015A	BC	2018.308.15.54.35.103012	2018.308.17.05.52.000000	
PME02030 Sensor ID	Eng	Dec	BothSensors		
PME02101 Calibration Mode	Eng	Dec	Cal5Meander		
ZME02611 MERMSensorSetCompVal	AMET015A	BC	2018.308.15.54.35.103014	2018.308.17.05.53.000000	
PME02030 Sensor ID	Eng	Dec	MAGIB		
PME02059 SensManualCompValX	Raw	Dec	0		
PME02060 SensManualCompValY	Raw	Dec	0		
PME02061 SensManualCompValZ	Raw	Dec	0		
ZME02611 MERMSensorSetCompVal	AMET015A	BC	2018.308.15.54.35.103016	2018.308.17.05.54.000000	
PME02030 Sensor ID	Eng	Dec	MAGOB		
PME02059 SensManualCompValX	Raw	Dec	0		
PME02060 SensManualCompValY	Raw	Dec	0		
PME02061 SensManualCompValZ	Raw	Dec	0		
ZME02702 MERMSSetCalibrationMode	AMET010A	BC	2018.308.15.54.35.103018	2018.308.17.13.01.000000	
PME02030 Sensor ID	Eng	Dec	BothSensors		
PME02101 Calibration Mode	Eng	Dec	Cal1Step		
ZME02611 MERMSensorSetCompVal	AMET010A	BC	2018.308.15.54.35.103020	2018.308.17.13.02.000000	
PME02030 Sensor ID	Eng	Dec	MAGIB		
PME02059 SensManualCompValX	Raw	Dec	0		
PME02060 SensManualCompValY	Raw	Dec	0		
PME02061 SensManualCompValZ	Raw	Dec	0		
ZME02611 MERMSensorSetCompVal	AMET010A	BC	2018.308.15.54.35.103022	2018.308.17.13.03.000000	
PME02030 Sensor ID	Eng	Dec	MAGOB		
PME02059 SensManualCompValX	Raw	Dec	0		
PME02060 SensManualCompValY	Raw	Dec	0		
PME02061 SensManualCompValZ	Raw	Dec	0		
ZME02704 MERMSSetMeasurementRange	AMET010A	BC	2018.308.15.54.35.103024	2018.308.17.13.04.000000	
PME02030 Sensor ID	Eng	Dec	BothSensors		
PME02103 Measurement Range	Eng	Dec	2048		
ZME02702 MERMSSetCalibrationMode	AMET010A	BC	2018.308.15.54.35.103026	2018.308.17.20.04.000000	
PME02030 Sensor ID	Eng	Dec	BothSensors		
PME02101 Calibration Mode	Eng	Dec	Cal2Count		

ZME02704 MERMSSetMeasurementRange AMET010A BC 2018.308.15.54.35.103028 2018.308.17.20.05.000000
PME02030 Sensor ID Eng Dec BothSensors
PME02103 Measurement Range Eng Dec 2048
ZME02705 MERM Set Instr Sci Mode AMET011A BC 2018.308.15.54.35.103030 2018.308.17.23.10.000000
PME02104 New Science Mode Eng Dec ScienceX
ZME02701 MERMSSetMeasurementRate AMET011A BC 2018.308.15.54.35.103032 2018.308.17.23.11.000000
PME08005 PID Eng Dec ScienceX
PME02030 Sensor ID Eng Dec BothSensors
PME02100 Measurement Rate Eng Dec 128
ZME02704 MERMSSetMeasurementRange AMET011A BC 2018.308.15.54.35.103034 2018.308.17.23.12.000000
PME02030 Sensor ID Eng Dec BothSensors
PME02103 Measurement Range Eng Dec 0128
ZME02612 MERMSensorSingleAutoComp AMET011A BC 2018.308.15.54.35.103036 2018.308.17.23.13.000000
PME02030 Sensor ID Eng Dec BothSensors
ZME00329 MERM Set HK Report Rate AMET011A BC 2018.308.15.54.35.103038 2018.308.17.23.14.000000
PME08003 SID Raw Dec 1
PME08004 Collection Interval Raw Dec 80
ZME00329 MERM Set HK Report Rate AMET011A BC 2018.308.15.54.35.103040 2018.308.17.23.15.000000
PME08003 SID Raw Dec 2
PME08004 Collection Interval Raw Dec 80
ZME00329 MERM Set HK Report Rate AMET011A BC 2018.308.15.54.35.103042 2018.308.17.23.16.000000
PME08003 SID Raw Dec 4
PME08004 Collection Interval Raw Dec 80
ZME00329 MERM Set HK Report Rate AMET011A BC 2018.308.15.54.35.103044 2018.308.17.23.17.000000
PME08003 SID Raw Dec 5
PME08004 Collection Interval Raw Dec 80
ZME02614 MERMSensorSetAutoHeater AMET011A BC 2018.308.15.54.35.103046 2018.308.17.23.18.000000
PME02078 OBSensAutoHeaterEnable Eng Dec Off
PME02096 IBSensAutoHeaterEnable Eng Dec Off
PME02094 OBHeaterTargetTemp Eng Dec 0.0
PME02095 IBHeaterTargetTemp Eng Dec 0.0
ZME02616 MERMSensorSetHeaterValue AMET011A BC 2018.308.15.54.35.103048 2018.308.17.23.19.000000
PME02030 Sensor ID Eng Dec BothSensors

PME02081 Sensor Heater Value Raw Dec 128
ZME02616 MERMSensorSetHeaterValue BC 2018.308.15.54.35.103050 2018.308.17.43.19.000000
PME02030 Sensor ID Eng Dec BothSensors
PME02081 Sensor Heater Value Raw Dec 0
ZME02705 MERM Set Instr Sci Mode AMET012A BC 2018.308.15.54.35.103052 2018.308.17.43.25.000000
PME02104 New Science Mode Eng Dec ScienceX
ZME02704 MERMSetMeasurementRange AMET012A BC 2018.308.15.54.35.103054 2018.308.17.43.26.000000
PME02030 Sensor ID Eng Dec BothSensors
PME02103 Measurement Range Eng Dec 0256
ZME02612 MERMSensorSingleAutoComp AMET012A BC 2018.308.15.54.35.103056 2018.308.17.43.27.000000
PME02030 Sensor ID Raw Dec 2
ZME02701 MERMSetMeasurementRate AMET012A BC 2018.308.15.54.35.103058 2018.308.17.43.28.000000
PME08005 PID Eng Dec ScienceX
PME02030 Sensor ID Eng Dec BothSensors
PME02100 Measurement Rate Eng Dec 128